Performance Evaluation of Water Collecting Systems for a Hybrid Dephlegmator

by
Jacques du Plessis

Thesis presented in partial fulfilment of the requirements for the degree of Master of Engineering (Mechanical) in the Faculty of Engineering at Stellenbosch University

Supervisor: Prof. Hanno Carl Rudolf Reuter

December 2014

Declaration

By submitting this thesis electronically, I declare that the entirety of the work contained therein is my own, original work, that I am the sole author thereof (save to the extent explicitly otherwise stated), that reproduction and publication thereof by Stellenbosch University will not infringe any third party rights and that I have not previously in its entirety or in part submitted it for obtaining any qualification.

.....

Date: .....

Abstract

Water collection systems are used in wet-cooling towers (WCTs) with fill over which water to be cooled flows and in evaporative air-cooled heat exchangers (EACHEs) having deluged tube bundles over which water flows to transfer heat from the tubes. They collect and remove water falling from the bottom of the fill or heat exchanger tube bundle while allowing air to pass with limited flow resistance. There are basically two types of collection systems, categorized as trough and basin systems. Trough systems comprise of multiple, evenly spaced parallel troughs extended in one direction with inclined capture plates to direct water into the troughs. The water collects in the troughs and drains under gravity to a collecting tank or manifold from where it is pumped to the sprayers. In basin systems water falls directly into an open basin under gravity where it is collected and can be pumped to the sprayers. The hybrid (dry/wet) dephlegmator (HDWD) for air-cooled steam condensers, which is being developed at Stellenbosch University as discussed by Heyns (2008), Owen (2013) and Anderson (2014), requires a more effective water collection system with a lower pressure drop than what current designs have to offer.

In this thesis, an existing trough system is systematically evaluated by means of various high speed camera and flow experiments to determine its performance characteristics and to find ways to improve its catchment effectiveness. A modification is proposed which increases the effectiveness from approximately 92% to 100 % with a relatively small increase in pressure drop, by adding a small deflector plate and reducing the spacing between adjacent troughs. Experimental data and CFD models are used to determine the performance characteristics of the modified trough system for design purposes.

For comparison, various basin system designs are proposed and investigated using CFD, where the baseline model is validated by means of experimental data of rectangular cooling tower inlets by Kröger (2004). Rectangular cooling tower inlets are relevant as they have a similar re-circulating flow pattern to what is seen with the water basin inlets at the vicinity of the inlet wall. The numerical data is correlated to determine empirical relations for the flow performance characteristics.

The comparison between the modified trough and the different basin systems yields that the trough system requires significantly less fan and pumping power than basin systems and the costs are also expected to be less.

Opsomming

Wateropvangstelsels word gebruik in nat koeltorings en verdamping verkoelers, waar waterdruppels in teen-vloei is met n lugstroom. Die stelsel vang die water wat val op en verwyder dit uit die lugstroom met 'n minimale lugweerstand. Daar is twee wateropvangstelsels wat as volg gekategoriseer word: trog stelsel en wateropvangbak stelsel. 'n Trog stelsel bestaan uit eweredige gespasieerde trôe parallel aan mekaar met 'n skuinsvlak om water in die kanaal op te vang. Water dreineer as gevolg van swaartekrag na 'n opvangs tenk waarvan dit terug gepomp word na die sproeiers. In 'n wateropvangbak stelsel val water direk in die bak en word terug gepomp na die sproeiers. 'n Lugverkoelde kondenserstelsels met 'n hibriede (droog/nat) deflegmator wat huidiglik by die Stellenbosch Universiteit ontwikkel word benodig 'n meer effektiewe wateropvangstelsel met 'n lae drukval.

In hierdie tesis word bestaande trog stelsels sistematies geëvalueer deur middel van verskeie toetse met 'n hoë spoed kamera en lugvloei eksperimente om die werkverrigtingskarakteristieke te bepaal en om die opvangsvermoë te verbeter. 'n Verbetering word voorgestel wat die opvangsvermoë verbeter van ongeveer 92 % na 100 % met 'n relatiewe klein verhoging in die drukval deur 'n klein leilem by te voeg en die spasiëring tussen trôe te verminder. Eksperimentele data en BVD (berekeningsvloeidinamika) modelle word gebruik om die werkverrigtings-karakteristieke te bepaal van die nuwe trog stelsel vir ontwerps doeleindes.

Die modelle is bekragtig deur gebruik te maak van literatuur van inlaatverlies korrelasies vir reghoekige koeltorings, soos gedoen deur Kröger (2004). Die inlaat van reghoekige koeltorings het soortgelyke vloeipatrone en vloeiwegbreking soos wat by die inlaat van die wateropvangbak stelsel gesien word. Die numeriese data word gebruik om 'n vergelyking vir die vloei karakteristieke te bepaal.

'n Vergelykende studie tussen die nuwe trog stelsel en die wateropvangbak stelsel het bewys dat die trog stelsel noemenswaardig minder waaier drywing en pomp drywing benodig.

Acknowledgments

I would like to say thank you to the following:

- Thank you God for giving me the perseverance and strength for every day.
- Thank you Prof. Reuter for his guidance, assistance and always pushing us to better ourselves.
- EPRI for funding the project.
- Mr. C. Zietsman, F. Zietsman, J. Stanfliet and the workshop team for always helping.
- My parents for always understanding, supporting me and loving me no matter what.
- Sonika my fiancé for being there when I needed you and supporting me every day, good or bad.
- Neil Anderson, Alain Michaels and Neil Fourie for friendship, help, advice, and assistance.

Contents

List of Figures

List of Tables

Nomenclature

A	Area, m^2
B	Buoyancy, breadth, m
D	Diameter, m
E	Energy, J
F	Force, N
G	Mass velocity, $kg/m^2.s$
g	Gravitational acceleration, m/s^2
H	Height, m
K	Loss coefficient
L	Length, m
$\dot{m}$	Mass flow rate, kg/s
N	Rotational speed, rpm
P	Power, W, Pressure, N/m^2
T	Temperature, K
t	Temperature, °C
V	Volume, m^3
v	Velocity, m/s
W	Width, m
x	Co-ordinate, m, spacing, m
y	Co-ordinate, m

Greek letters

α	Kinetic energy correction factor
Δ	Differential

θ	Angle, °
μ	Dynamic viscosity, kg/m-s
ν	Kinematic viscosity, m^2/s
ρ	Density, kg/m^3

Dimensionless groups

Re	Reynolds number

Subscripts

a	Air
b	Basin, buoyancy
bb	Ball bearing
bl	Blades
c	Casing
ch	Channel
ct	Cooling tower
d	Drag, drop, dynamic
db	Delugeable bundle
dp	Deflector plate
f	Frontal , fan
ft	Finned tube
h	Hub, hydraulic
he	Heat exchanger
m	Mechanical
i	Initial, inlet
p	Primary, pump

pr	Projected
rz	Rain-zone
s	Secondary, shroud, static
t	Total
tr	Trough
w	Water

List of abbreviations

ACC	Air cooled condenser
ANSI	American National Standards Institute
ASHRAE	American Society of Heating, Refrigerating and Air Conditioning Engineers
CFD	Computational fluid dynamics
DPM	Discrete phase model
FPS	Frames per second
HDWD	Hybrid (dry/wet) dephlegmator
HSDC	High speed digital camera
HVAC	Heating, ventilating, and air conditioning
LCD	Liquid-crystal display
NDWCT	Natural draft wet cooling tower
PJM	Pressure jump method
RPM	Revolutions per minute
VFD	Variable frequency drive

1. INTRODUCTION

1.1 Background

In South Africa more than 80 % of electricity is generated by means of conventional fossil fuelled thermal power plants. Thermal power plants reject more than half of the fuel input heat to the atmosphere by means of a cooling system. Cooling is needed to condense the steam leaving the turbine in order to pump it back to the boiler. Depending on the rated output, the climate and availability of adequate cooling water, these cooling systems can either be dry-cooled, wet-cooled or a combination referred to as hybrid or dry/wet cooling. Due to the shortage of adequate water resources, more modern power plants make use of direct dry-cooling to condense steam. Direct dry air-cooled condensers (ACC's) have finned tube heat exchanger bundles arranged in a number of parallel delta or A-frame streets. Each street consists of between four to six main condenser fan units and one secondary condenser or dephlegmator used to remove non-condensable gases from the primary condensers and to prevent sub-cooling and freezing of condensate. The performance of such a system is coupled to the dry-bulb temperature. Because dry-cooled air condensers are generally used in hot arid or semi-arid regions, the high ambient dry-bulb temperatures result in high steam turbine back pressures and thus lower overall power plant efficiency. The reduction in performance due to the high dry-bulb air temperature may result in a loss of income and higher flue gas emissions per unit of power generated.

Therefore, a need arises to increase the cooling performance during the peak demand or times of high ambient air temperatures. A patented hybrid (dry/wet) dephlegmator (HDWD) cooling system, developed at Stellenbosch University, can be deployed due to the lower water usage than wet systems and improved performance during periods of high ambient temperatures as shown by Heyns (2008), Owen (2013) and Anderson (2014). The advantage of a dry/wet cooling system is that the system has the cooling characteristics of both dry and wet cooling systems, however with a reduction in overall water consumption, depending on the duration of wet operating and the design. Investigations on the layout, design and performance of a HDWD are discussed by Heyns (2008), Owen (2013) and Anderson (2014). Figure 1.1 depicts an induced draft and a forced draft HDWD fan unit where typically one HDWD fan unit will be utilized per ACC street comprising between 4 to 6 fan units. During periods of high demand or high ambient air temperature, deluge water is sprayed over the tubes of the horizontal bundle to cool the tubes through heat and mass transfer, essentially operating as an evaporative cooler. The deluge water needs to be collected below the dephlegmator tubes and re-circulated.

The water collection system can either be made up from multiple parallel troughs or a water basin system. This study will focus on the design and layout of the water collection system for such a HDWD.

The water collection system needs to be effective in collecting the deluge water and draining it to a re-circulating pump, without excessively obstructing or blocking air flow to the delugeable tube bundles. This study investigates different water collection system concepts and determines their performance characteristics experimentally and by means of CFD.

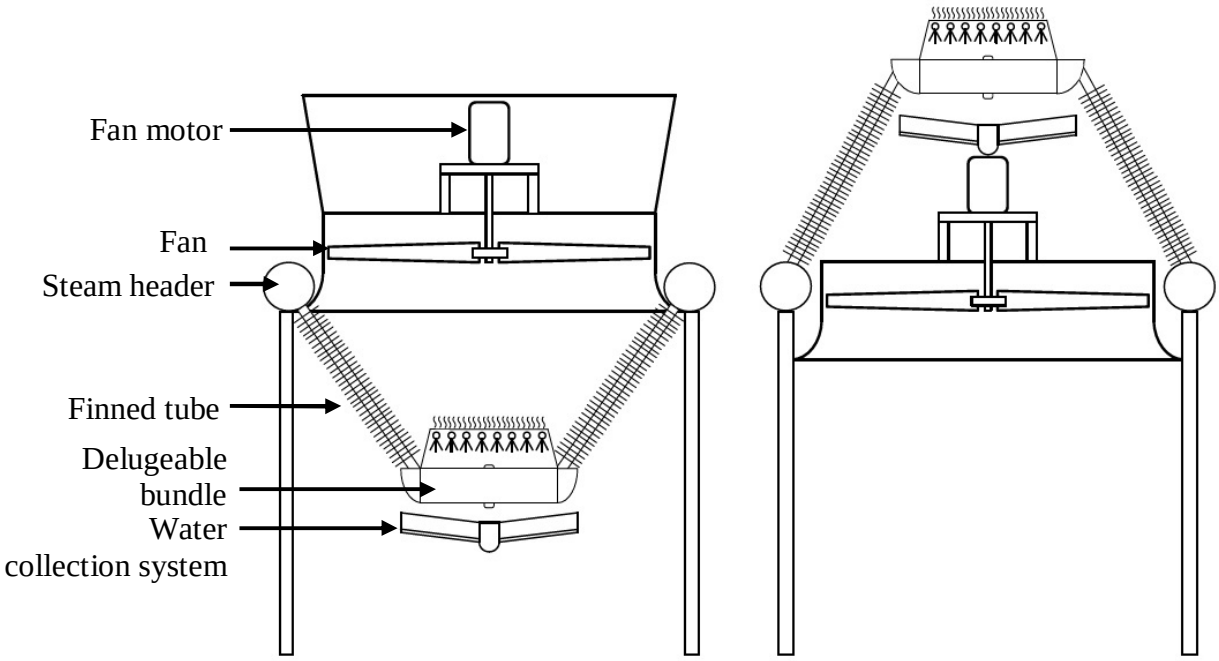

(a) Induced draft fan unit (b) Forced draft fan unit

Figure 1.1: Hybrid (dry/wet) dephlegmator

1.2 Water collection under the hybrid (dry/wet) dephlegmator

A water collection system separates water from an upward flowing air stream allowing air to pass through as freely as possible with minimal flow losses. Deluge water falling vertically down under the force of gravity is collected below the delugeable bundle. The water is drained away to a deluge water tank and fed back to the pump supplying the sprayers as shown in Figure 1.2 below.

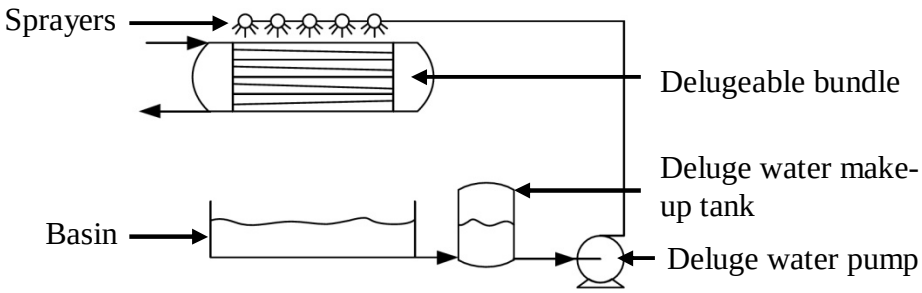

Figure 1.2: Deluge water cycle schematic with basin

A loss in deluge water through spilling or splashing is not permitted as water is a costly, scarce natural resource and due to pollutant chemicals added to the deluge water that could negatively impact the environment by ending up in the ground water. Deluge water collection can either be done by multiple water troughs or by means of a basin with one or more lateral air-inlets as shown Figure 1.3 (a) and (b) respectively. The water troughs allow the counter-flowing air to flow vertically through each water trough while the water is collected in channels. The water basin system collects the water like a pond under the delugeable bundle and the cross-counter flowing air enters laterally and is turned through 90 ° in the rain-zone. Pumping power is required to re-circulate the deluge water from the collection tank to the sprayers above the tube bundle.

The geometry and design of the above mentioned water collection systems result in different air-side flow patterns and pressure drop which needs to be minimised to reduce the fan power required. Fan and pumping power contribute to the parasitic power needed to operate a power station, reducing the net output capacity of a power station. The study develops correlations for loss coefficients for various trough and basin geometries which can be used for design purposes.

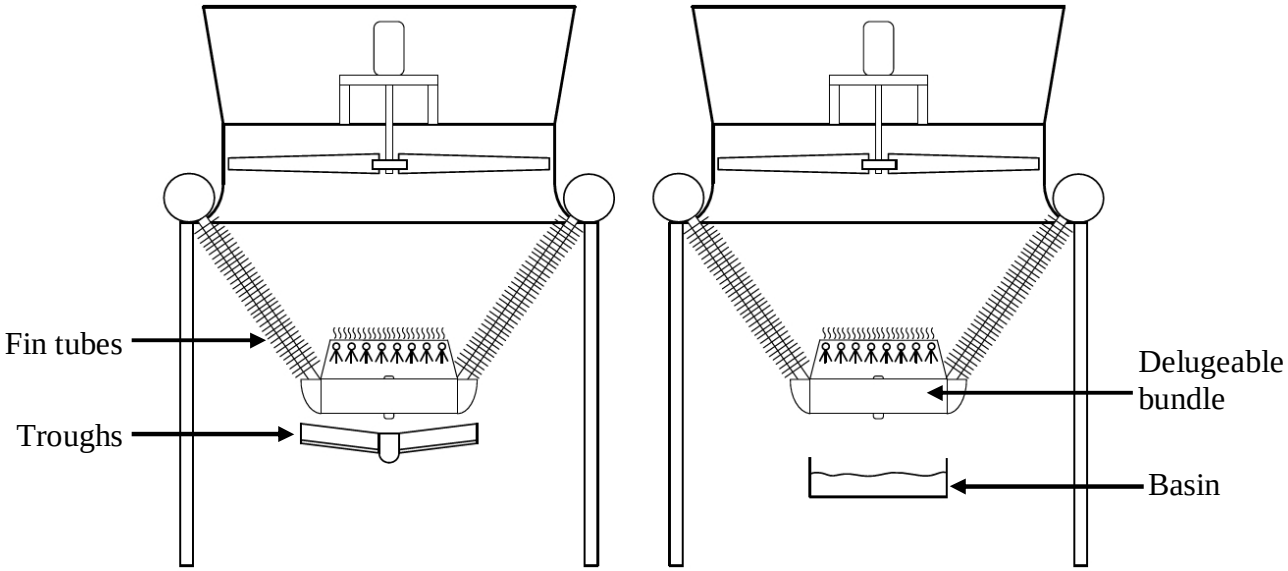

(a) Water trough collection system (b) Water basin collection system

Figure 1.3: An induced draft HDWD showing different water collection systems

1.3 Motivation

By reducing the air-side pressure drop of a water collection system the fan power required is reduced, which in turn increases the operating efficiency of a power plant. A well designed water collection system could also reduce the pump head required for the deluge water re-circulation pump and ensure that no water is lost due to spilling or splashing, reducing the pumping power consumption and operating cost of the cooling system. An effective water collection system may be

used in many industrial applications such as the refrigeration and air-condition industry, counter-flow fill test facilities, evaporative coolers and wet cooling towers. This thesis will focus on finding all the necessary information and parameters to design a water collection system which can be used below the second stage delugeable heat exchanger bundles of a HDWD to collect the deluge water.

1.4 Objectives

The objectives for the study are as follows:

a) Evaluate, test and improve existing water collecting trough system employed in the counter-flow fill test facility at Stellenbosch University.
b) Develop an effective water trough and basin design for collecting water underneath the dephlegmator tubes.
c) Investigate the air-side flow patterns for the proposed water trough and basin designs.
d) Develop empirical correlations for air-side loss coefficient for the water trough and basin system with various geometric and air inlet parameters using CFD, to be used by a design engineer.
e) Compare the performance of the two water collection system concepts.

1.5 Research methodology

The research methodology is as follows:

a) A stream of single water droplets is tested with a high speed digital camera at the point of impingement on a water trough similar to that of the troughs found in the Stellenbosch University counter-flow fill test facility.
b) A high speed digital camera is used to find a solution to increase the water collection effectiveness to 100 %.
c) The troughs in the counter-flow fill test facility are modified and tested. The results are used to validate a CFD model to further investigate the effect of the geometric parameters on the trough loss coefficients.
d) CFD models are developed for different basin system designs, which are validated by means of empirical data for cooling tower air inlets. The model is used to develop empirical relations for the inlet loss coefficient
e) The water trough system and the water basin system are compared with each other to find the best solution for each ACC layout and dephlegmator design.
f) Recommendations are made for the design of water collection system for industrial implementation.

1.6 Thesis outline

Chapter 1 gives background information on what water collection systems are and why there is a need for water collection systems. The layout for an induced draft and a forced draft HDWD is also shown. The motivation is provided for the research as well as the objectives and research method, and ultimately the thesis outline is presented.

The literature review is covered in Chapter 2. In this chapter the two concepts are explained, namely the water trough system and basin system. Previous designs are discussed as well possible areas to improve upon. The rectangular cooling tower inlet loss coefficient and the rain-zone loss coefficient correlations used in the analysis are also presented.

In Chapter 3 the water trough and flat plate drop impingement tests are presented. The tests are done with a high speed digital camera to observe the dripping, splashing, straddling and cutting patterns of water after impinging on a water trough and a flat plate inclined at a given angle to the horizontal. The results are used to improve the current water troughs found in the counter-flow fill test facility at Stellenbosch University by adding a deflector plate to the back of the water trough.

In Chapter 4, an experimental investigation is done on the water troughs in the counter-flow fill test facility before and after the addition of the deflector plate. The pressure drop and water collection effectiveness is tested in the counter-flow fill test facility. The results are used to validate a CFD model and to develop empirical relations for the loss coefficient. The water draining characteristics of the water trough are also investigated theoretically and experimentally.

Chapter 5 consists of a CFD investigation on different water basin designs. The CFD models used are validated with work done by Kröger (2004) on rectangular cooling tower inlets as well as work done by Kröger and De Villiers (1997) on loss coefficients of a rain-zone. The geometry of the water basin is explored. The basin is simulated for an induced draft (dry and wet), induced draft cascaded and a forced draft layout. The results are used to develop an empirical relation for the inlet loss coefficients.

A comparison between the water trough system and the water basin system is presented in Chapter 6. The compromise between the loss coefficient and the pumping head required is considered, to determine which parameter has the greatest effect on the energy used to operate the water collection system depending on how often the deluge water is used. Design recommendations are made with regards to the trough and basin geometry.

The equations used to determine the fluid properties needed for all calculations in the thesis are presented in Appendix A. Calibration details of the instrumentation

are presented in the Appendix B and C. Sample calculations of the water draining characteristics of the water trough are presented in Appendix D. The input data to the CFD models are presented in Appendix E. A sample calculation for the inlet loss coefficient of the water basin with an induced draft including a rain-zone and a 2.5 m lateral inlet is shown in Appendix F.

2. LITERATURE SURVEY

2.1 Water collection systems

As discussed before, water collection systems can be put in two categories, the trough system and the basin system. The air flowing from below the water troughs passes through between the troughs in counter-flow as shown in Figure 2.1 (a). For basin systems, the air has to flow around the water basin and enter laterally, as shown in Figure 2.1 (b).

For both systems, the water is collected and pumped back to the sprayers. The pump head required may be different depending on the design of the water collection system and the water level in the collection tank.

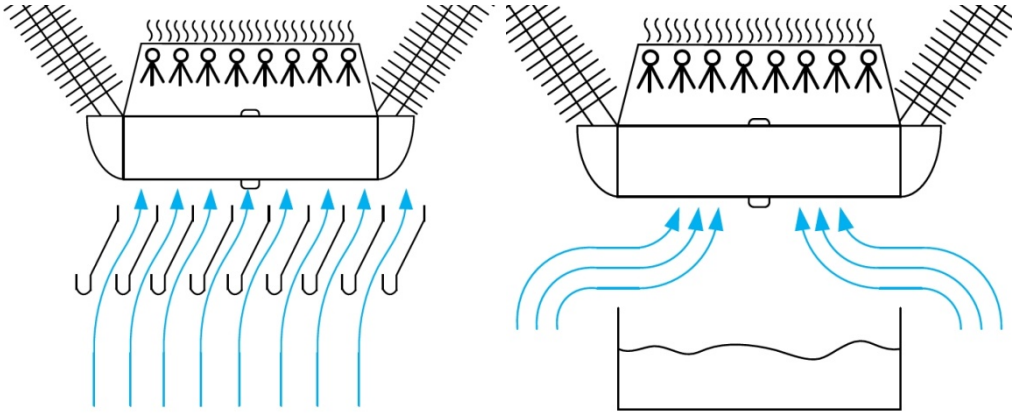

(a) Water troughs with vertical flow (b) Water basin with lateral inlet flow

Figure 2.1: Water collection system showing different air inlet flow patterns

Water collection systems have been used in evaporative coolers and wet cooling towers for many years. Previous designs like the patent filed by Lefevre (1985) are shown in Figure 2.2 (a) below for water troughs used in a natural draft wet-cooling tower (NDWCT). Multiple water troughs are situated parallel to each other and each top edge of the trough aligns with the lower edge of the adjacent trough. Air is in counter-flow to the water which is falling under the force of gravity. The troughs have primary and secondary collection channels to collect water adhering to both the front and back sides of the trough.

In Figure 2.2 (b), a patent by Korsell (1984) is shown for a water basin design below a rain-zone with air being sucked through lateral inlets. The water is collected and drained away from a central point to a pump.

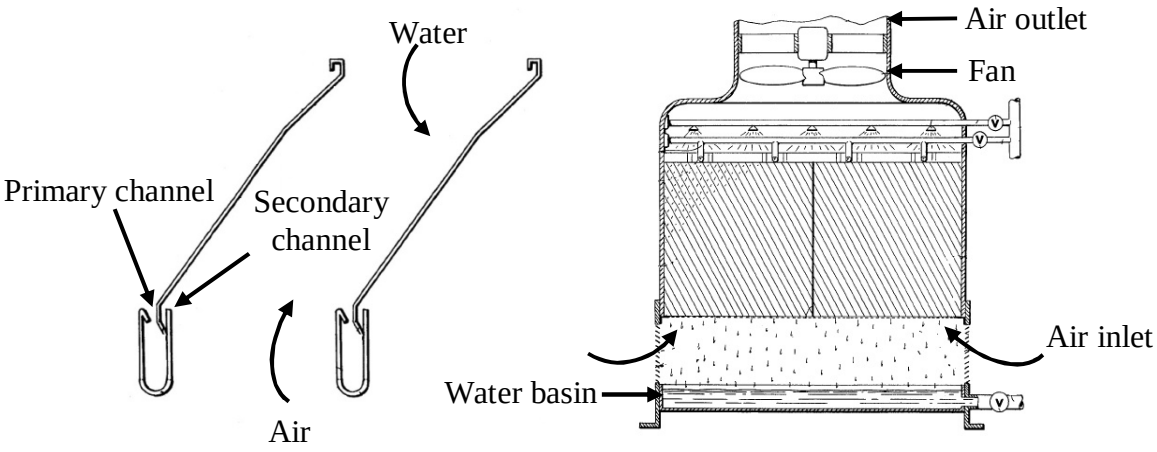

(a) Water trough system (Lefevre 1985) (b) Water basin system (Korsell 1984)

Figure 2.2: Patented water collection systems

A similar water trough concept as discussed above is applied in modern cooling towers, as seen in Figure 2.3 (a). Hamon Thermal Europe (2013) makes use of large water troughs in their NDWCT design. Seen in Figure 2.3 (b) Tower Tech (2011) has a more complex water trough design in their TTXL series of compact counter-flow cooling towers with secondary water channels, to collect water adhering to the outside of the water trough. The advantage of the water trough system is to reduce the water pumping head between the water collection tank and the sprayers and have a uniform air distribution throughout the rain-zone. Furthermore, forced draft fans have lower fan power consumption due to the lower air temperature resulting in lower volume flow rates.

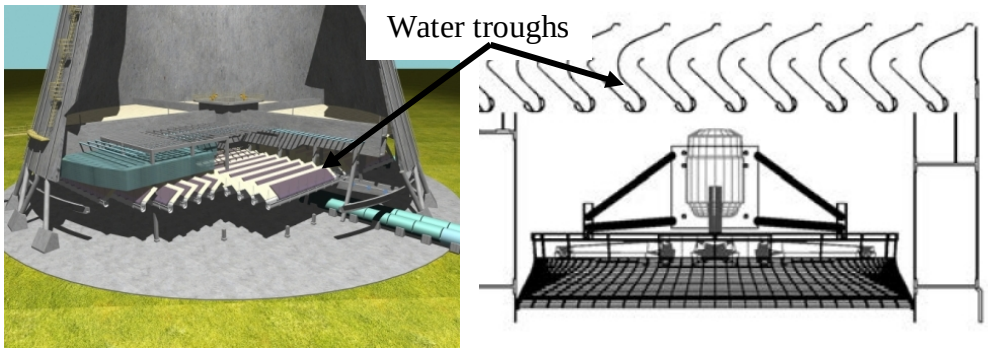

(a) Water troughs in a NDWCT (Hamon Thermal Europe 2013)

(b) Water troughs in a counter flow forced draft cooling tower (Tower Tech 2011)

Figure 2.3: Modern water collection troughs

Similarly the counter-flow fill test facility at Stellenbosch University makes use of two layers of water troughs rotated 90° to each other as seen in Figure 2.4. According to work done by Bertrand (2011) about 8 % of the water still passes

through the first layer of the collection system and about 4 % of the total volume of water still passes through the bottom layer. Thus the two layer trough design is ineffective and has a high air resistance.

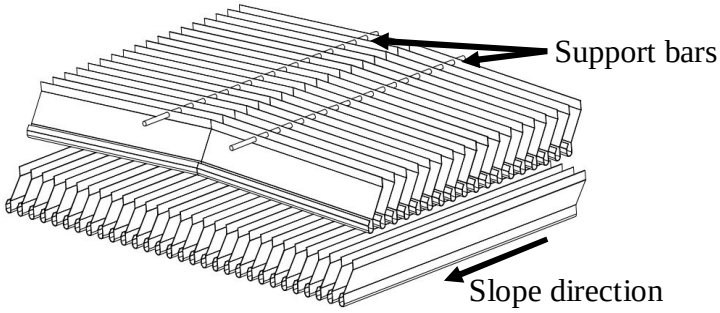

Figure 2.4: Two layers of water troughs from the counter-flow fill test facility at Stellenbosch University

As shown in Figure 2.5 below a simplified water basin design can be seen in a NDWCT. The round cooling towers make use of a lateral air inlet around the base of the tower with a pond below the rain-zone also used by Hamon Thermal Europe (2013).

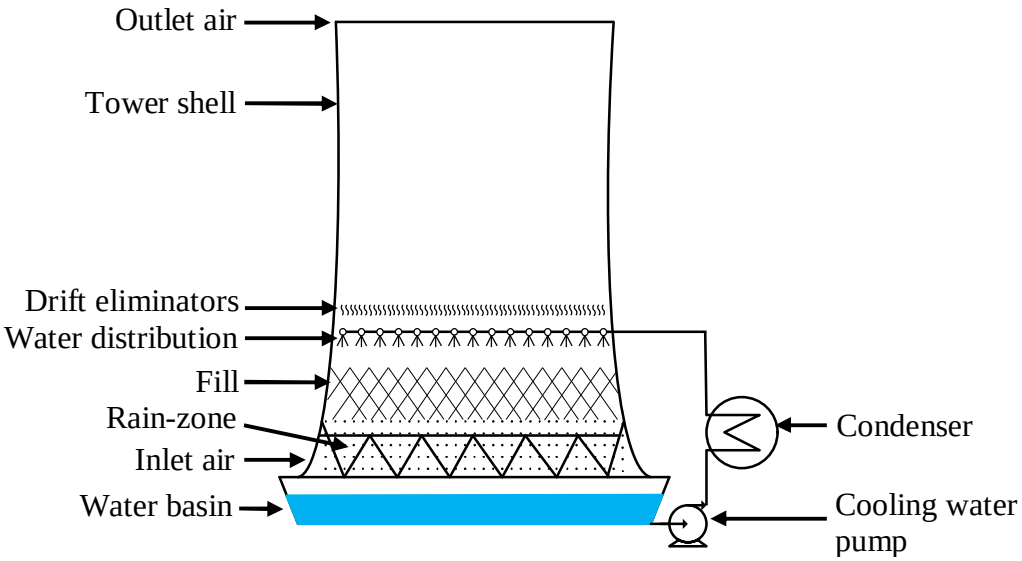

Figure 2.5: NDWCT water basin system

2.2 Air-side pressure drop

Air-side inlet losses are caused by a combination of flow separation and flow re-circulation which is caused by a reduction in flow area, forcing the air to accelerate. Bertrand (2011) developed the following empirical correlation (equation 2.1) for pressure drop over the dry water troughs, by testing the double layer water trough system in the fill test facility at Stellenbosch University.

The water trough design is used as a reference case and improvements are needed to reduce the pressure drop and increase the water collection effectiveness.

$$\Delta P_{tr} = 1.563 G_a{}^2, \mathrm{N/m^2} \tag{2.1}$$

Terblanche and Kröger (1994) developed an empirical correlation (defined by equation 2.2 below) from experiments done on a scale model for inlet loss coefficients for rectangular, mechanical induced draft cooling towers with a horizontal heat exchanger. The flow field is similar to the cross counter-flow field of the water basin with flow separation and re-circulation at the inlet. A CFD investigation done by Reuter (2010) on the inlet pressure drop of round natural draft wet-cooling towers with varying geometric parameters found that the tower diameter to inlet height ratio $\left(\frac{d_i}{H_i}\right)$ had the greatest effect on the inlet loss coefficient. He also found a good agreement between a scale model CFD, full scale CFD and the scale model experimental work done by Terblanche and Kröger (1994), verifying the accuracy. According to a comparison between the various turbulence models done by Reuter (2010), on inlet losses of round cooling towers, the *k-ε* Realizable turbulence model is best suited for typical inlet loss simulations. He stated that the *k-ε* Realizable turbulence model produced similar results to the experimental data of Terblanche and Kröger (1994) in the region of the tower shell and inlet, typically where flow separation takes place. It was also proven that in both the round and rectangular cooling tower the inlet loss coefficient can be reduced by adding rounded inlets or platforms.

$$K_{ct} = \left[1.1 + 1.1\left(\frac{W_i}{H_i}\right)^3 - 0.05\left(\frac{W_i}{H_i}\right) exp\left(\frac{W_i}{H_i}\right)\right] \times K_{he}{}^{\left[-0.29+0.079cos\left(\frac{W_i}{H_i}\right)+0.102sin\left(\frac{W_i}{H_i}\right)\right]} \tag{2.2}$$

where $0 \leq \frac{W_i}{H_i} \leq 5$ and $4 \leq K_{he} \leq 80$

With a HDWD, the loss coefficients of the first stage finned tube heat exchanger and the second stage bare tube bundles are needed. According to Kröger (2004) the following correlation may be used for the finned tube loss coefficient under isothermal flow conditions.

$$K_{ft} = 4177.08481 Ry^{-0.4392686} \tag{2.3}$$

The characteristics flow number R_y (equation 2.4 below) is determined with the minimum frontal area, the mean dynamic viscosity and the mean air temperature.

$$Ry = \frac{m_a}{\left(\frac{A_{fr}\mu_a n_{tb1}}{n_{tb2}}\right)}, \mathrm{m^{-1}} \tag{2.4}$$

and the pressure drop correlation for the bare tube bundle is shown below.

$$K_c = \frac{1}{Re_D^{0.16}}\left[1 + \frac{0.47}{(a-1)^{1.06}}\right] \quad (2.5)$$

where $a = P_t/d_o$

2.3 Droplet formation

The deluge water mass flow rate and drop sizes will influence the water collection system design and collection effectiveness. The water drop size distribution found in a NDWCT rain-zone is different when compared to an evaporative cooler due to the packing used. According to Kröger (2004), Terblanche (2008) and Reuter (2010), film and trickle fills produces drops with a Sauter mean diameter (defined by equation 2.6) ranging between 5 and 6 mm, while the drop size below a given splash fill varies between 3 and 4 mm.

$$d_{32} = \frac{\sum nd^3}{\sum nd^2} \quad (2.6)$$

The droplet formation below the second stage bare tube bundle of a HDWD is different from drops forming below fill due to the differences in geometry.

From research done by Killion and Garmimella (2003) on liquid films falling over horizontal tube banks, it was noted that the formation of droplets is linked to the Rayleigh instability phenomenon. After the film around the tube has thickened, the drops start to form below the tube. When a critical wave length is reached, due to an internal oscillation and the force of gravity, and the fluid has accumulated sufficiently, the surface tension cannot bind the fluid to the tube anymore and a droplet breaks off. Killion and Garmimella (2003) also stated that the drops falling from the preceding row of tubes have an effect on the drop detachment spacing from the bottom of the tube and initial velocity after detaching from the tubes.

Yung (1980) also investigated liquid when falling over horizontal tubes in evaporative coolers. According to Yung (1980), the primary drop detaches from the bottom of the tube, forming a narrow liquid column, resulting in 4 to 5 smaller secondary drops to form that follow the primary drop. Yung (1980) proposed the following equation for the primary and secondary drop sizes formed under a horizontal tube. According to Yung (1980) a droplet diameter distribution between 1 mm and 4 mm can be expected with a primary drop size of 8 mm.

$$d_p = 3\sqrt{\frac{\sigma}{\rho_w g}} \text{ , m} \quad (2.7)$$

with $0.24 < \frac{d_s}{d_p} < 0.46$

2.4 Pressure drop coefficients for rain-zone

Simulating a rain-zone numerically can be computationally expensive and time consuming and a one-dimensional empirical model based on a monodisperse drop diameter can accurately simplify the model. Kröger and De Villiers (1997) presented the following empirical relation for the loss coefficient of counter-flow rain zones, which was determined using a numerical Euler-Lagrangian model.

This correlation (equation 2.9) was verified by means of experimental tests in a counter-flow test section. According to CFD work done by Pierce (2007) on pure counter-flow rain zones, the loss coefficient correlation produced accurate results and can be used to validate a CFD model within the applicable range of application.

$$K_{rz} = a_v v_w \left\{ \begin{array}{c} 10645988 a_\mu \mu_a - 130.774 a_p \rho_a - 32.6634 + 888.6645 \\ \times [2.45287 (a_v v_i)^{-1.93315} + 0.34] \\ \times [4.03861 exp(-574.542 a_L d_d) + 0.493] \\ \times exp\left[\begin{array}{c} (65.26215 a_L d_d + 0.74827) \\ \times \ln[6.09836\, exp(0.0767 a_L H_i) - 6.1] \end{array} \right] \end{array} \right\} \quad (2.8)$$

where

$$a_\mu = 3.061 \times 10^{-6} \left[\frac{\rho_w^4 g^9}{\sigma_w} \right]^{0.25}$$

$$a_p = \frac{998}{\rho_w}$$

$$a_v = 73.298 \left[\frac{g^5 \sigma_w^3}{\rho_w^3} \right]^{0.25}$$

$$a_L = 6.122 \left[\frac{g \sigma_w}{\rho_w} \right]^{0.25} \quad (2.9)$$

with $0.927 \leq \rho_a \leq 1.289$ kg/m^3, $0.002 \leq d_d \leq 0.008$ m, $1 \leq v_i \leq 5$ m/s and $0.5 \leq H_i \leq 5.5$ m

Kröger and De Villiers (1997) also found a correlation (equation 2.10 below) for the loss coefficient through a cross-counterflow rain-zone as encountered in rectangular cooling towers with lateral air inlets and vertical outlet.

Since equation (2.10) is based on idealised potential air flow patterns, the effect of the rain zone on the air inlet loss coefficient of cooling towers with lateral inlets needs to be taken into account. Kröger and De Villiers (1997) presented the following correlation (equation 2.11) for a correction factor C_{rz}, that is used to correct the inlet loss coefficient in the presence of a rain zone.

$$K_{rz} =$$

$$a_v v_w \frac{3}{2}\left(\frac{H_i}{d_d}\right)\left\{\begin{array}{c} 0.219164 + 8278.8a_\mu\mu_a - 0.30487a_\rho\rho_a \\ +0.954153 \times [0.328467exp(135.7638a_L d_d) + 0.47] \\ \times [26.28482(a_L H_i)^{-2.95729} + 0.56] \\ \\ \times exp\left[\begin{array}{c} \ln[0.204814\, exp(0.133036a_L W_i) + 0.21] \\ \times [3.9186\, exp(-0.3a_L H_i)] \\ \times [0.31095\, \ln a_L d_d + 2.63745] \end{array}\right] \\ \\ \times [2.177546(a_v v_a)^{-1.46541} + 0.21] \end{array}\right\} \quad (2.10)$$

with $10 \leq T_w \leq 40$ °C, $0.927 \leq \rho_a \leq 1.289$ kg/m^3, $0.002 \leq d_d \leq 0.007$ m, $0.0075 \leq v_w \leq 0.003$ m/s, $2 \leq H_i \leq 8$ m, $1 \leq v_a \leq 5$ m/s and $2 \leq W_i \leq 20$ m

$$C_{rz} = 1 - G_w\left(0.123 - 12.1d_d - 272.26d_d + 5.04e^{-4} \times e^{\frac{0.466w_i}{H_i}}\right) \times (1 - 1.16e^{-3}e^{G_a}) \quad (2.11)$$

where $3 \leq W_i/H_i \leq 7.5$, $0.003 \leq d_d \leq 0.006$ m, $1 \leq G_w \leq 3$ kg/m^{2}s and $2 \leq G_a \leq 6$ kg/m^{2}s

2.5 Conclusion

The literature survey shows that assorted water collection systems in wet cooling towers and evaporative coolers are used in industry. Each trough system is unique in design, scale and geometry which have a varying effect on the flow characteristics. Inlet loss coefficients for water troughs are specific to each design and geometry. The literature does not provide significant information on water collection effectiveness and loss coefficients for the trough systems.

Research has been done on inlet pressure drop due to the reduction in area and flow re-circulation in rectangular mechanical draft cooling towers (RMDCT) and NDWCTs, but not specifically for a basin collection system as required for a HDWD. CFD models can be used for the investigation on the water basin inlets, similar to CFD work done by Reuter (2010) for the NDWCT. The empirical correlations for the loss coefficients of counter-flow rain-zones and inlet loss coefficient of rectangular cooling towers with lateral air inlets can be used to validate the CFD models respectively. Existing water collection systems discussed in the literature survey will be investigated and improved on to find the best suited design for the specific application of the HDWD. A reduction in inlet losses and effective water catchment can be achieved by making use of experiments and CFD. The available literature lacks research on the air-side pressure drop of the available water trough designs and proposed water basin inlets.

3. WATER TROUGH AND FLAT PLATE DROPLET IMPINGEMENT TESTING

3.1 Introduction

Tests are done on a single water collecting trough, identical in design to those in the counter-flow fill test facility at Stellenbosch University. According to tests done by Bertrand (2011) these water troughs do not collect all the water, therefore there is a need to investigate reasons for their ineffectiveness and to find a better solution. For the purposes of the water basin design, a stream of single water drops are tested on a flat plate at different plate inclinations and injection point heights to determine the splash drop trajectories after impinging on a flat plate inclined at different angles. Following is an experimental investigation to determine the dripping, splashing, straddling and cutting patterns after water dripping from a tube, impinges on different locations of a collecting trough with a specific design.

3.2 Experimental investigation of drop flow patterns after impinging on different parts of a single water collecting trough

3.2.1 Introduction

This section investigates the flow patterns after impingement of a single stream of water drops at different locations on a water collection trough simulating water drops falling from a heat exchanger tube onto water troughs. Figure 3.1 below is a schematic of a water trough which is a replica of the collection trough used in the counter-flow fill test facility at Stellenbosch University.

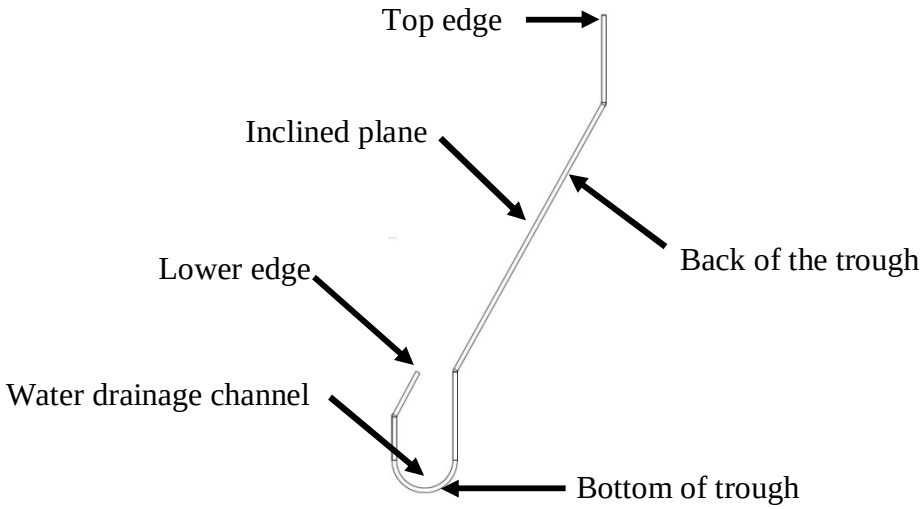

Figure 3.1: Water collection trough identical to those from the counter-flow test facility

The two layers of the collection troughs in the counter-flow fill test facility do not collect all the water as they were designed to do. The tests are conducted to find possible reason why water passes through and to investigate ways to improve their performance. A Point Grey high speed digital camera (HSDC) is used to capture still images of impinging water drops on the trough. These images are processed with ImageJ®, a Java based image processing and analysis software to determine the drop flow patterns.

Figure 3.2: Point Grey high speed digital camera

3.2.2 Experimental apparatus

With reference to Figure 3.3 below, a single water trough, identical to the water collection trough system, found in the counter-flow fill test facility at Stellenbosch University is positioned upright.

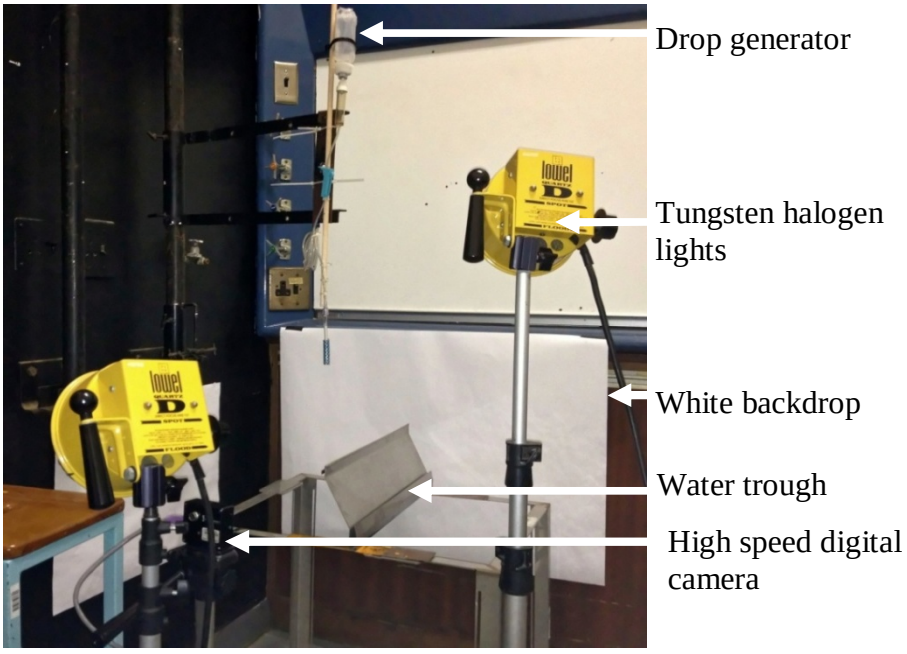

Figure 3.3: Water trough drop impingement test apparatus

The drop generator has a 4 mm outlet tube where the drop is formed. The drop generator's height above the top edge of the trough is set to 100, 200 and 300 mm respectively for the different tests. A high speed camera is fixed at one point and used to record the water drop impingement at 150 frames per second (fps) and a picture resolution of 640 x 480 pixels. A white backdrop is used to make the drops more visible and increase the contrasts. Two 1000 W tungsten halogen static lights are used for back lighting.

3.2.3 Experimental procedure

During the tests the high speed digital camera is fixed in one position and focused on the water trough, at the point of impingement. Each recording is done over 15 seconds at 150 fps producing 2250 still photos. Three areas of the water trough are focused on in isolation namely the top edge, the inclined plane and the lower edge of the water trough, as described in Figure 3.1. Water drops are allowed to impinge while the high speed camera is recording. Each frame is analyzed individually to plot the flow patterns.

3.2.4 Experimental apparatus calibration

The experimental apparatus is calibrated with a 5 mm by 5 mm black and white grid paper. The grid paper is recorded at the camera's focus point (point of impinging). The number of pixels in the *x* and *y* direction is measured and related to distance in mm.

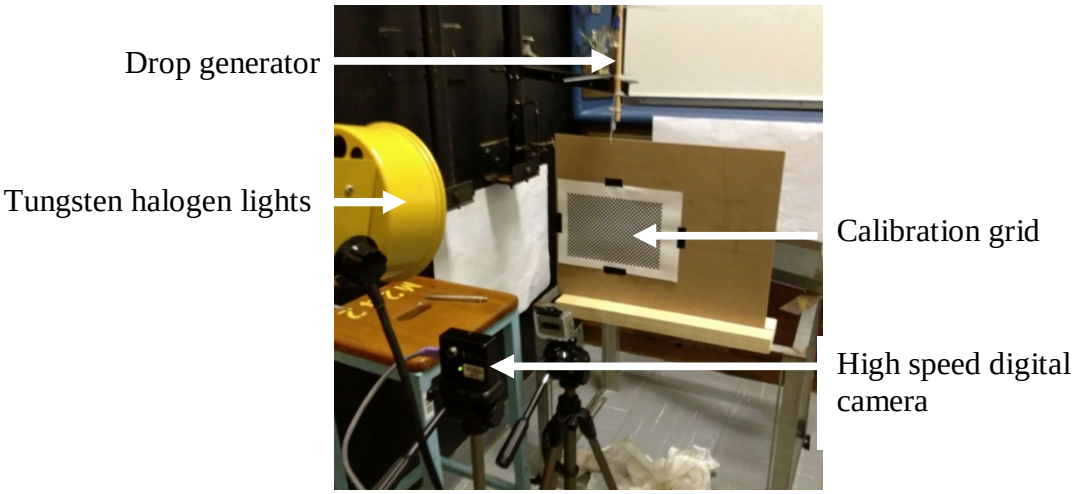

Figure 3.4: High speed camera calibration with grid paper

Similar to what Oosthuizen (1995) and Terblanche (2008) have done, the drop diameter is measured directly from the photo, with each pixel representing a length. The edges of the drops must be clearly visible for this technique. The drop's projected area is counted in terms of pixels and multiplied by the calibrated

value to find the area, from which the diameter is calculated by using equation (3.1).

$$d_d = \left(\frac{4A_{pr}}{\pi}\right)^{0.5}, \text{m} \qquad (3.1)$$

where A_{pr} is the projected area of the drop.

3.2.5 Experimental results

Following is a frame by frame analysis on how the water drops react after impinging on the different areas of the water trough. Firstly it is visually noted that the drop height range tested had no noticeable effect on the drop dripping, splashing, swinging and straddling patterns after impinging on the trough. Water falling on the inclined plane, simply falls into the water channel and is drained away not causing splashing or leaks.

Referring to Figure 3.5, a water drop impinging on the top edge of the vertical plate at the top of the trough is cut in two parts. One part falls onto the inclined plane and drains into the water channel. The other part adheres to the back of the trough and partially drips off, missing the neighbouring trough, causing water to pass through the collecting system.

Water adhering to the back of the trough, runs down and drips off at the bottom of the trough, which is problematic. This causes the water troughs to let water pass through. Preventing the water to adhere to the back of the trough and directing it to the neighbouring trough could potentially prevent water from bypassing the troughs.

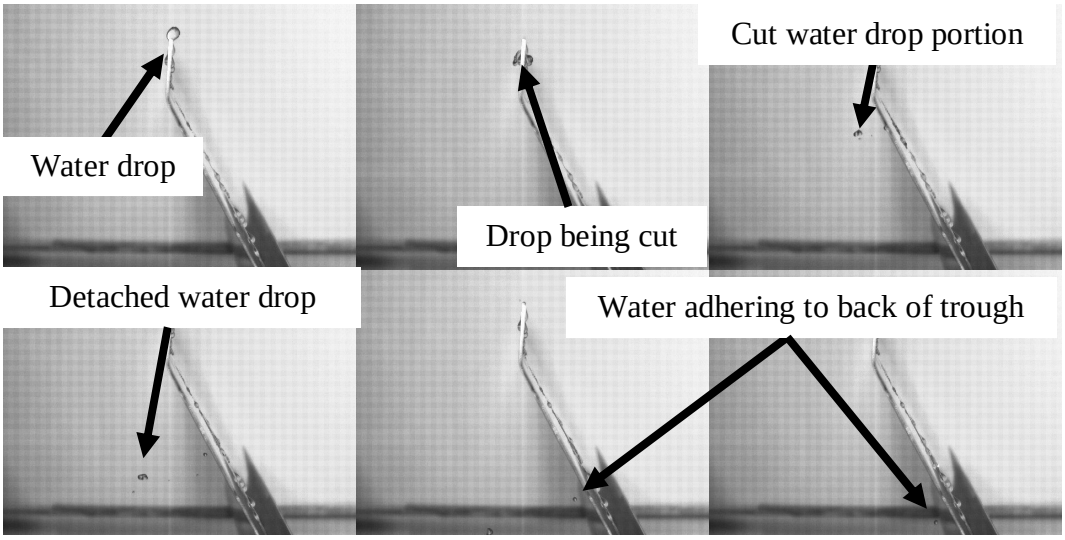

Figure 3.5: Drop impinging on top edge

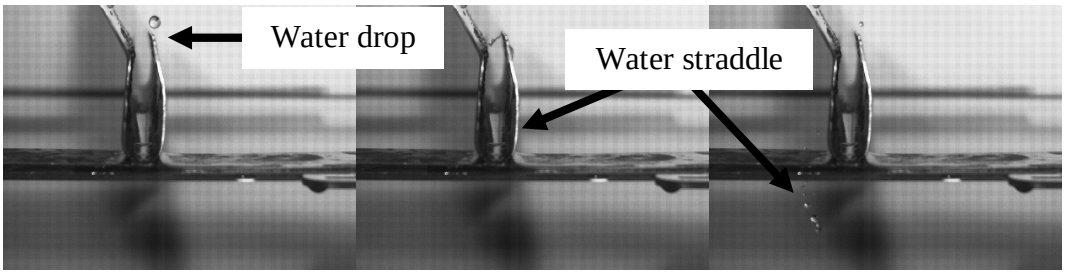

Figure 3.6: Drop impinging on the lower edge

With reference to Figure 3.6, a water drop impinging on the lower edge of the trough is cut in two parts. One part falls into the water channel and the other portion runs down the outside of the water channel, either dripping off at the bottom or swinging off. Water drops impinging on the lower edge of the troughs should be prevented. Redirecting water away from the lower edge prevents water from running down the trough and dripping off between the troughs.

The experimental results identify the shortcomings in the design of the water collection troughs in the counter-flow fill test facility at Stellenbosch University. By making a modification to the water troughs the water collection effectiveness can be increased.

3.2.6 Modifications made to the water trough

Three different deflector plate concepts are explored and fitted to the top edge of the water trough. A deflector plate can be easily retrofitted to the existing system, without removing the troughs from the counter-flow fill test section. The deflector plate is used to redirect the water impinging on the upper edge to the neighbouring water trough, preventing the water to adhere to the back of the trough and to prevent water from impinging on the lower edge. The addition of a deflector plate will however increase the air resistance.

In Figure 3.7 the three concepts are shown. The deflector plates are made from 0.9 mm stainless steel sheet metal. The lip is bent around the top edge of the water trough. Each deflector plate is tested in the same way the single water trough was tested. Deflector plate 1 is at an offset to deflect the drops away from the back of the trough. The lower edges of the deflector plate are sharpened to reduce the surface area for the water to attach itself and accumulate.

Deflector plate 2 has a saw tooth shaped cut along the length of the plate preventing water to accumulate at the lower edge of the plate.

Deflector plate 3 is a straight flat plate, guiding the drops to run vertically down and to fall into the adjacent water trough.

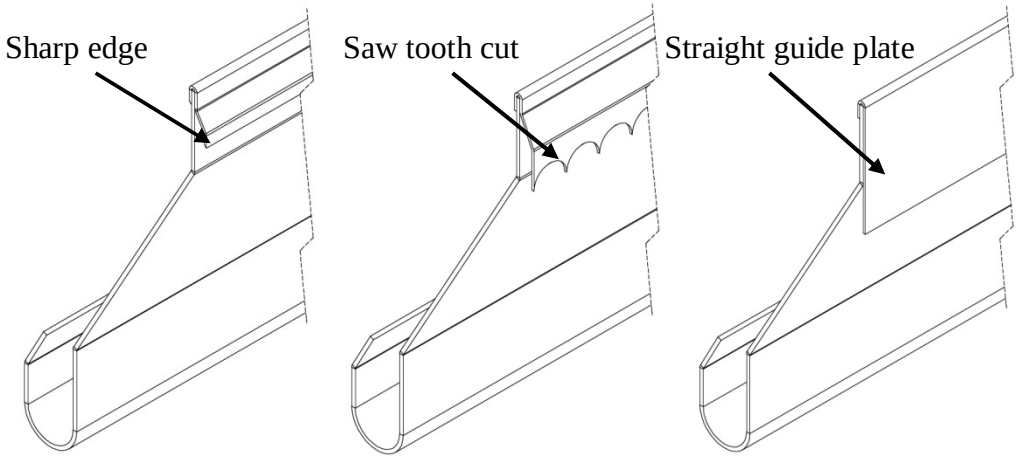

(a) Deflector plate 1 (b) Deflector plate 2 (c) Deflector plate 3

Figure 3.7: Sectional isometric view of the deflector plate designs

Following are the test results of the deflector plate recorded with the HSDC.

With reference to Figure 3.8 below, the water drops impinging on the deflector plate 1 (Figure 3.7 (a)) are cut and splash on the inclined surface causing the drop to break up. The water drop breaks up and adheres to the deflector plate. The drop swings off towards the back side of the trough due to the surface tension of the water. The drop misses the adjacent water trough and falls through, causing the drops to bypass.

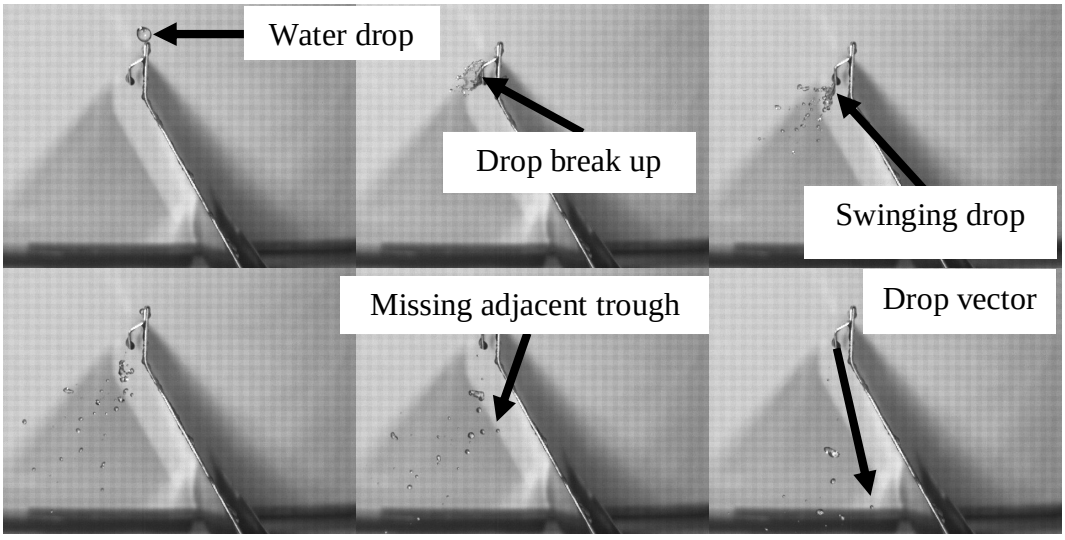

Figure 3.8: Drop impinging on top edge with deflector plate 1

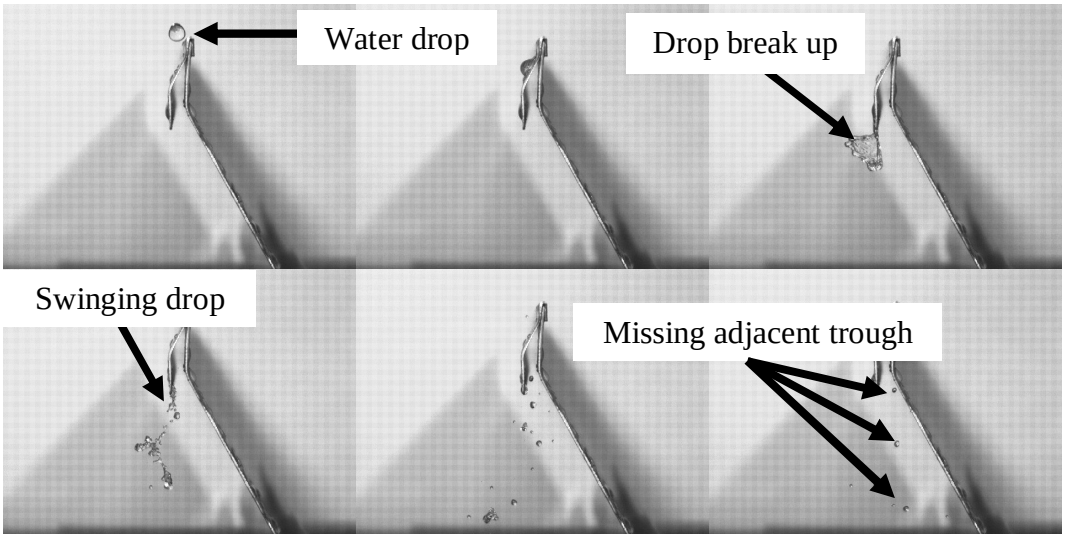

Figure 3.9: Drop impinging on top edge with deflector plate 2

In Figure 3.9 above, the deflector plate 2 can be seen (Figure 3.7 (b)) as a variation of deflector plate 1, but with a saw tooth edge based on work done by Terblanche (2011) on saw toothed profile slats. The saw tooth cut on the edge of the deflector plate prevents water from accumulating on the bottom edge of the plate and decreases the water drop diameter dripping off.

It is noted that the water drop swings around the deflector plate towards the back of the trough due to the combination of the offset of the deflector plate from the top edge and the surface tension of the liquid.

Despite the saw tooth edge, the results are similar to the deflector plate 1, with the swinging drop missing the adjacent trough and causing water to bypass the trough system.

Deflector plate 3 (Figure 3.7 (c)) is a straight deflector plate, 60 mm in height, with a 30 mm protruding edge fixed to the top of the water trough. In Figure 3.10 below it can be seen that the deflector plate guides the water drop vertically down in line with the adjacent trough without swinging the drop, due to the momentum of the drop. The water drop is guided onto the adjacent water trough and collected effectively.

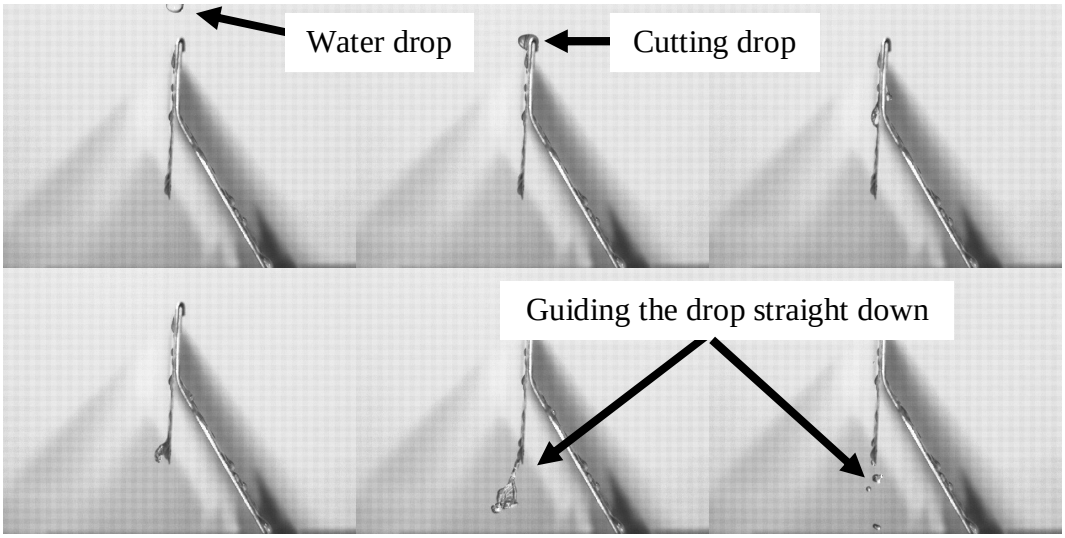

Figure 3.10: Drop impinging on top edge with deflector plate 3

3.2.7 Discussion of results

From the visual tests results presented on the single water trough, it can be concluded that the top edge and lower edge of the trough are identified as problematic. For both scenarios, the water drop is cut and the portion of the drop running down the outside of the trough drips off at the bottom of the trough, causing water to bypass. Adding a deflector plate to the trough may redirect the water away from running down the outside of the trough.

Deflector plate 1 and 2 are not successful in redirecting all of the water drops onto the adjacent water trough due to the surface tension of the water flinging the drops onto the back of the water trough. The water drop effectively falls through between the two troughs or impinges on the lower edge of the neighbouring trough.

Deflector plate 3 is successful in redirecting all of the water drops onto the adjacent water trough. The drop runs vertically down detaching from the base of the deflector plate due to the momentum and falls onto the adjacent water trough. Deflector plate 3 will increase the water collection effectiveness with an increase in the air-side pressure drop.

3.3 Flat plate water drop splash experiment

3.3.1 Introduction

Similar to the tests done above, a high speed camera is used to record a stream of single water drops dripping under the force of gravity on a flat plate while the angle of the plate, with respect to the horizontal plane, is varied along with the water injection point heights. The flat plate represents the inclined surface of the

trough as well as the wall of a basin system under the delugeable bundle of an HDWD. The forward and backwards splash patterns are recorded to find the best suited angle and drop height to minimize splashing. The information gathered is used in the design for an effective water collection basin system. A high speed digital camera is used to capture still images of impinging water drops on the trough at 150 fps. The images are processed frame by frame, with ImageJ®, a Java based image processing and analysis software to determine the drop splash patterns.

3.3.2 Experimental apparatus

With reference to Figure 3.11, a galvanized sheet is used as a flat impact plate. The plate angle is varied with a pivot bracket in the middle. The drop generator is a medical drip arrangement. The drop generator's height above the point of impingement can be set between 250 and 1750 mm. A Point Grey high speed digital camera records the water splash at 150 fps and a picture resolution of 640 x 480 pixels. The camera is facing the point of impingement, perpendicular to the drop and in-line with the plate. The droplet splash pattern can be recorded in the *x* and *y* direction only. A white backdrop is used to make the drops more visible and increase the contrasts. Two 1000 W tungsten halogen static lights are used for back lighting.

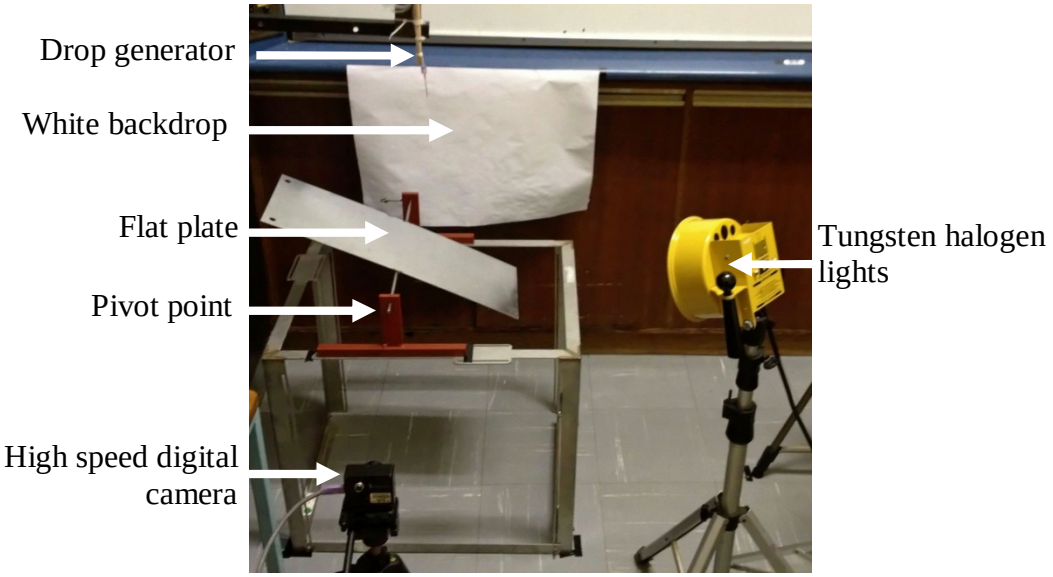

Figure 3.11: Flat plate drop impingement test apparatus

3.3.3 Experimental procedure

The high speed digital camera is fixed throughout testing and is focused on the point of impingement. The flat plate is dried off, and cleaned with acetone to get rid of impurities and any micro oil layers. The flat plate is left to be wetted by the drops for at least a minute before each test. Falling drops colliding with stagnant

drops on the plate influence the splashing. Similar to before, each recording is done over 15 seconds at 150 fps producing 2250 still photos. Between each test run the base plate angle is varied between 0° and 60° to the horizontal with 10° increments while the drop height is varied between 250 mm to 1750 mm with 250 mm increments for each angle. The flow rate of the drop generator is set to produce at least one drop per second. The drop generator produces a 4.5 mm diameter drop. ImageJ® software is used to trace the water droplet splash. Each drop has an *x* and *y* co-ordinate in terms of pixels. In Figure 3.12 below a screen shot shows how the drop splash trajectory is traced with the analysis software. The pixels are related to distance by multiplying with the calibrated value. The results are plotted on a two dimensional plane to find the splash distance and trajectory.

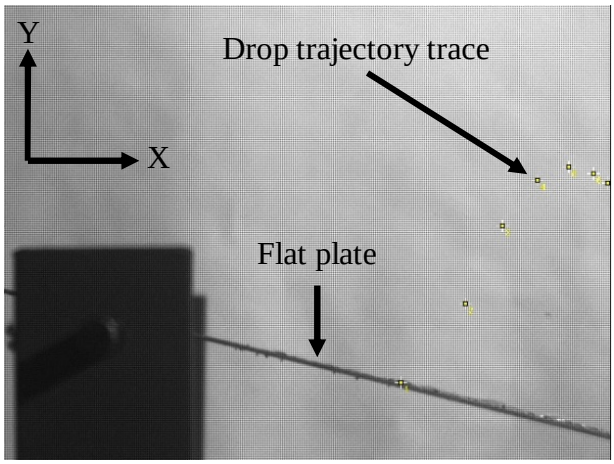

Figure 3.12: Drop trajectory measurements

3.3.4 Experimental apparatus calibration

Similar to the previous experiment the apparatus is calibrated with a 5 mm by 5 mm grid paper. The grid paper is recorded at the focus point (point of impinging). The amount of pixels in the *x* and *y* direction is measured and related to distance in mm. With each pixel representing a distance the water drop diameter and velocity are measured. A 4.5 mm drop is used for calibrating the drop impinging velocity. The droplet velocity before the point of impingement is measured with the high speed camera and the grid paper. The measured velocity is compared to the theoretical velocity which is calculated from the measured drop diameter. The measurements are taken over two frames and three frames to ensure accuracy. The droplet velocity is calculated with the Newton drag method. See Appendix B for the calibration details, sample calculation and the verification done with steel ball bearings.

3.3.5 Experimental results

The following are the results for the splash trajectory plots for various droplet free falling heights and flat plate angles plotted from the high speed photos.

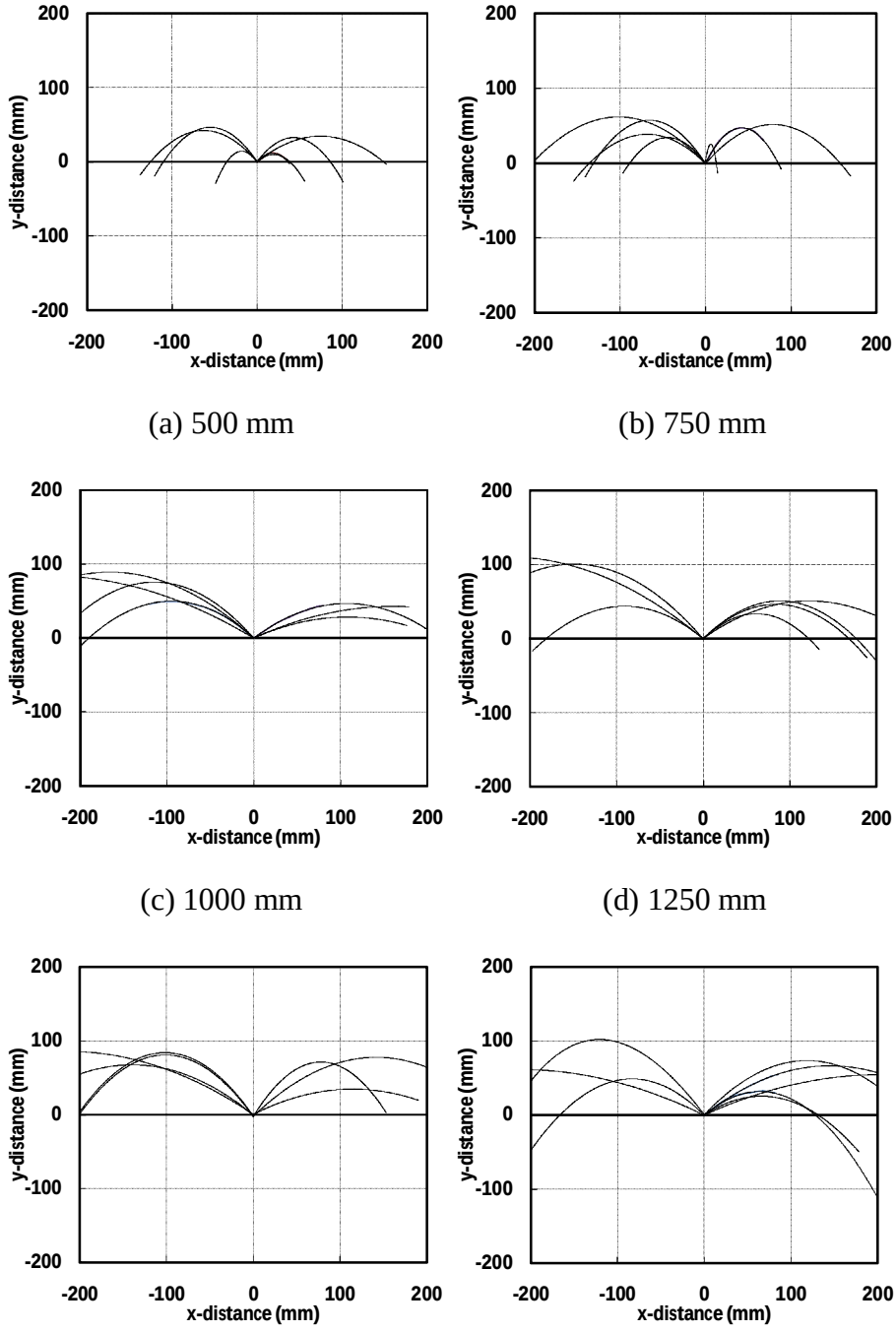

(a) 500 mm (b) 750 mm

(c) 1000 mm (d) 1250 mm

(e) 1500 mm (f) 1750 mm

Figure 3.13: Splash trajectories with a plate angle of 0° to the horizontal for different falling distances before impingement

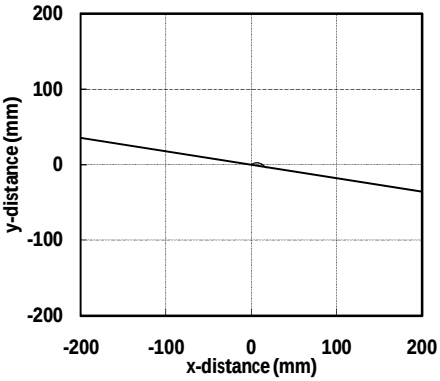

(a) 250 mm

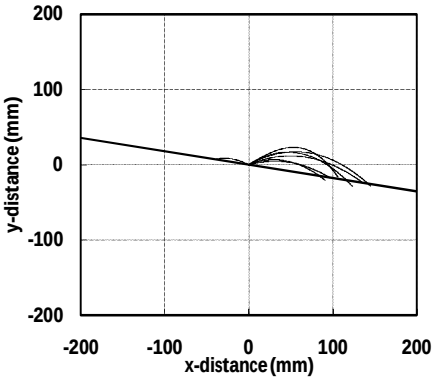

(b) 500 mm

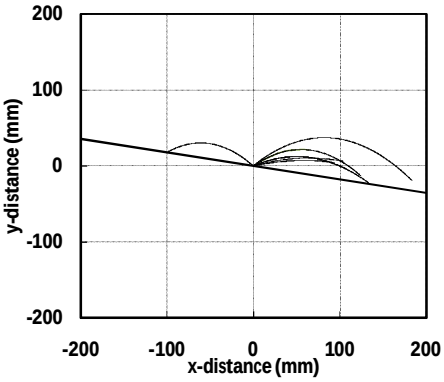

(c) 750 mm

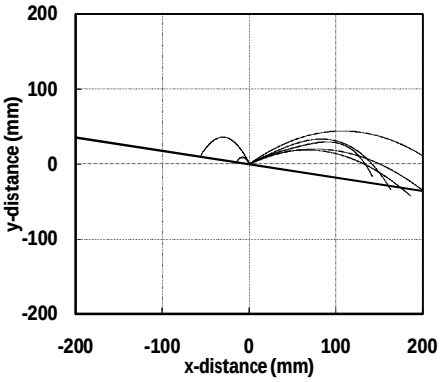

(d) 1000 mm

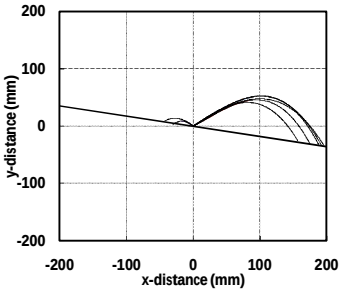

(e) 1250 mm

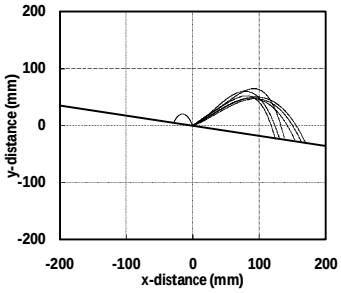

(f) 1500 mm

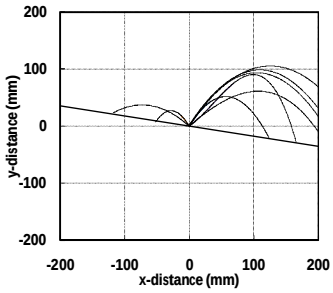

(g) 1750 mm

Figure 3.14: Splash trajectories with a plate angle of 10° to the horizontal for different falling distances before impingement

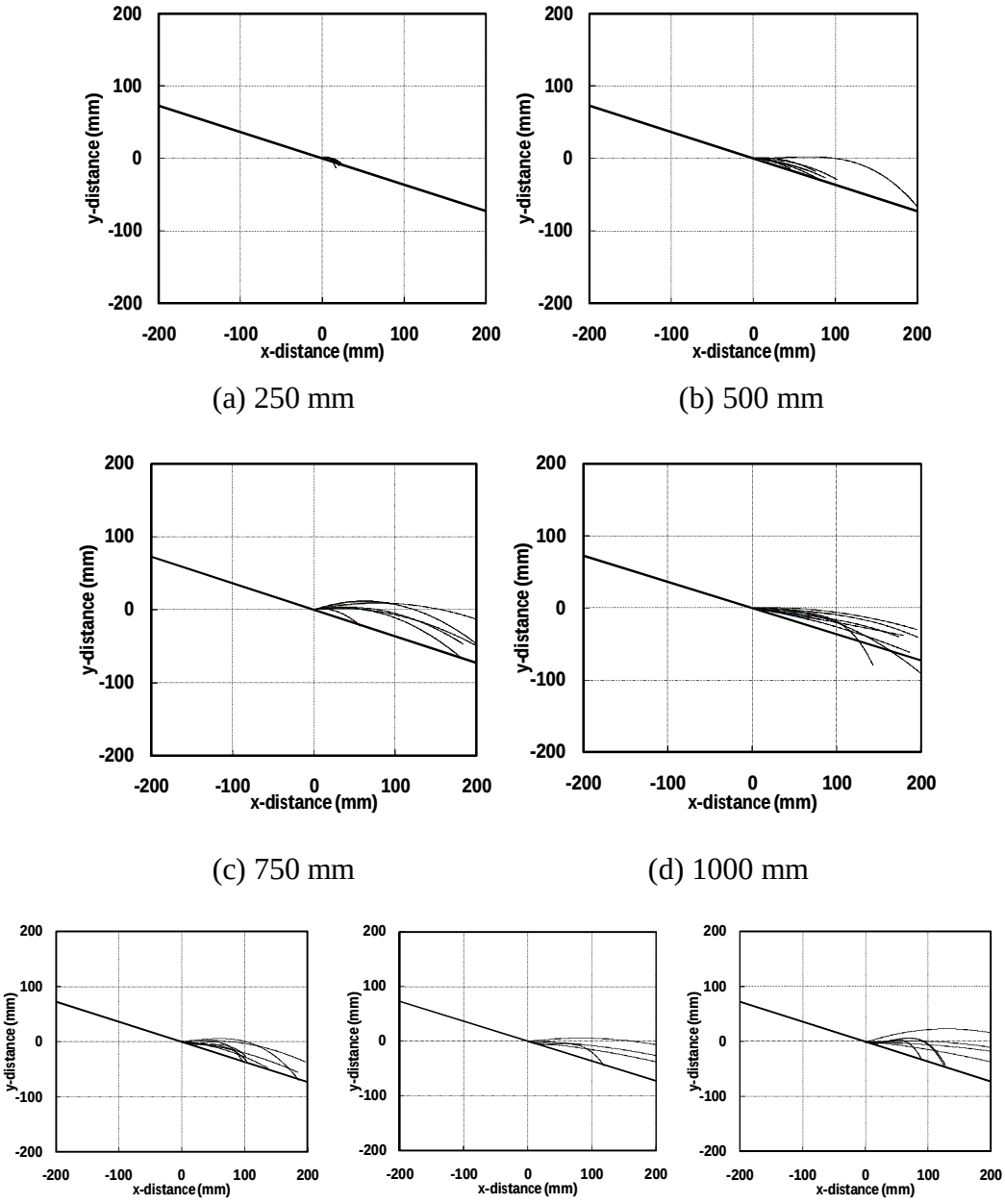

(a) 250 mm (b) 500 mm

(c) 750 mm (d) 1000 mm

(e) 1250 mm (f) 1500 mm (g) 1750 mm

Figure 3.15: Splash trajectories with a plate angle of 20° to the horizontal for different falling distances before impingement

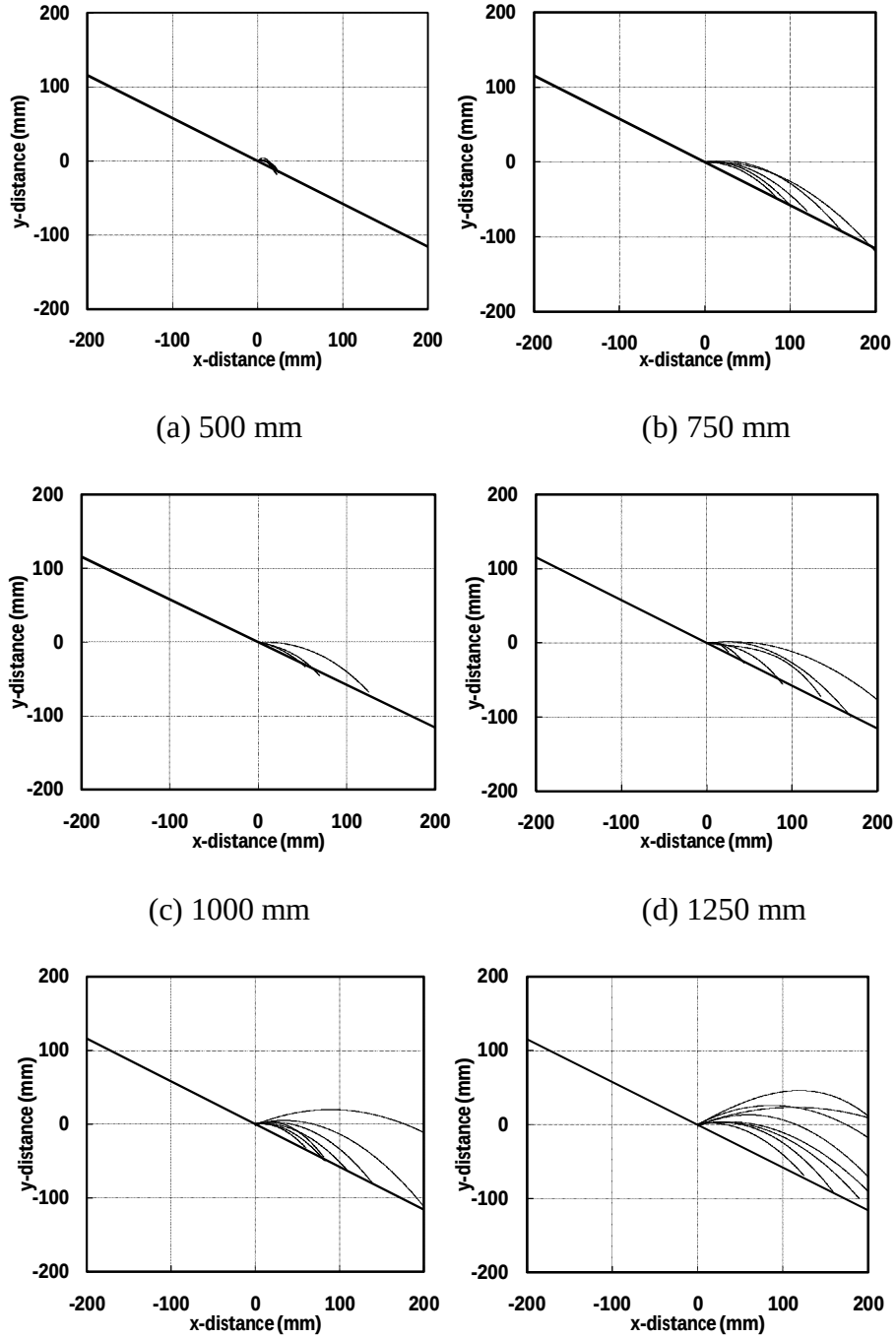

(a) 500 mm (b) 750 mm

(c) 1000 mm (d) 1250 mm

(e) 1500 mm (f) 1750 mm

Figure 3.16: Splash trajectories with a plate angle of 30° to the horizontal for different falling distances before impingement

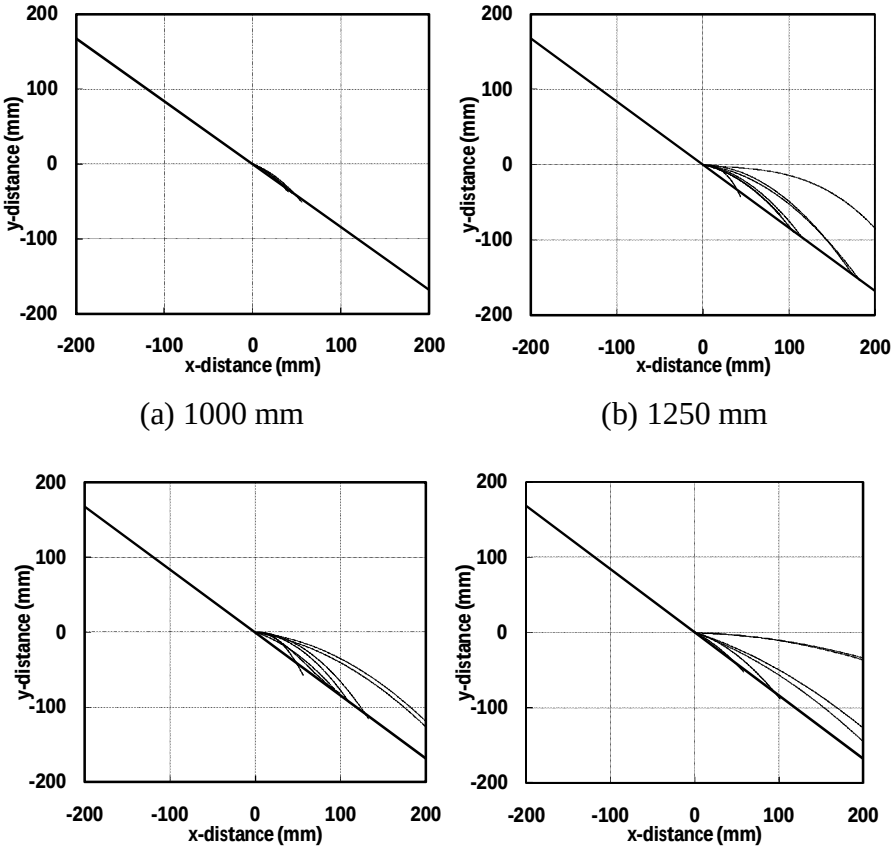

(a) 1000 mm (b) 1250 mm

(c) 1500 mm (d) 1750 mm

Figure 3.17: Splash trajectories with a plate angle of 40° to the horizontal for different falling distances before impingement

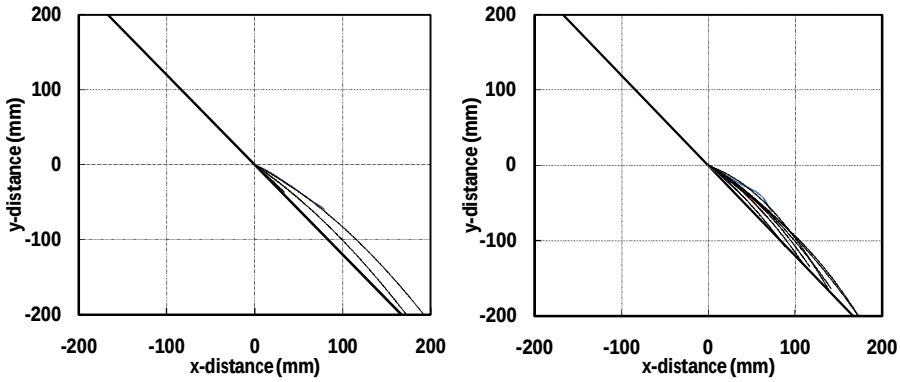

(a) 1000 mm (b) 1250 mm

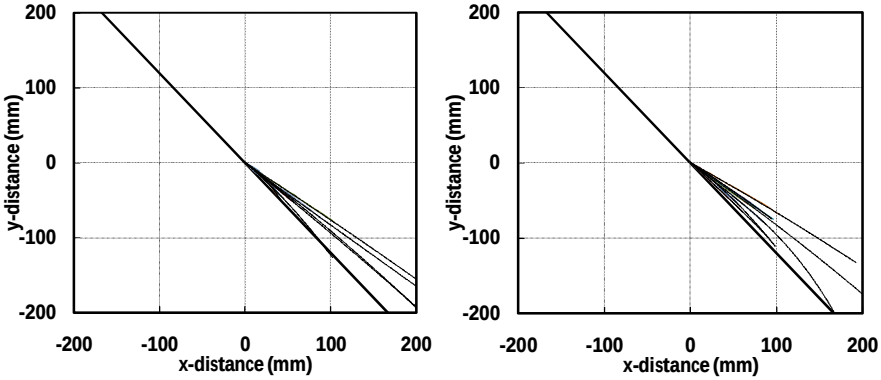

(c) 1500 mm (d) 1750 mm

Figure 3.18: Splash trajectories with a plate angle of 50° to the horizontal for different falling distances before impingement

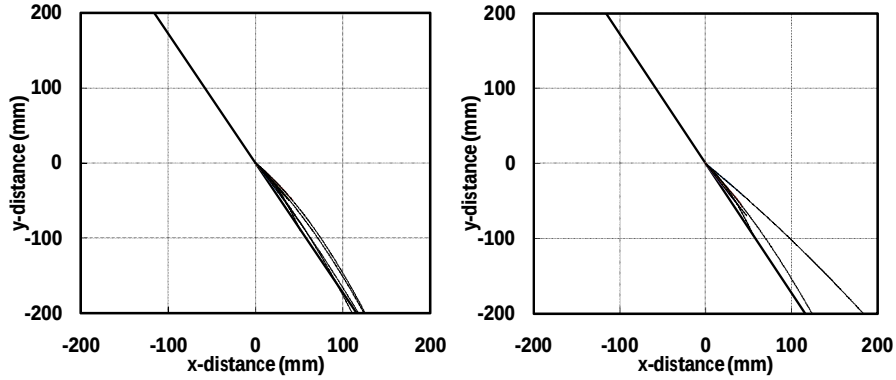

(a) 1500 mm (b) 1750 mm

Figure 3.19: Splash trajectories with a plate angle of 60° to the horizontal for different falling distances before impingement

3.3.6 Discussion of results

As expected, the higher the injection point, the greater the splashing distance, due to the increase in the drop velocity. From a plate inclination angle of 20° and greater no backwards splashing is noted in the negative x-direction for all drop heights.

With a plate angle of 60° there was no splashing seen between the heights of 250 mm and 1250 mm and very low splashing from 1500 mm onwards. The information can be used to determine the angle of the inclined surface of the water trough and the angle of a basin wall to minimize splashing.

4. INVESTIGATION AND MODIFICATION OF THE WATER TROUGH SYSTEM USED IN AN EXISTING COUNTER-FLOW FILL TEST SECTION

4.1 Introduction

This chapter examines the existing water collecting trough system in the Stellenbosch University counter-flow fill test facility as well as the modifications required to improve the water collecting effectiveness of the troughs. The counter-flow fill test facility is used to conduct the trough tests. Water collection performance and air-side pressure drop tests are conducted on the water troughs in the counter-flow fill test facility. Both tests are repeated after a 30 mm deflector plate is added to the top edge of the water trough as discussed in Chapter 3. The pressure drop tests results are used to validate a two dimensional CFD model. The CFD model is used to explore the varying geometry and the effect it has on the trough loss coefficient (K_{tr}).

4.2 Experimental apparatus

The tests are conducted in the counter-flow test facility which comprises of two sections namely, the horizontal section (Figure 4.1) which has a 2 x 2 m cross-section and a vertical section (Figure 4.2) which has a 1.5 x 1.5 m cross-section. The troughs are tested in the vertical section. With reference to Figure 4.1, air is drawn in through the horizontal 2 x 2 m inlet section (1). The air entering the horizontal section flows through a cross-flow fill test section (2), mixing vanes (3), settling screen (4) and three air flow nozzles (5) measuring the air flow rate. The mixing vanes ensure a uniform air temperature and the settling screen breaks up any large vortices which have formed for accurate flow measurements. The air is drawn in by a centrifugal fan (6) driven by a 50 kW electric motor which is controlled by a variable-frequency drive (VFD). Downstream from the centrifugal fan the air passes a series of 90° turning guide vanes (7) to enter the 1.5 x 1.5 m vertical section.

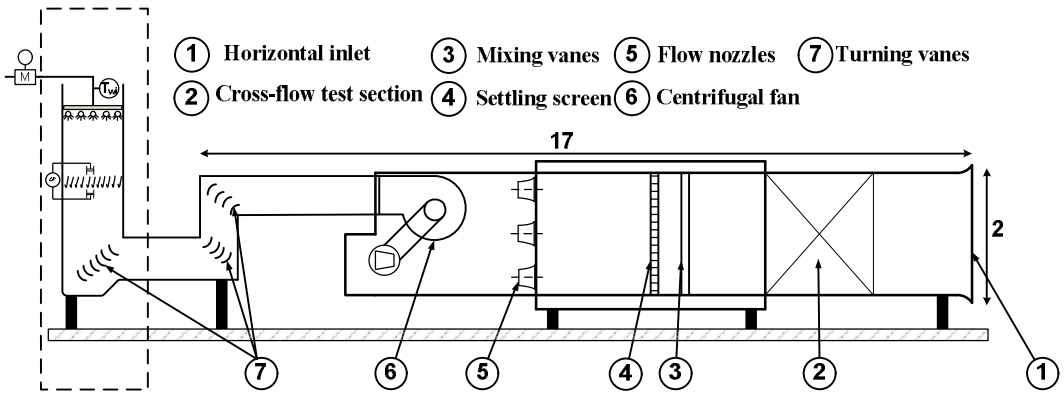

Figure 4.1: Schematic of counter-flow fill test facility at Stellenbosch University

Four pairs of thermocouples are located in the horizontal section to measure the dry and wet-bulb temperatures. Air is drawn over the wetted wicks by an aspiration fan as prescribed by ANSI (1986).

The nozzle plate has an option of 5 nozzles which can be used depending on the desired Reynolds number required for testing. For the purpose of testing the water troughs only the top three nozzles are opened. Air is drawn through the nozzle plates while the pressure drop is measured over the ASHRAE 51-75 elliptical nozzles. The measured pressure drop is used to calculate the air mass flow rate (m_{avm}).

After the horizontal section the air enters the 1.5 x 1.5 m vertical section of the test facility as seen in Figure 4.2 below. Two layers of water collecting troughs (8) are situated in the vertical section with the two layers rotated 90° to each other as discussed in Chapter 2. Differential pressure taps (9) are located below and above the water troughs to measure the pressure difference over the troughs with two Endress and Hauser differential pressure transducer. The cooling water is supplied by a spray frame (10) which can be adjusted in height above the water troughs. Drift eliminators (11) are situated on top of the spray frame. The inlet water temperature is measured with thermocouples (12) in the spray frame supply pipe. A magnetic flow meter (13) is used to measure the water flow rate.

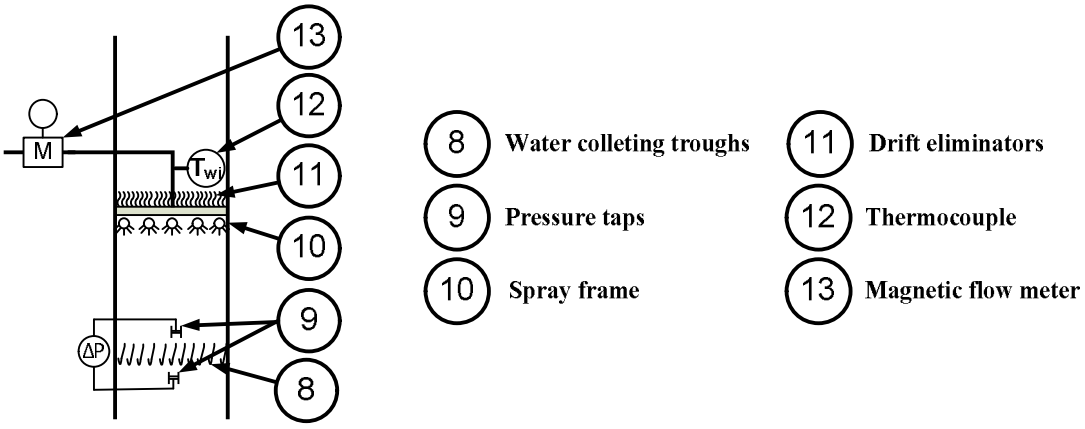

Figure 4.2: Schematic of the vertical section of the counter-flow fill test facility

The spray frame is 1.48 x 1.48 m in size which delivers a uniform water distribution. The spray frame comprises of 57 pipes arranged in two rows with a 50 mm triangular pitch. The sprayer pipes have a tube-in-tube design as shown in Figure 4.3.

The inner tubes have 2 mm holes along the top of the tube and the spray tubes have 1 mm holes along the bottom. Each hole is 10 mm apart as shown in Figure 4.3. The angle (α) between the sprayer holes are 30° for the bottom row and 20° for the top row. The sprayer holes are set at this angle to ensure a horizontal

velocity component to prevent the water from free falling in the vertical direction. This is important when testing fills with open vertical channels.

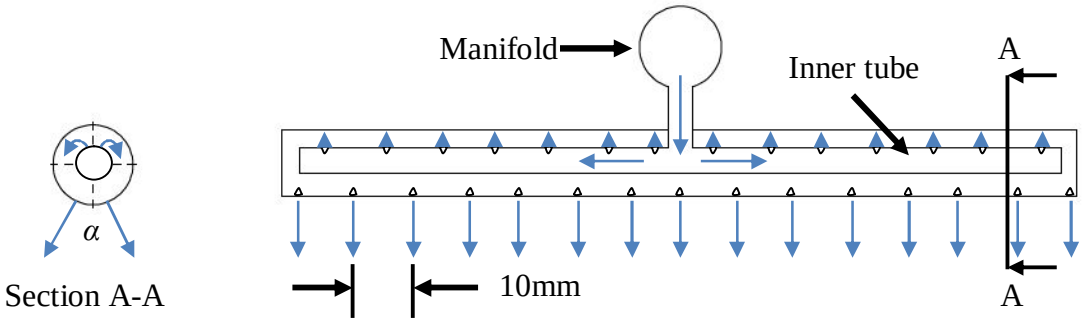

Figure 4.3: Spray frame schematic

The water troughs are tested twice. Firstly the original water troughs are tested as done by Bertrand (2011). This is done to compare the results to the modified trough with a 30 mm deflector plate, as discussed in Chapter 3, to increase the water collection effectiveness. The bottom layer of troughs is inaccessible and cannot be modified. The dimensions of the original and modified water trough are shown in Figure 4.4 below. Each row of water troughs are 50 mm apart. As indicated by the dotted line in Figure 4.4, the top edge of the water trough lines up with the inner edge of the adjacent water channel.

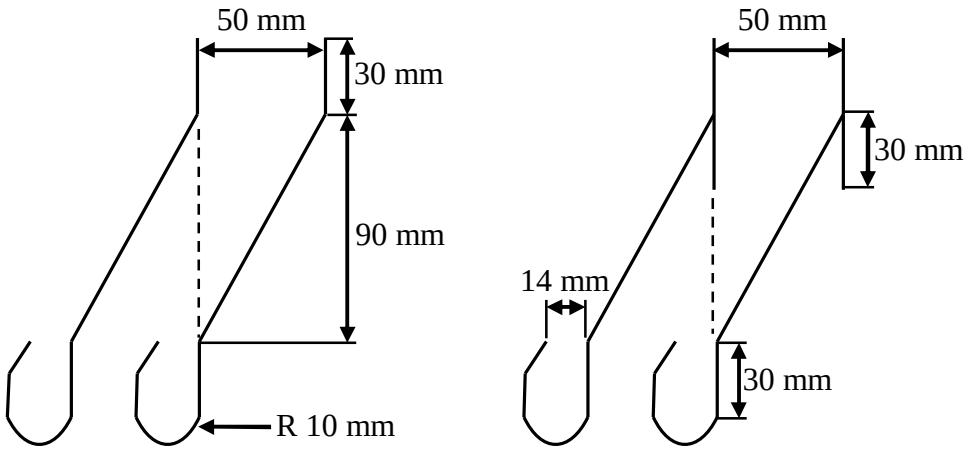

(a) Original water trough (b) Modified water trough

Figure 4.4: Water trough design with dimensions

4.3 Measurements techniques and procedure

The water supplied to the spray frame is measured with an electromagnetic flow meter. The flow rate is varied by adjusting a gate valve located on the supply pipe. There are five straight pipe diameters upstream of the flow meter and two straight pipe diameters downstream as specified by the manufacture to eliminate

disturbance in the flow. Details of calibration the electromagnetic flow meter are shown in Appendix C. Water collected by the top and bottom layers troughs are collected separately in calibrated tanks, to find the volume of water collected by each layer.

With reference to Figure 4.5 the Endress and Hauser differential pressure transducer (A) shown is used to measure the pressure drop over the elliptical nozzles. Differential pressure transducer (B) and (C) are used to measure the pressure drop over the water collecting troughs. The differential pressure transducers have working ranges of 10 000 (A), 1000 (B) and 2500 (C) N/m^2 respectively. Calibration details are shown in Appendix C.

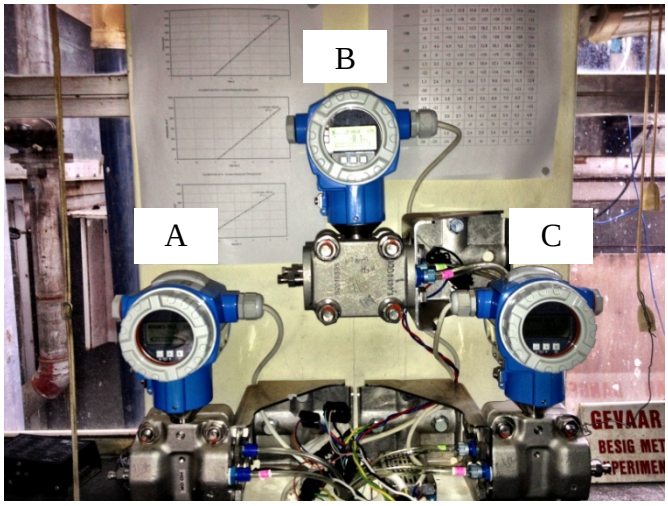

Figure 4.5: Endress and Hauser differential pressure transducers

The air-side pressure drop over the water collecting troughs is measured with four H-taps per differential pressure transducer. Two are located above the water troughs and two below the water troughs. One of the four H-taps is shown in Figure 4.6. The H-taps are fixed to a frame which can be moved around on top of the water collecting troughs.

The pressure taps are connected to the differential pressure transducer with 8 mm clear tube. Clear tubes are used to make condensation visible to prevent blocking. An average reading is taken from the two differential pressure transducers.

The pressure drop over the water troughs is used to determine the trough loss coefficient (K_{tr}) as defined in equation (4.1) below, where the velocity used is the free stream velocity, also measured with the elliptical nozzles.

$$\Delta p = K_{tr} \frac{1}{2} \rho_a v^2, \mathrm{N/m^2} \qquad (4.1)$$

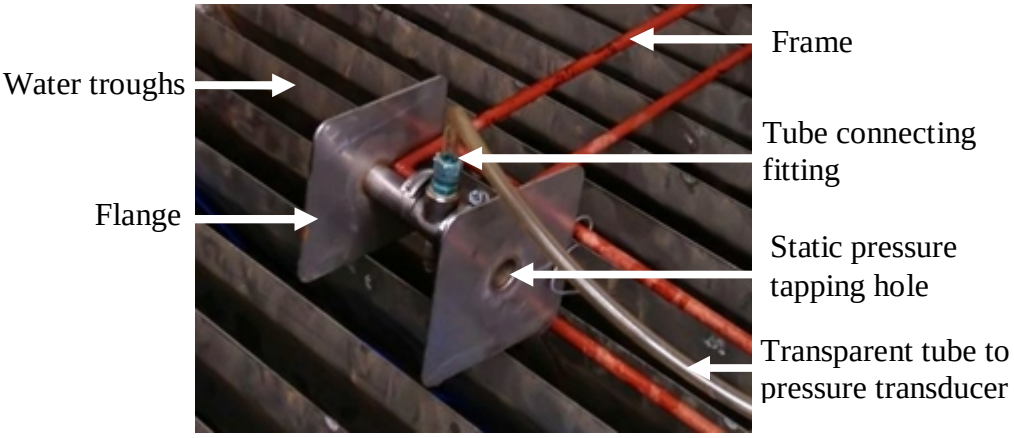

Figure 4.6: H-tap for static pressure measurements

4.3.1 Water collection performance tests procedure

The water collection effectiveness of the troughs is tested on the original and the modified troughs. As seen in Figure 4.7 below two calibrated tanks are used to collect the water from the two layers of troughs separately.

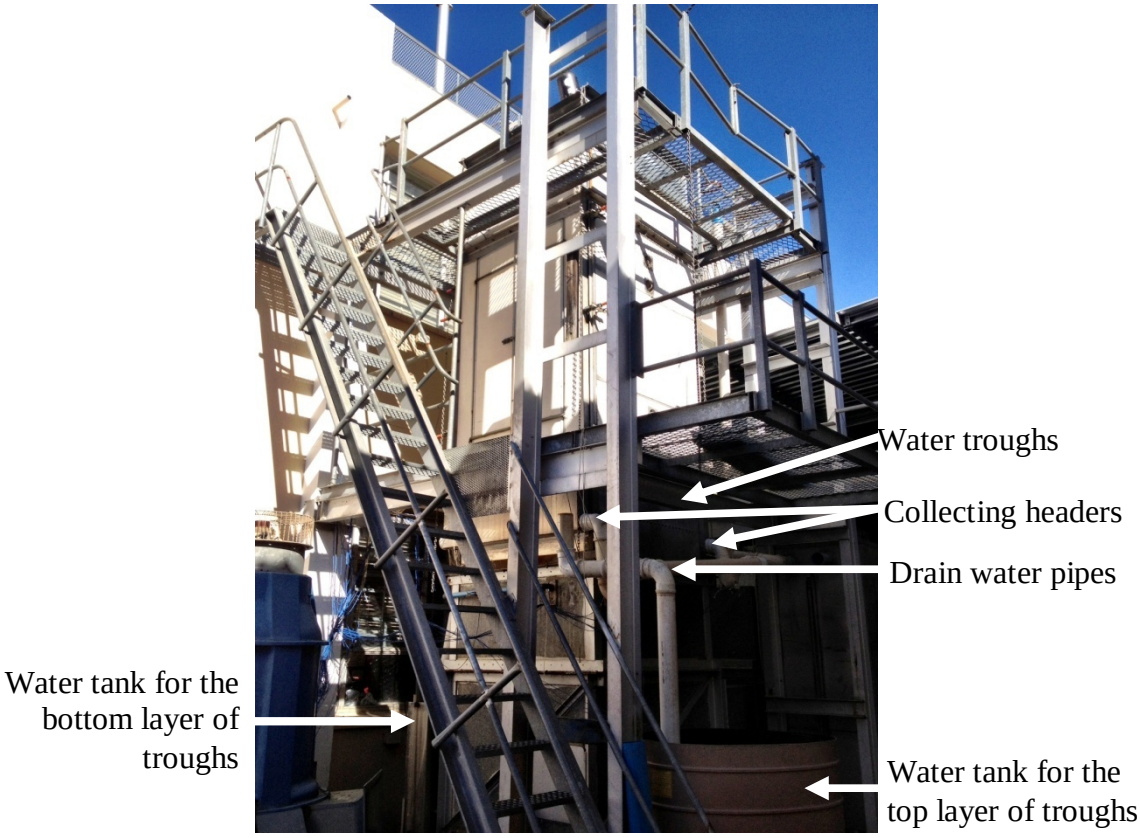

Figure 4.7: Vertical counter-flow test section

During the experiment the air mass velocity (G_a) is varied over a range of 0, 1, 2, 3 and 3.5 kg/m^{2}s while the water mass velocity (G_w) is fixed at 1.5, 3 or 4.5 kg/m^{2}s. The total amount of water entering the system is measured with the electromagnetic flow meter and the water collected in each layer of the troughs is measured in the tanks. The experiment is done twice for repeatability. The results are expressed in terms of percentage volume of water bypassing each layer of the troughs. The results will show the increase in water collection effectiveness due to the modifications made.

4.3.2 Air-side pressure drop tests

The air-side pressure drop is measured for both the original and the modified water trough to determine the additional pressure drop due to the 30 mm deflector plates. The air mass velocity (G_a) is varied over a range of 1, 1.5, 2, 2.5, 3, 3.5 kg/m^{2}s by changing the frequency on the variable-frequency drive connected to the fan motor.

The water mass velocity (G_w) is varied from 0, 1.5, 3 and 4.5 kg/m^{2}s to see the effect the deluge water has on the air-side pressure drop. The water trough drainage pipes are filled to prevent air from escaping from the test section. The H-taps are placed in the middle of the water trough test section. Each data set is averaged from ten data points at the specific air mass velocity.

4.4 Experimental results

Following are results presented for the original and the modified water troughs. The results are used to compare the gain in water collection effectiveness and the increase in air-side pressure drop due to the addition of the 30 mm deflector plate.

4.4.1 Water collection performance results

The water collecting effectiveness is presented for each water mass velocity (G_w) at different air mass velocities (G_a). The results are expressed as a percentage of water, which bypasses the top layer water troughs. The water mass balance is shown in equation (4.2) below. The final bypass is the water bypassing both layers.

$$m_{bypass} = (m_{flow\ meter} - m_{1st\ layer}) = m_{2nd\ layer} + m_{final\ bypass} \qquad (4.2)$$

From Figure 4.8 it is seen that the water collecting effectiveness is fairly linear apart from the last data point, where the air mass velocities (G_a) is at a maximum of 3.5 kg/m^{2}s. Before the deflector plate is added it is noted that a minimum of 7.7 and a maximum of 14.7 % by volume is passing through the top layer. As seen in Figure 4.8 (a), the modified trough allows an average of just over 6 % of water to pass through the top layer. In Figure 4.8 (b) it is seen that the modified trough allows an average of just less than 4 % of water pass through and in Figure 4.8 (c)

it is seen that the modified trough allows more than 4 % of water pass through the top layer of troughs.

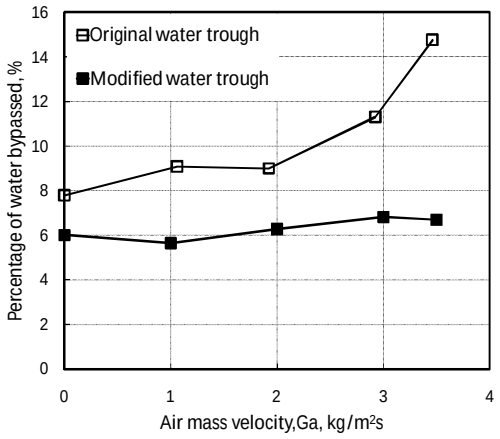

(a) G_w = 1.5 kg/m^{2}s

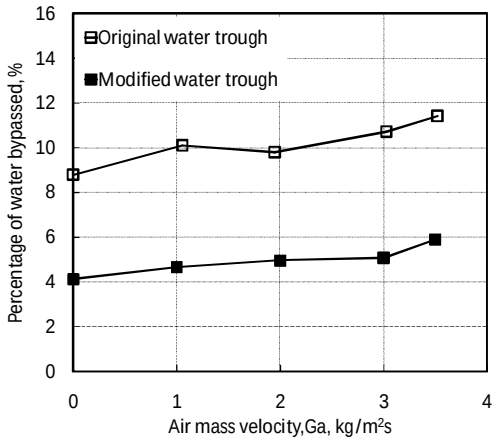

(b) G_w = 3 kg/m^{2}s

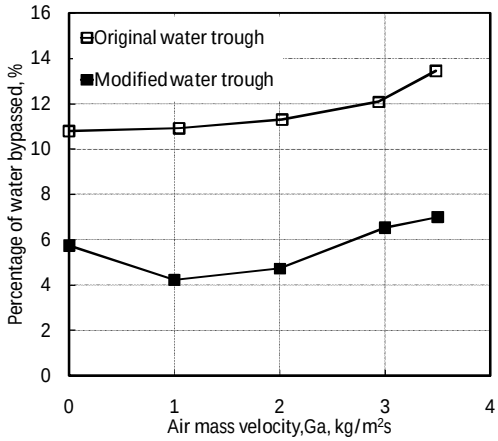

(c) G_w = 4.5 kg/m^{2}s

Figure 4.8: Percentage water passed through the first layer of troughs at different water mass flow velocity before and after the modification

From the results presented in Figure 4.8, it is noted that overall the deflector plate has made an improvement to the water collecting performance. After further investigating the modified water troughs and test section it is seen that the remaining water passing through is caused by wall effects as shown in Figure 4.9 below. Water adhering to walls of the counter-flow fill test facility runs down, either passing the troughs where they are integrated in the wall, or they fill the first and last water trough causing it to overflow. Water running down the walls is clearly visible from the top of the troughs as well as the bottom of the two layers.

In Figure 4.9 the amount of water passing both water trough layers due to wall effects is shown. It can be seen that between 3.3 and 5.9 % of the water is passing both water trough layers and only between 2 and 6 % of the water is collected in the bottom layer troughs. The results of the wall effects are clearly shown and the effect thereof on the water collection effectiveness tests. The difference between the total bypass shown in (Figure 4.8) and the wall effects (Figure 4.9) is the percentage of water bypassing the first layer of troughs. Accurate testing can be done by isolating the water troughs and eliminate the wall effects as discussed later.

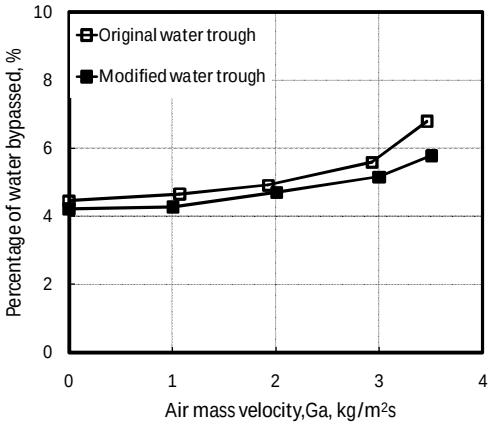

(a) G_w = 1.5 kg/m^{2}s

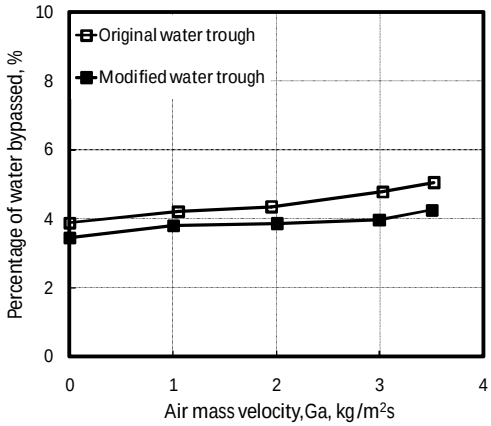

(b) G_w = 3 kg/m^{2}s

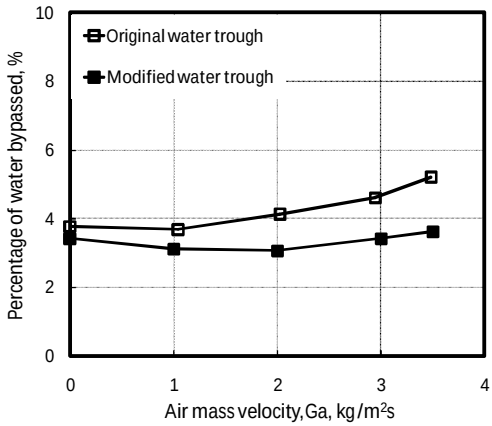

(c) G_w = 4.5 kg/m^{2}s

Figure 4.9: Percentage water passed through both trough layers due to wall effects

4.4.2 Water trough pressure drop test results

In Figure 4.10 (a) below, the pressure drop test results are presented for the original water troughs in the counter-flow fill test facility with deluge water present. The test is conducted between a minimum air mass velocity of 1 kg/m^{2}s

and a maximum air mass velocity of 3 kg/m^{2}s. The water mass velocity is between 0 and 4.5 kg/m^{2}s. The test results show the effect of the wetted troughs. There is a slight increase in pressure drop due the water resistance on the troughs. The dry water troughs have a loss coefficient (K_{tr}) = 3.7 for both layers and the wetted troughs have a maximum loss coefficient of 4.5 at a water mass velocity of 4.5 kg/m^{2}s. An increase in the pressure drop of 5, 15.4 and 29.7 % is seen for the water mass velocity of 1.5, 3, and 4.5 kg/m^{2}s respectively.

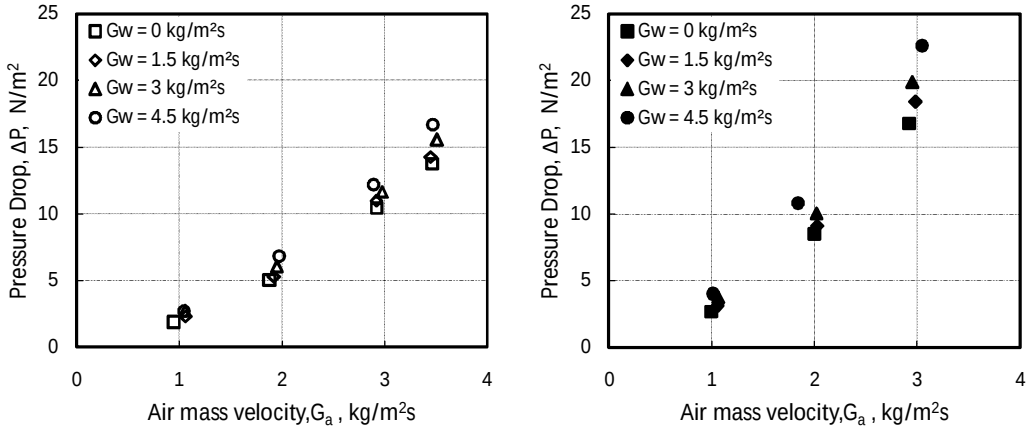

(a) Original water trough (b) Modified water trough

Figure 4.10: Air-side pressure drop over the water troughs with deluge water present

In Figure 4.10 (b) above the pressure drop test results are presented for the modified water troughs in the counter-flow fill test facility. The test is conducted between a minimum air mass velocity of 1 kg/m^{2}s and a maximum air mass velocity of 3 kg/m^{2}s. The water mass velocity is between 0 and 4.5 kg/m^{2}s. As expected the dry trough loss coefficient (K_{tr}) was increased significantly with the addition of the deflector plate to 5.3. The wetted water trough has a maximum loss coefficient of 6.8 at a water mass velocity of 4.5 kg/m^{2}s. An increase in the pressure drop of 11.3, 18.5 and 31.2 % is seen for the water mass velocity of 1.5, 3, and 4.5 kg/m^{2}s respectively. The modified water trough will require greater fan power to overcome the additional air resistance.

4.4.3 Discussion of results

The results show that by modifying the top layer of water troughs in the counter-flow fill test facility the water collection effectiveness is increased. Further visual investigation with a water proof digital GoPro camera inside the counter-flow fill test section above and below the water troughs revealed that the wall effects is causing by water running down the walls of the test section, bypassing the troughs, and causes the troughs at the outer edges to flood and over flow. Between 3.3 and 5.9 % of the water bypass the troughs due to wall effects. This is shown in Figure 4.9. The troughs need to be at a steeper angle to be able drain the water off

and not overflow. For an accurate indication of the water collection performance the wall effects should be eliminated. The true performance of the water troughs can be measured in an isolated scale test rig to confirm the water collection effectiveness. Further the test results show that the changes made to the water trough system have increased the air-side loss coefficient (K_{tr}) of the system from 3.7 to 5.3 for both trough layers. A well designed single layer water trough may be more effective than the two layer water trough system. Furthermore, a CFD sensitivity analysis on the water trough will yield the best suited geometry for the trough design by lowering the loss coefficient and understanding the flow characteristics. The pressure drop tests results can be used to validate a CFD model to further investigate the geometry of the troughs.

4.5 Water collection performance for an isolated water trough test rig

4.5.1 Introduction

This section presents water collection performance tests done on isolated water troughs in the horizontal cross-flow test section as discussed before. A small scale test rig is built to eliminate the wall effects by isolating the water troughs, only allowing water to impinge on the inner central area as seen from above. The small test rig is more adjustable, in terms of trough spacing and tilt angle for water drainage.

4.5.2 Experimental apparatus

Because of accessibly and space constraints the tests are conducted in the 2 x 2 m horizontal cross-flow test facility as shown in the schematic drawing in Figure 4.1. Similar as with the counter flow test section the same calibrated electromagnetic flow meter is used to measure the flow rate. A seen in Figure 4.11, seven water troughs, 500 mm in length, are fixed to a frame with threaded rods allowing the spacing between each trough to be adjusted. This is done to find the effect of the trough spacing on the water collection performance. Both the original and modified water troughs are tested with the small scale test rig.

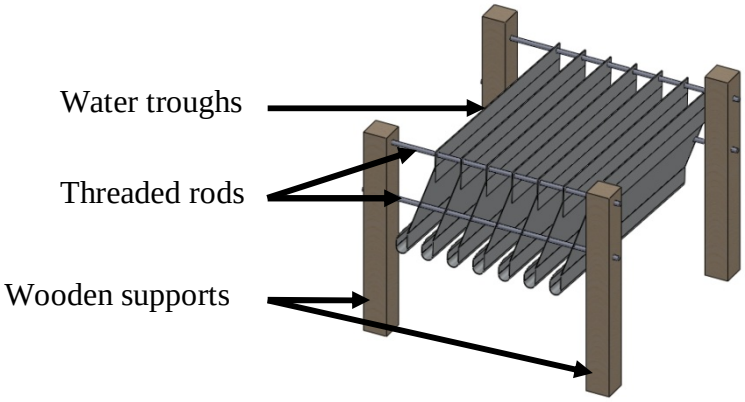

Figure 4.11: Collecting troughs test frame

The test rig is suspended from the roof of the 2 x 2 m cross-flow test section, preventing possible water splashing from support structures holding the troughs in place.

The troughs are fixed at a slope, allowing the water to drain under gravity while the higher end is closed off to prevent water from overflowing. The spray frame is closed off with sheet metal to prevent water from impinging on the surrounding edges of the water troughs. This eliminates wall effects only exposing the inner central area of the water troughs to the rain-zone as shown in Figure 4.12.

A container is located in the centre, directly below the water troughs to capture any water passing through the water troughs test frame.

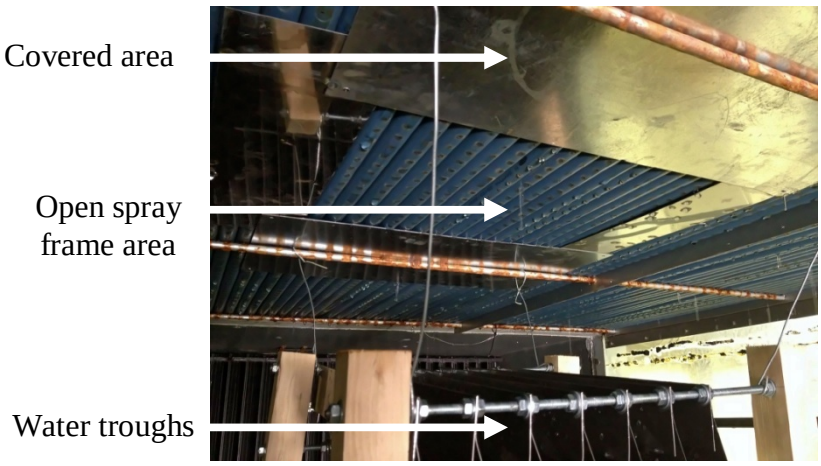

Figure 4.12: Trough test rig with the reduced spray frame test area

4.5.3 Experimental procedures

The water mass velocity (G_w) is kept constant at 1.5 kg/m^{2}s throughout the testing. The desired water flow rate is obtained by adjusting a valve on the supply pipe.

Three test runs are done for different time durations, firstly a 5 minute test followed by a 10 minute and lastly a 30 minute test. The mass of the collected water in the container below the water troughs is measured after each test.

Each set of tests is repeated for 50 mm, 45 mm and 40 mm spacing (Δx_{tr}) shown in Figure 4.13. The water below the rain-zone is pumped back to the supply pump reservoir with a second pump.

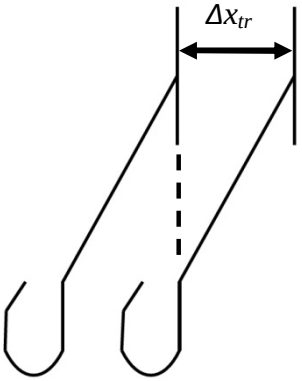

Figure 4.13: Adjacent troughs spacing

4.5.4 Experimental results

In Figure 4.14 below the test results of the water collection effectiveness tests are presented for the tests done on the original and modified water troughs.

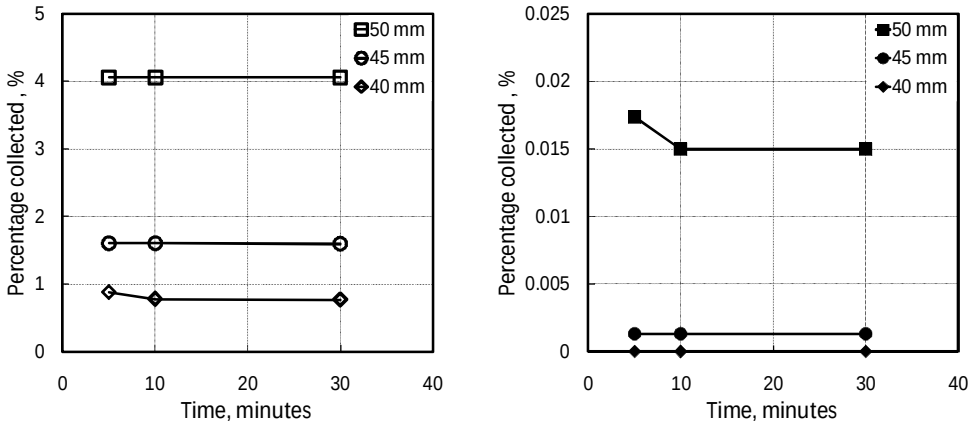

(a) Original water trough (b) Modified water trough

Figure 4.14: Isolated trough collection performance for different trough spacing

The results correlate well with the tests results with the single trough presented in section 3.2 and the results from the counter-flow fill test facility, presented in section 4.4. The original water trough's water collection effectiveness is increased by reducing the trough spacing. More of the drops swinging off the back of the trough are collected in the neighbouring trough as shown in section 3.2. The wall effects are successfully eliminated with the small test rig by isolating the troughs and spray frame. The effect of the deflector plate is seen as the water collection effectiveness is increased from 4 % to 0.015 % for a trough spacing of 50 mm. No water is collected below the troughs with a trough spacing of 40 mm. The water from the deflector plate, is successfully guided onto the neighbouring trough, not allowing water to pass between the troughs.

4.5.5 Discussion of results

The wall effects of the counter-flow fill test facility shown in Figure 4.9 are eliminated with the isolated trough tests. With the isolated trough tests (Δx_{tr} = 50 mm), 4 % of the water bypasses the original troughs and 0.015 % of the water bypasses the modified troughs. The water collection effectiveness test result presented in section 4.4.1, conducted in the counter-flow fill test facility, show that 4.4 % of the water bypasses the original troughs and 0.5 % of the water bypasses the modified troughs. The difference can be due to water adhering to pressure transducer piping and thermocouple wires. The influence of the trough spacing on the water collection effectiveness is shown in Figure 4.14. As the trough spacing is reduced, the percentage bypass decreases. Intuitively it can be seen that there will be an increase in the air-side loss coefficient as the effective frontal flow area is reduced.

4.6 Water draining performance of the water channel at different angles

4.6.1 Introduction

This section presents the water drainage characteristics of the water trough's open channel at various angles to the horizontal. The tests are conducted to find the water depth in the channel at different water mass flow rates, for a given angle. The test result may be used to find a best suited design angle of the water troughs to ensure proper water run out to the collection tanks and prevent the troughs from overflowing. The water depth in the troughs needs to be minimized as this can cause splashing from falling drops.

4.6.2 Experimental apparatus

The tests are conducted in a single water channel, identical in design to the channel of the water troughs from the counter-flow fill test facility at Stellenbosch University.

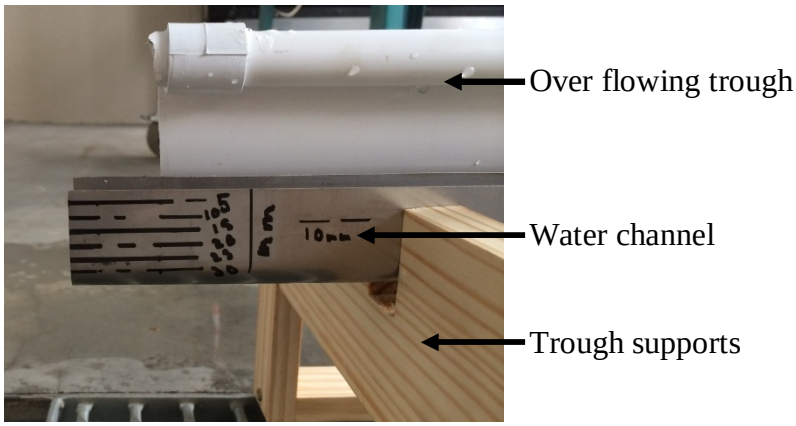

Figure 4.15: Drainage channel apparatus with water level markings

As shown in Figure 4.15 the water channel is made from 0.9 mm stainless steel, 2.5 m in length and open at both ends. Water level markings are made on the trough to record the water level at the outlet. The water outlet height is measured from the reference lines on the water channel. An overflowing trough is used to feed the water channel to simulate a uniform water distribution. During testing the water mass flow rate is varied while the water channel is set to different angles of 1.3, 2.2, 5.4 and 9 degrees. The total water mass flow rate is measured with a calibrated water tank, used to collect the water at the outlet of the channel. Each measurement is done twice for repeatability.

4.6.3 Experimental results

The measured and calculated water depths are compared in Figure 4.16 below. Manning's empirical equation (4.3) is used to calculate the water depth (Δy). A sample calculation of the calculated water depth is shown in Appendix D.

$$\dot{V}_2 = \frac{a}{n} A_c R_h^{2/3} S_o^{1/2} \text{ , m}^3/\text{s} \tag{4.3}$$

where n is the Manning coefficient and is 0.012 for stainless steel and a = 1 and

$$A_c = (W \times \Delta y) + \frac{1}{2}\left(\pi \frac{D^2}{4}\right) \tag{4.4}$$

$$R_h = A_c / P \tag{4.5}$$

$$S_o = \Delta x / \Delta y \tag{4.6}$$

A linear relationship is noted in the water depth for a given water channel angle. For mass velocity of 1.7 kg/m^{2}s, the water channel needs to drain 0.2125 kg/s, and the water depth will depend on the angle of the water channel.

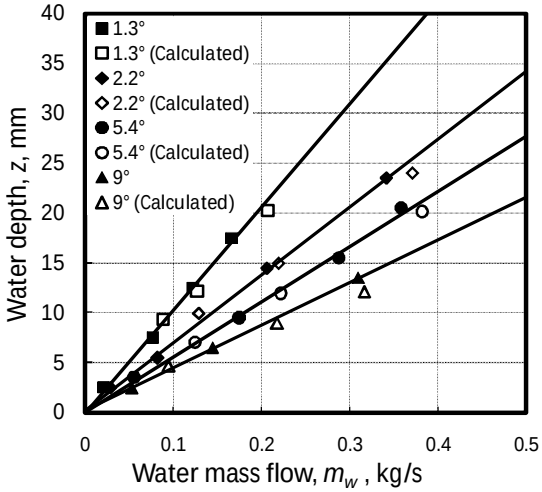

Figure 4.16: Water depth test result and calculated results for different angles

4.6.4 Discussion of results

A good correlation can be seen between the measured water depth and the calculated water depth, even with the theoretical model used to calculate the water depth. The open channel flow calculations is based on work done by Gauckler and Manning taken from (Cengel and Cimbala, 2006). For a specific water channel angle, the water level increases linearly when increasing the water flow rate. Increasing the water channel angle, increases the water draining rate. The results show that the outlet depth can be predicted accurately by means of the theoretical model.

4.7 CFD analysis on geometry variables of a water trough

4.7.1 Introduction

In this section a two-dimensional CFD model is developed in FLUENT® 14.0 to simulate air flowing through the water troughs. Two-dimensional CFD models are used to reduce computing time and computing resources needed. The model is validated with the water trough air-side pressure drop tests results as discussed in section 4.4.2. The validated model is used to find the effect of variance of geometric parameters on the air-side loss coefficient. The results are used to develop a loss coefficient correlation for design purposes.

4.7.2 CFD model and setup

As shown in Figure 4.17 below a two-dimensional domain is used with periodic boundaries on each side, to represent the multiple water troughs in the counter-flow fill test facility. The structured mesh is shown through the domain with mesh inflation around the water trough edges.

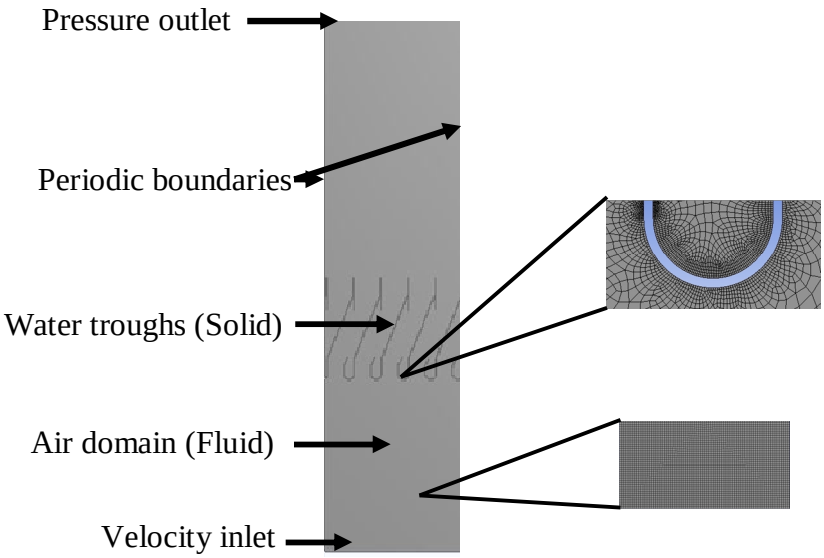

Figure 4.17: Mesh and boundary conditions for the two-dimensional CFD domain

Periodic boundaries allows for a repeated pattern. Vectors leaving the left side will enter the right side and vice-versa. The inlet boundary is a velocity inlet boundary and the outlet is a pressure outlet.

All the CFD models are simulated with dry air at 288.16 K with a constant density of 1.225 kg/m^3. The *k*-ε Realizable turbulence model with standard wall functions is used as it predicts areas where flow separation takes place well, as stated by Reuter (2010). The *k*-ε Realizable turbulence model by Shih (1995) is the latest edition to the three *k*-ε variations, and has mainly two differences from the standard *k*-ε model. A new improved equation is used for turbulent viscosity (μ_t) and an improved transport equation for the dissipation rate (ε), which performs better than the standard *k*-ε turbulence model.

4.7.3 CFD validation and results

A grid independence study is conducted. The CFD model is validated by conducting a grid independence test and a comparison to the air-side pressure drop experimental test results, for both the original and modified water trough as shown in section 4.4.2. A area weighted average is to obtain the pressure values. The simulation is run over a range of air mass velocities to produce the same data point to the experimental tests.

The CFD model only simulates one layer of water troughs. The pressure drop is doubled to compensate for the second layer of water troughs. In the case of the modified water trough model the pressure drop from the original water and the modified water trough are added. The total pressure drop distribution over the single original and modified water trough is shown in Figure 4.18, where the effect of the deflector plate on the total pressure distribution can be seen.

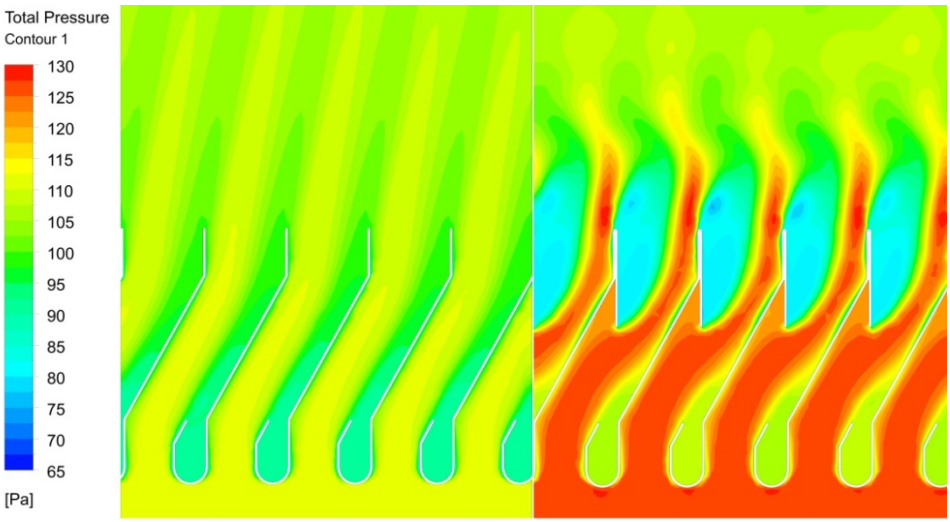

(a) Original trough (b) Modified trough

Figure 4.18: CFD results for the total pressure distribution for the trough

The CFD and experimental test results are shown in Figure 4.19 below. When comparing the experimental and CFD results for both cases it is seen that the CFD is slightly underestimating the pressure drop. The differences between the experiment and CFD results can be attributed to a combination of possible measurement uncertainties such as air flow rate or pressure drop measurements.

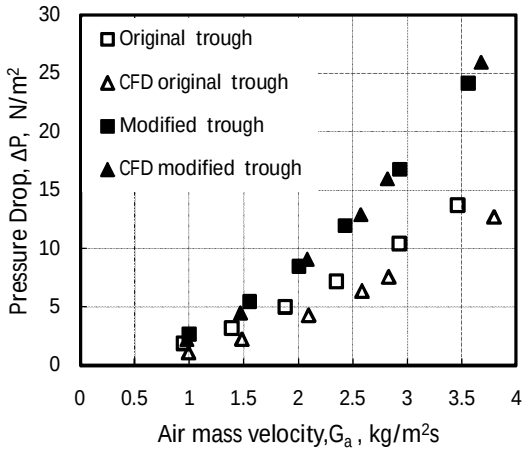

Figure 4.19: Experimental and CFD pressure drop data for the trough

A grid independence test is conducted on the model with the original water troughs at 3 m/s inlet velocity. Face sizing with mesh refinement is used to mesh the domain with five different quadrilateral cell sizes used for the grid independence test namely 15, 10, 8, 4, and 3 mm, with a maximum amount of 24 289 elements and a minimum amount of 5194 elements used.

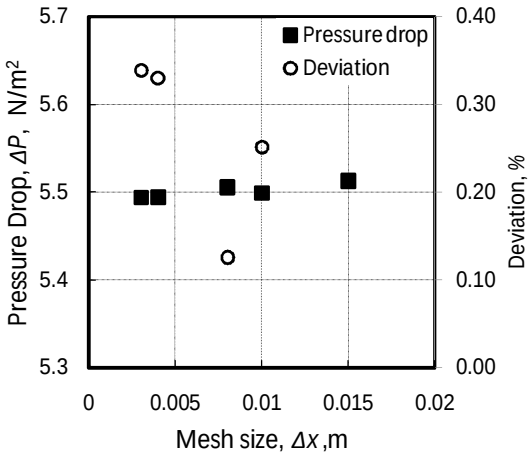

Figure 4.20: CFD predicted pressure drop over the troughs for different mesh element sizes

Shown in Figure 4.20 is the pressure drop over the water troughs for different grid sizes. The reduction in element size does not have a significant effect on the pressure drop results. The deviation shown is the difference from the previous to the new pressure drop due to the change in mesh size. The maximum difference in

pressure drop is 0.35 %. From the grid independence test results an element size of 4 mm is considered to be sufficient to use for the CFD model.

4.7.4 Influence of geometric variables on inlet loss coefficient for the modified trough

The validated CFD model is used to investigate the effects of different geometric variables on the inlet loss coefficient (K_{tr}). The modified trough with the 30 mm deflector plate, as tested in the counter-fill test facility, is used as a reference case. For the parametric study the channel radius (R_{ch}), trough height (H_{tr}), deflector plate length (L_{dp}) and the trough spacing to the next trough (Δx_{tr}) are varied as shown in Figure 4.21.

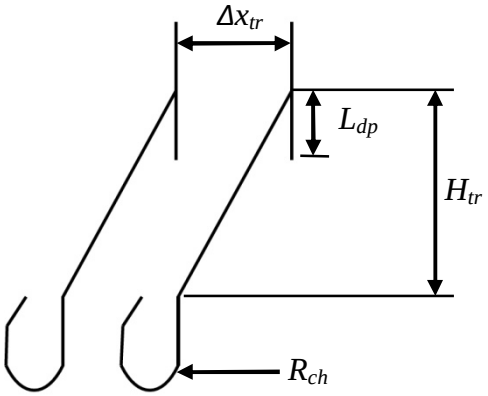

Figure 4.21: Modified trough with geometry variables

The following dimensions are used for the reference geometry: R_{ch} = 10 mm; H_{tr} = 90 mm; L_{dp} = 30 mm and Δx_{tr} = 50 mm. The regression has a R^2 value of 0.975.

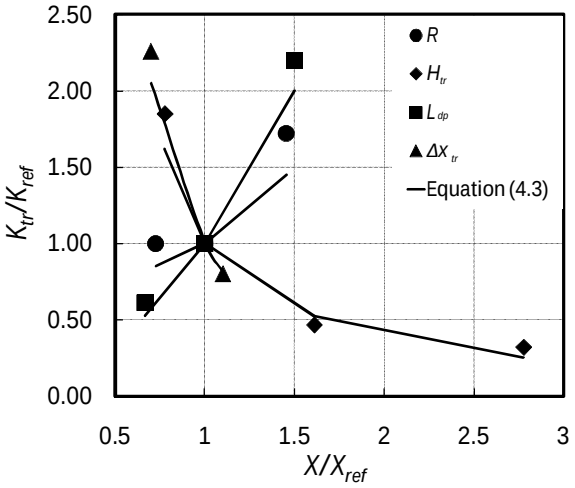

Figure 4.22: CFD trough loss coefficient data and regression

The following relation between the geometry variables and loss coefficient is proposed for the trough with the deflector plate.

$$K_{tr} = 4549.35\, R_{ch}^{0.82}\, H_{tr}^{-1.34}\, L_{dp}^{1.57}\, \Delta x_{tr}^{-2.1} \quad (4.3)$$

with $8 \leq R_{ch} \leq$ 16 mm, $70 \leq H_{tr} \leq$ 250 mm, $20 \leq L_{dp} \leq$ 45 mm and $35 \leq \Delta x_{tr} \leq$ 55 mm

4.7.5 Discussion of the parametric study results

A two-dimensional CFD model in FLUENT® with periodic boundaries is used to simulate air flow over the water troughs as tested in the counter-flow fill test facility. The test results in section 4.4.2 are used to validate the CFD model. The validated model is used to do a mesh element independence test by changing the mesh element size. A 4 mm mesh element size is adequate to capture the re-circulating flow field and yield accurate results by reproducing the experimental test results.

A maximum discrepancy of 7% is seen between the test results and CFD results. The validated CFD model is used to explore the effects that the different geometric parameters have on the trough loss coefficient (K_{tr}).

4.8 Conclusion

The test results presented for the water collection effectiveness of the water collecting trough system in the counter-flow fill test facility at Stellenbosch University show that the trough system does not collect the water properly. Water is found to bypass the troughs even with the addition of a deflector plate to the top layer of water troughs in the counter-flow fill test facility. This was found to be caused by wall effects. The trough spacing to the neighbouring trough is decreased and a deflector plate is proposed to improve the water collection effectiveness.

A smaller test rig is designed, built and tested to eliminate the wall effects of the counter-flow fill test facility. The modified water trough tests are repeated using the smaller test rig in the cross-flow test facility. The results show that the modified trough has 100 % effectiveness when the trough spacing is reduced to 40 mm.

A test channel was designed, manufactured and tested to investigate the water level in a channel at different water inlet flow rates uniformly distributed along the channel's length. The rate at which water is drained out of the collecting troughs is dependent on the angle of the troughs. Open channel flow theory correlates well with the test results of the trough draining channel. The water depth needs to be minimized as this can cause splashing.

The original two layer water troughs has a loss coefficient (K_{tr}) = 3.7 and a loss coefficient = 5.3 after the deflector plate was added. The pressure drop tests results are used to validate a two-dimensional CFD model in FLUENT® for modelling air-side pressure drop of the water troughs. A maximum discrepancy of 7% is seen between the test results and the CFD results. An increase in the pressure drop of 11.3, 18.5 and 31.2 % is seen for the water mass velocity of 1.5, 3, and 4.5 kg/m^{2}s respectively for the two layer water trough system in the counter-flow test facility. The CFD model is used to conduct a parametric study to determine the effect of varying geometric parameters. The regression curves are used to determine an empirical relation between the loss coefficient (K_{tr}) and different trough geometries. The empirical relation is shown in equation (4.3).

5. CFD ANALYSIS OF AIR INLETS FOR INDUCED AND FORCED DRAFT BASIN DESIGNS

5.1 Introduction

Water basin systems are highly effective in collecting water falling as rain through an air-stream and are used successfully in evaporative coolers and wet-cooling towers as discussed in section 2.1. A water basin system collects deluge water falling under gravity directly into a collecting basin. Air generally enters horizontally through one or more lateral inlets and is turned through 90° to flow out vertically. Water basin systems do not have leakage problems, but the inlets are limited by space and can restrict air-flow. An induced draft and forced draft HDWD collecting basin design is shown in Figure 5.1, respectively. The different inlet air-flow patterns are shown for each design. A forced draft HDWD basin design has space constraints causing a reduction in lateral air inlet height as seen in Figure 5.1 (b). Intuitively it can be seen that the forced draft HDWD basin design will have a larger air-side pressure drop when compared to the induced draft design. The air-flow patterns around a HDWD collecting basin design are different to evaporative coolers or wet-cooling towers' collecting basins. With the HDWD collecting basin design the air flows vertically and around the basin to enter horizontally through the lateral inlets as opposed to horizontally and through the lateral inlet with evaporative coolers or wet-cooling towers.

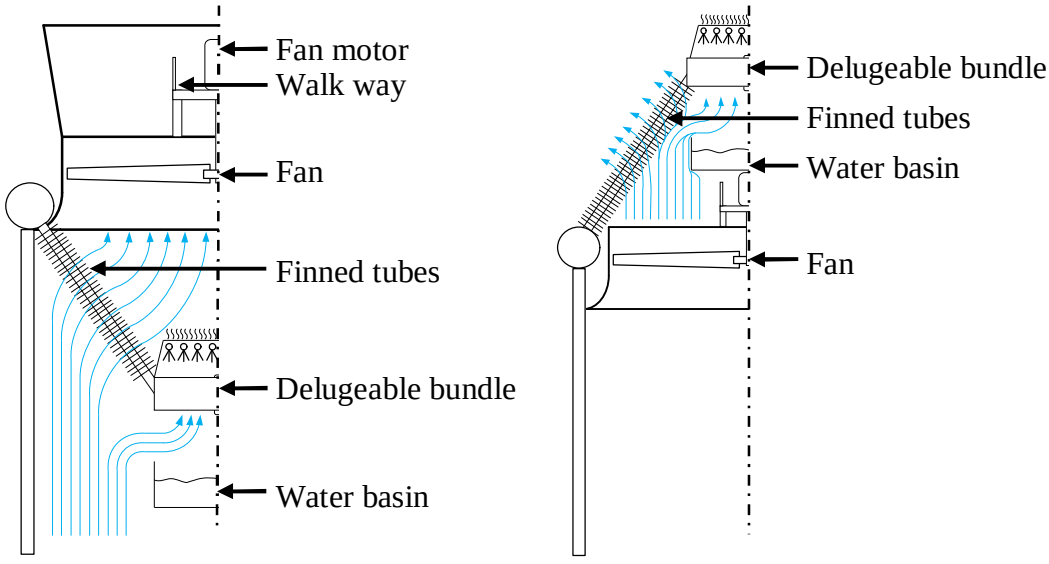

(a) Induced draft (b) Forced draft

Figure 5.1: HDWD water basin system showing different air inlet flow patterns

Water basin systems are categorized as single water basins or cascading basins. Figure 5.2 shows a single collecting basin, with one air-inlet per side and a cascaded collecting basin with more than one air-inlet each side. The different

inlet air-flow patterns are shown for each configuration. A cascading basin design has a larger inlet area, reducing the flow resistance. For design purposes sufficient space between the delugeable bundle and the fan is needed to ensure that the basin fits in. The basin inlet loss coefficient (K_{db}) is needed to find the air-side pressure drop over the basin inlet. The water volume of a deluge system is needed to ensure the collecting basin can accommodate all the deluge water when the deluge water system is not running. The inlet loss coefficient is needed to determine the fan power required. The water basin of a HDWD collects the water which then runs to the lowest point in the basin. The water is pumped from this point back to the deluge water sprayers. Each basin design has a different pump head to overcome and to feed the sprayers above the delugeable bundle.

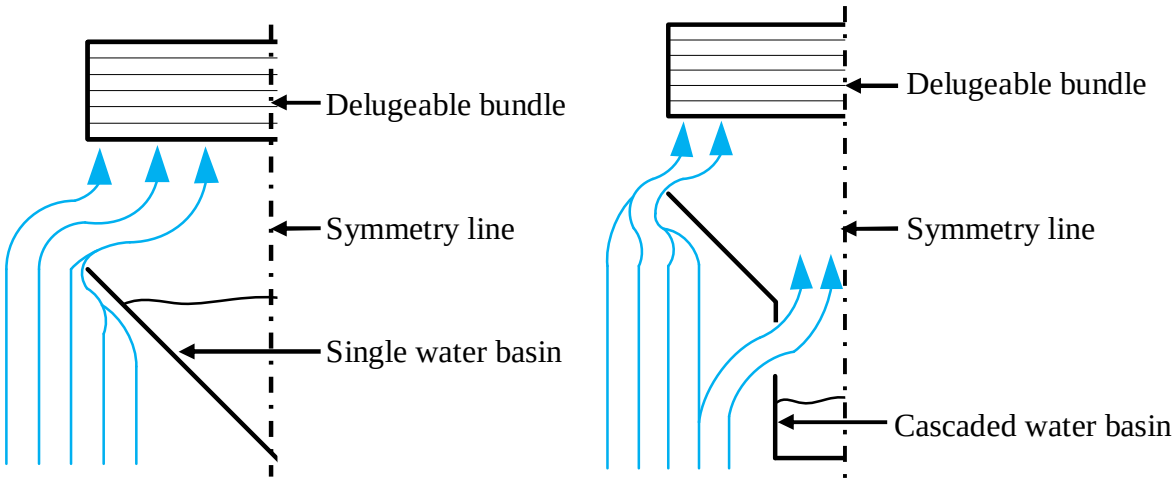

(a) Single collecting basin (b) Cascading collecting basin

Figure 5.2: Different water collecting basin configurations showing typical air-inlet flow patterns

A substantial amount of research has been done on inlet losses of round natural draft wet-cooling towers (NDWCT) and rectangular cooling towers. Kröger (2004) did experimental work on a small scale model of a round natural draft cooling tower and rectangular cooling tower. Reuter (2010) confirmed the accuracy in results by comparing the CFD results to the experimental data and investigated scaling effects. Two-dimensional, symmetrical CFD models are developed in FLUENT® 14.0 to model air-flow through the lateral basin inlets with and without a rain-zone present. The collecting basin design inlet is unique for the proposed HDWD patent and no correlations were found to predict the inlet loss coefficients as the flow patterns are different to those of evaporative coolers or cooling towers as discussed above. Terblanche and Kröger (1994) developed an empirical correlation (defined by equation 2.2) from experiments done on a scale model for inlet loss coefficients for rectangular, mechanical induced draft cooling towers with a horizontal heat exchanger. The empirical data obtained from this correlation is used to validate the CFD model and to confirm the accuracy of the model through the later inlets. The CFD model is used to do a geometric study on

the induced and forced draft basin design to find the effect that varying different parameters has on the basin inlet loss coefficient (K_{db}). The CFD results are used to develop a relation for the inlet loss coefficient for design purposes.

A reduction in the flow cross-sectional area as found at the basin inlet causes velocity gradients. Velocity gradients in flow fields cause shear stress in the working fluid, in turn this cause's viscous dissipation of mechanical energy. Mechanical energy is defined as $E_m = P/\rho + \alpha_e v^2/2 + gz$, where α_e is the kinetic energy coefficient. The dimensionless loss coefficient for incompressible flow in horizontal ducts is defined as.

$$K = \frac{\left(\frac{p_1}{\rho}+\frac{\alpha_{e1}v_1^2}{2}\right)-\left(\frac{p_2}{\rho}+\frac{\alpha_{e2}v_2^2}{2}\right)}{\frac{v^2}{2}} = \frac{\left(p_1+\frac{\alpha_{e1}\rho v_1^2}{2}\right)-\left(p_2+\frac{\alpha_{e2}\rho v_2^2}{2}\right)}{\frac{\rho_i v^2}{2}} = \frac{P_{t1}-P_{t2}}{\frac{\rho_i v^2}{2}} \quad (5.1)$$

where P_t is the total pressure and the subscripts 1 and 2 refer to the control volumes at inlet and outlet respective. According to Kröger and De Villiers (1997) the inlet loss coefficient (K_{ct}), for an isothermal model, can be expressed as follows for dry operation:

$$K_{ct(dry)} = \frac{\frac{P_1}{\rho_1} - \left(P_2/\rho_2+\frac{\alpha_{e\,2}v_2^2}{2}\right)}{\frac{v_2^2}{2}} - K_{he} \quad (5.2)$$

and as follows for wet operation:

$$K_{ct(wet)} = \frac{\frac{P_1}{\rho_1} - \left(P_2/\rho_2+\frac{\alpha_{e\,2}v_2^2}{2}\right)}{\frac{v_2^2}{2}} - K_{he} - K_{rz} \quad (5.3)$$

where K_{he} is the loss coefficient of the delugeable bundle and K_{rz} is the rain-zone loss coefficient (equation 2.9) from Kröger and De Villiers (1997). Equation (2.9) is limited to one lateral inlet, therefore it can only be applied to the single water basin.

Kröger and De Villiers (1997) showed that a rain-zone has a dampening effect on the velocity distribution resulting in a reduction in inlet loss coefficient. To compensate for the differences in the dry and wet inlet loss coefficient (K_{ct}) a rain-zone inlet loss correction factor (C_{rz}), smaller than unity is used as shown in equation (5.4) below.

$$C_{rz} = \frac{K_{ct(wet)}}{K_{ct(dry)}} \quad (5.4)$$

5.2 Validation of the CFD model

The following are the procedures used to validate the CFD model used for modelling air flow through the water basin inlets. The validated CFD model is use to do a parametric study. The validity of the CFD analysis is dependent on the similarities between the CFD model and experimental work from previous research.

For the validation the CFD model is compared with results from experimental work done by Kröger and Terblanche (1994) on induced draft rectangular tower inlets with a horizontal heat exchanger. The empirical data of the induced draft, rectangular tower cannot be used directly for the HDWD basin design because the air-flow patterns of an induced draft rectangular tower are different to that of the HDWD basin design. The induced draft rectangular tower draws air in horizontally through lateral inlets, not vertically as with the HDWD basin design.

For the wet operating conditions a CFD rain-zone model is compared with results from work done by Kröger and De Villiers (1997) on the pressure drop of the rain-zones in induced draft cooling towers and an inlet loss correction factor. The CFD model is further validated by conducting a mesh element size independence test for different mesh sizes.

Figure 5.3 is a schematic of the CFD model geometry for the rectangular inlet used for the validation tests. The tower width (W_i) to inlet height (H_i) ratio is varied over a range. The CFD results are compared to the following correlation for the inlet loss coefficient developed from experimental work by Kröger and Terblanche (1994). According to Kröger and Terblanche (1994) a kinetic energy coefficient (α) of unity may be used as the velocity distribution at the outlet is uniform.

$$K_{ct} = \left[1.1 + 1.1\left(0.5\frac{W_i}{H_i}\right)^3 - 0.05\left(0.5\frac{W_i}{H_i}\right)e^{\left(0.5\frac{W_i}{H_i}\right)}\right] \times K_{he}^{\left[-0.29+0.079cos\left(0.5\frac{W_i}{H_i}\right)+0.102sin\left(0.5\frac{W_i}{H_i}\right)\right]} \quad (5.5)$$

with the range $0 \leq 0.5W_i/H_i \leq 2.5$ and $4 \leq K_{he} \leq 80$.

A large air domain at the left boundary is used to simulate stagnant, ambient air. The air leaves through the heat exchanger with an outlet velocity of 3 m/s, regulated by the ,mass flow inlet. The half width (W_i) to inlet height (H_i) ratio is varied over a range of 1 to 2.5. The heat exchanger is modelled as a porous medium with a loss coefficient (K_{he}) = 38 taken from experimental work by Anderson (2014).

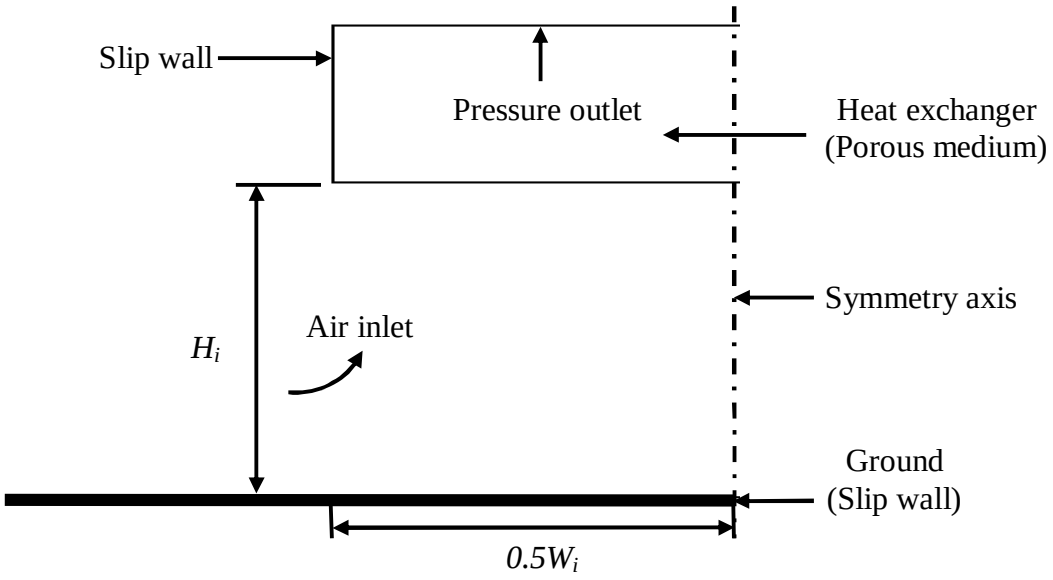

Figure 5.3: Rectangular tower with horizontal heat exchanger

The porous medium in FLUENT® is modelled as a source term in the momentum equation:

$$S_{i,mesh} - \frac{\partial p}{\partial x_i} - \frac{\partial}{\partial x_i}(\tau_{ij}) = \frac{\partial}{\partial t}(\rho U_i) + \frac{\partial}{\partial x}(\rho U_i U_j) \tag{5.6}$$

where the source term is related to a pressure drop over the mesh.

$$S_{i,mesh} = \frac{-\Delta p_{mesh}}{\Delta n} \tag{5.7}$$

The resistance over the porous medium due to the inertial (equation 5.8) term.

$$C_z \frac{1}{2} \rho \Delta n = 23.275 \tag{5.8}$$

With a density of 1.225 kg/m^3 and height (Δn) of the porous medium of 0.8 m, C_z is equal to 47.5 m^{-1}.

Equation (5.2) is used to find the tower inlet loss coefficient and in Figure 5.4 the CFD results are compared to the empirical correlation (equation 5.5) discussed above.

The CFD results slightly over-predict the inlet loss coefficient. This is similar to the trend found by Reuter (2010) on NDWCT and Kröger and De Villiers (1997). The reason for this is that the flow re-circulation at the basin inlet in the vicinity of the wall, is not captured fully in the CFD model as well as it is with the experimental work. An uncertainty in the measurement instrumentation used for the experiment can also attribute to the problem. The over prediction of the inlet

loss coefficient is especially true at the higher values of inlet width to height ratio (lower values of H_i) due to the increasing effect of flow re-circulation at the inlet. Despite the above mentioned the numerical model does simulate the flow field reasonably well and there is a good correlation shown between the CFD and experimental data providing confidence in the model with a maximum deviation of 6.8 %.

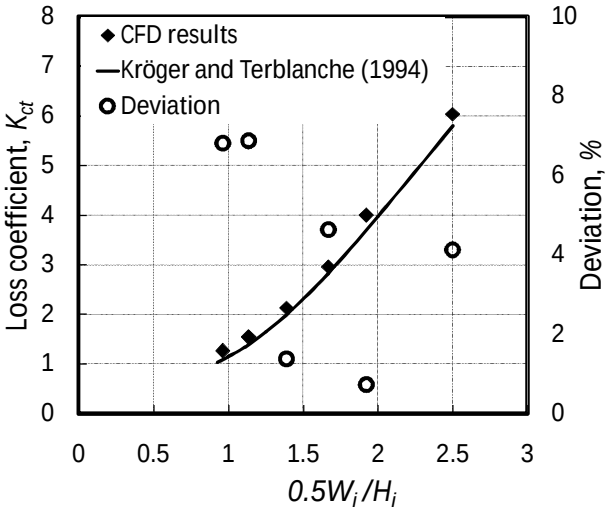

Figure 5.4: Comparison between the inlet loss coefficient correlation and CFD results for a rectangular tower with horizontal heat exchanger

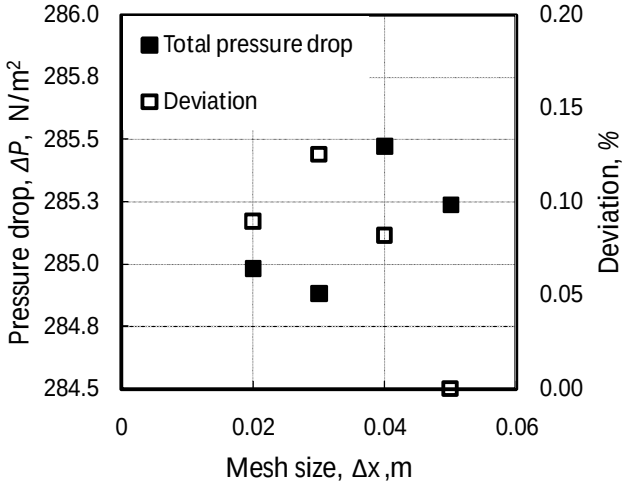

Figure 5.5: Mesh element independence test results

The same model as above is used to conduct the mesh element independence test to confirm the correct mesh size is used and to see the effect that the mesh size has on the loss coefficient. The test is conducted with quadrilateral cells with mesh refinement and a maximum element size of 50 to a minimum of 20 mm with 10 mm increments. From the mesh independence test results it is seen that the

differences in the total pressure drop for the various mesh sizes can be neglected, as an average deviation of 0.26 Pa is noted. A mesh size of 20 mm will be adequate to capture the recirculation and flow separation in the flow field for future simulations as proven with the comparison with the experimental work. More details about the mesh are shown in Appendix E.

According to Kröger and De Villiers (1997) the presence of a rain-zone decreases the tower inlet loss coefficient, while Pierce (2007) showed a rain-zone makes the velocity distribution more uniform throughout a cooling tower. A purely counter-flow rain-zone is used to validate the CFD model and to compare the results with the experimental relation from Kröger and De Villiers (1997) as shown in equation (2.8) in section 2.4. For a purely counter-flow rain-zone the analysis is essentially one-dimensional, thus the total pressure drop of the test domain is due to the drag force of the drops acting on the air.

The discrete phase model (DPM) is used to simulate a rain-zone in FLUENT® model. Water drops are injected at the air outlet with the spherical drag law. With regards to the tracking parameters, the maximum number of steps are set to 50 000, while the step length factor is set to 2, and for every 10th continuous phase iteration, the DPM runs 1 iteration. A monodisperse droplet distribution is used and droplet deformation is neglected to replicate the conditions as with the counter-flow rain-zone analysis of Kröger and De Villiers (1997).

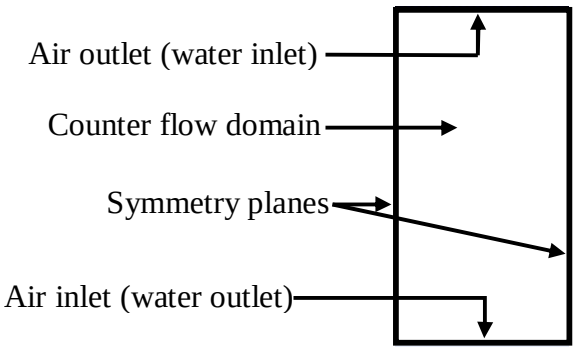

Figure 5.6: Counter-flow domain and boundary conditions

By increasing the rain-zone loss coefficient the tower inlet loss coefficient is dampened. In Figure 5.7 below it can seen that the CFD model predicts the rain-zone loss coefficient reasonably accurate at different drop diameters but, similar to the results found by Pierce (2007) the CFD model over predicts the loss coefficient at the smaller drop diameters and slightly under predicts the loss coefficient at the larger drop diameters.

The rain-zone analysis done by Kröger and De Villiers (1997) on rectangular cooling towers with an induced draft shown by the empirical relation in equation (2.9) is used for the CFD analysis of the induced draft basin. The empirical correlation is developed and limited for an induced draft design with a single

lateral inlet on each side of the tower. Therefore the correlation may not be applied to the forced draft or the cascaded basin design due to the multiple lateral inlets. For this reasons the forced draft design and cascaded basin design is simulated for dry operating conditions only.

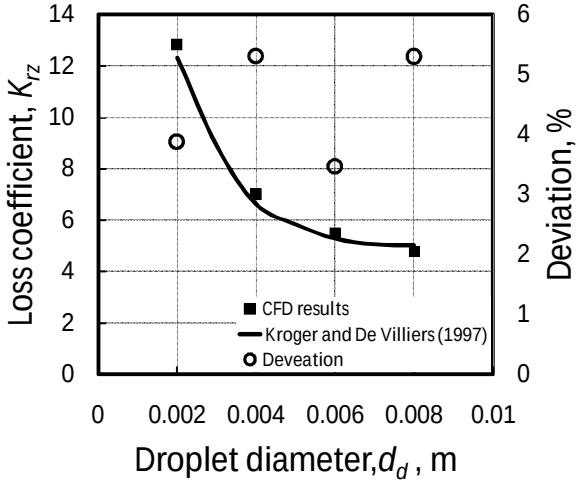

Figure 5.7: Counter-flow rain-zone loss coefficient result for the CFD model and experimental relation from Kröger and De Villiers (1997)

To further establish confidence in the CFD rain-zone model, the inlet loss correction factor (C_{rz}) of the induced draft case is compared to an empirical correlation by Kröger and De Villiers (1997) as shown in equation (5.9) below. The inlet loss coefficient is a function of all the variables that characterize the inlet and rain-zone losses. Kröger and De Villiers (1997) excluded the "weaker" variables, not having a major effect on the inlet loss correction factor. The variables that are included are, W_i, H_i, d_d , G_w and G_a. The empirical correlation is only applicable to induced draft rectangular cooling towers and compared to the reference case of the induced draft basin model while varying the water mass velocity.

$$C_{rz} = 1 - G_w\left(0.123 - 12.1d_d - 272.26d_d + 5.04e^{-4} \times e^{\frac{0.466w_i}{H_i}}\right) \times (1 - 1.16e^{-3}e^{G_a}) \quad (5.9)$$

where $3 \leq W_i/H_i \leq 7.5$, $0.003 \leq d_d \leq 0.006$ m, $1 \leq G_w \leq 3$ kg/m^{2}s and $2 \leq G_a \leq 6$ kg/m^{2}s

Equation (5.4) is used with the induced draft CFD results to find the inlet loss correction factor. In Figure 5.8 below it can be seen that the CFD model's inlet loss correction factor (C_{rz}) correlates well to the work by Kröger and De Villiers (1997). The water mass velocity is varied over a range to produce the curve. The results establish more confidence in the CFD models as it shows the repeatability of the CFD code. Kröger and De Villiers (1997) stated that the prediction for inlet

correction factor for circular cooling towers are more accurate and that the influence of the inlet correction factor may be neglected for rectangular tower, but may be used when a conservative design approach is used.

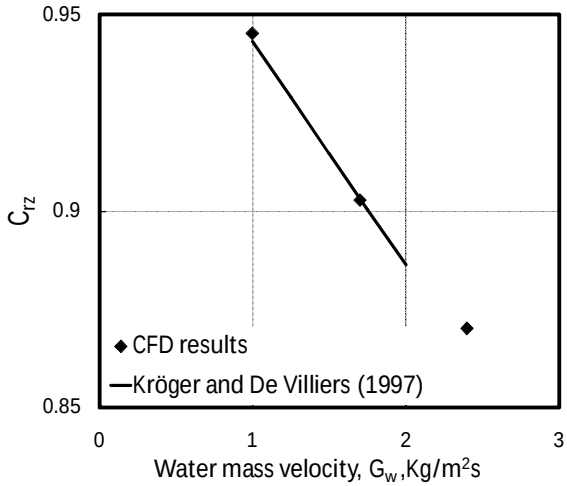

Figure 5.8: Inlet loss correction factor for the induced draft rectangular cooling tower air-inlet model and empirical relation from Kröger and De Villiers (1997)

5.3 Induced draft HDWD basin CFD modelling

Induced draft HDWD collecting basins are modelled with CFD to find the flow characteristics. As shown in Figure 5.2 two basin types are considered, namely a single basin (V-shape, W-shaped and rectangular-shaped) with one lateral inlet per side and a cascaded basin design (V-shape and rectangular-design), which has two or more lateral inlets. The CFD model is used to do a parametric study on different basin designs.

5.3.1 Single collecting basin design model setup

For the induced draft case air is drawn in from the bottom of the array of air-cooled condensers. As shown in Figure 5.9 some air is drawn in to pass through the finned tubes and the rest passes through the basin inlet and the delugeable bundle. A generic model is prepared in FLUENT® for the V-shape basin. The model is setup with a symmetry line on the HDWD centreline to reduce the computing resources needed. Another symmetry line is used on the left side of the domain to compensate for the adjacent air-cooled condenser street.

The width of the domain is 5.32 m, while the delugeable bundle is 2.5 m wide and 0.8 m in height. The air domain is large enough to model stagnant ambient air entering from the bottom. There is no pressure gradient in the inlet domain itself. There are two outlets namely outflow 1 and outflow 2. The outflow 1 is air passing through the delugeable bundle, while outflow 2 allows air to flow over the finned tubes. The HDWD is modelled as a porous medium with the reference loss

coefficient (K_{he}) taken from experimental work done by Anderson (2014) on the characteristics of the delugeable bundle.

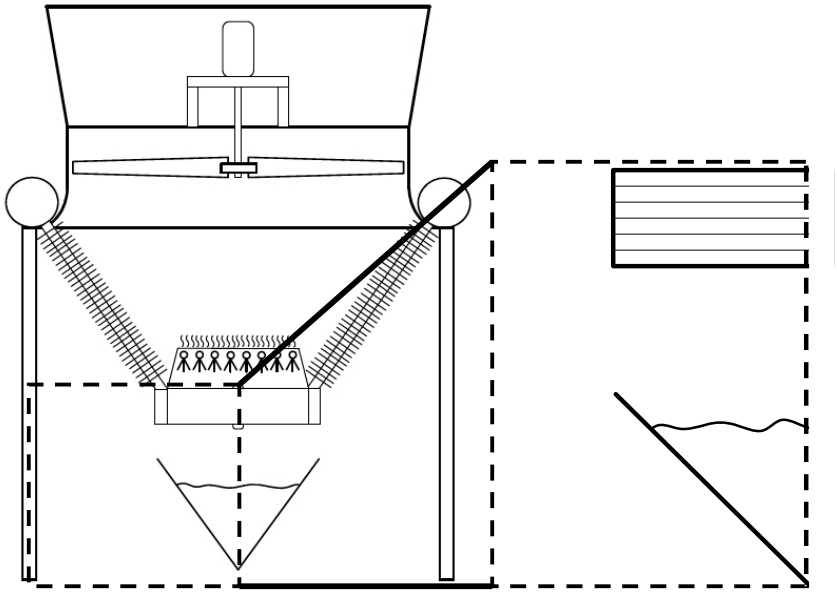

Figure 5.9: Induced draft symmetrical model layout

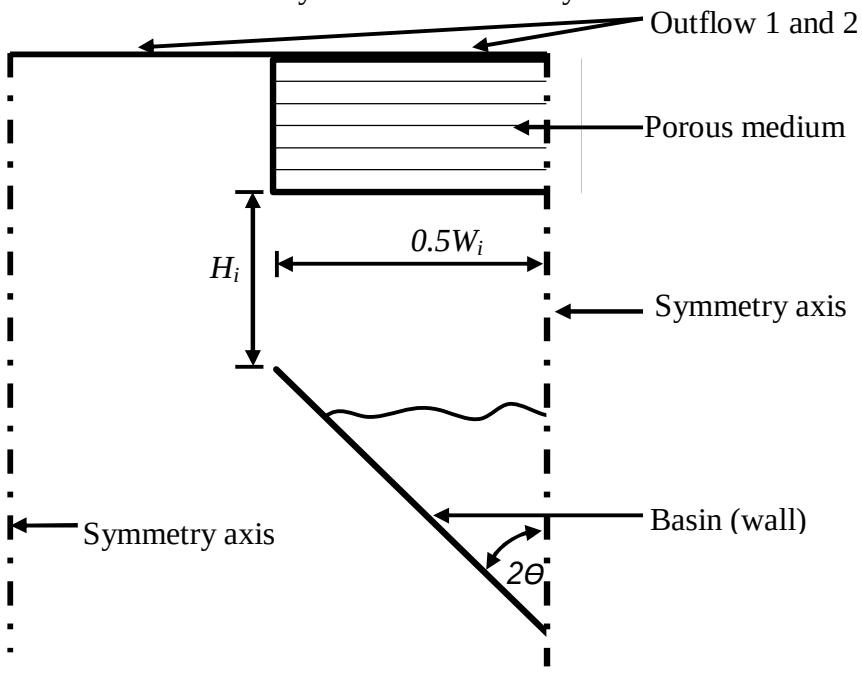

Figure 5.10: CFD model setup and boundary conditions for the induced draft basin

The discrete phase model (DPM) is used in FLUENT® to simulate the wet operation with the rain-zone. The air outflow 1 is set as the inlet for the rain-zone and the water drops are trapped in the basin. The water basin has a maximum

capacity of 6.25 m^3 per meter along the length. The spherical drag law is used with a uniform drop distribution. The drop diameter is set to 4 mm as discussed in section 2.3, and the water mass velocity (G_w) is varied between 1 and 2.4 kg/m^2s. The geometry parameters are varied for the wet operation models similar to what is done with the dry operation.

5.3.2 Single collecting basin design results

As mentioned above a W-shaped and rectangular-shaped basin were considered, but discarded due to the high loss coefficient. Shown in Figure 5.11 (b) is the W-shaped basin geometry with two large areas of flow separation and also a greater inlet velocity at the top edge in the vicinity of the wall. From the results it is decided to discard the W-shaped collecting basin and investigate the V-shaped basin in more detail. Sample calculations for the loss coefficient of the induced draft basin are shown in Appendix F. Tests with rounded inlets were also considered, but it was noted that because the air enters from the south (bottom) boundary of the domain, the air flows vertically upwards, after which it is turned to enter the basin laterally and leave vertically. The rounded inlets obstruct the natural flow of the air flowing into the basin inlet subsequently increasing the loss coefficient.

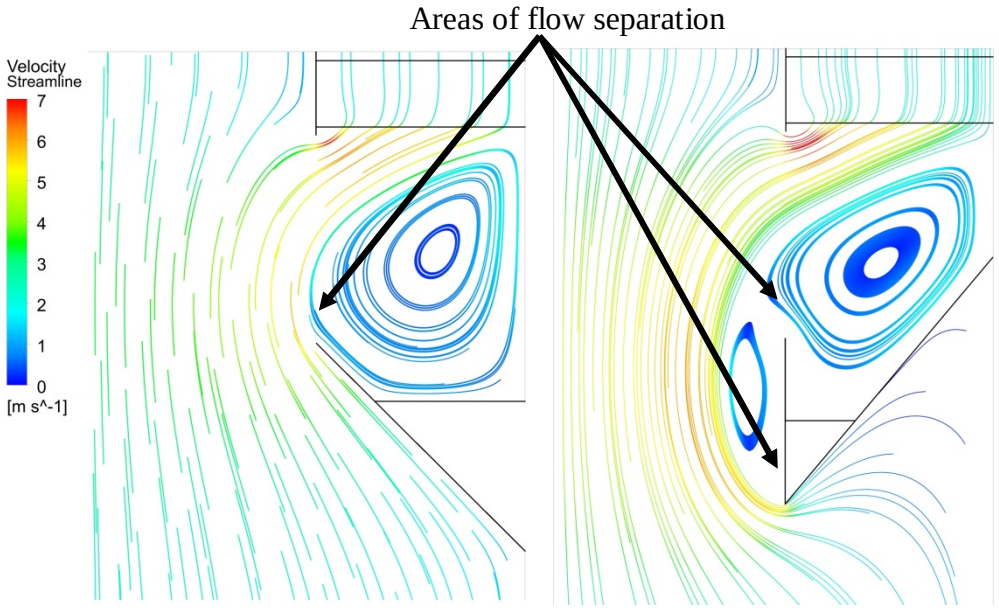

(a) V-shape (b) W-shape

Figure 5.11: Velocity path lines showing the flow separation

For this investigation the V-shaped basin has a reference case where the half inlet width to inlet height ratio ($0.5W_i/H_i$) is 1, the basin angle (Θ_{db}) = 90, and the heat exchanger has a loss coefficient (K_{he}) of 38. The water level inside the water basin had no significant effect on the loss coefficient and therefore was discarded for

the parametric study. The discrete phase model (DPM) in FLUENT® is used to add a rain-zone. This is done to see the effect a rain-zone will have on the inlet loss coefficient ($K_{db(wet)}$) and to find an empirical relation for wet operation. See Appendix F for a sample calculation of the loss coefficient of the rain-zone. In Figure 5.12 below, the regression curves for the induced draft V-shaped basin is shown. The data regression curves have a R^2 value of 0.99, confirming a good curve fit.

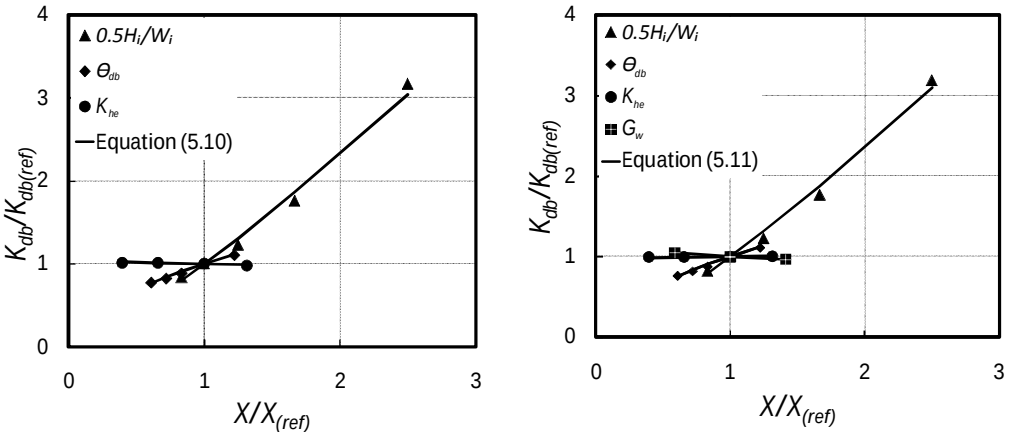

(a) Without rain-zone (b) With rain-zone

Figure 5.12: Inlet loss coefficient regression curves for the induced draft layout

The following empirical relation is proposed for the induced draft V-shaped single basin inlet loss coefficient without a rain-zone.

$$K_{db(Dry)} = 0.801\left(0.5\frac{W_i}{H_i}\right)^{1.22} \Theta_{db}{}^{0.539} K_{he}{}^{-0.026} \tag{5.10}$$

valid for $0.8 \leq 0.5W_i/H_i \leq 3$, $55 \leq \Theta_b \leq 110$ and $15 \leq K_{he} \leq 50$.

and with a rain-zone present:

$$K_{db(Wet)} = 0.619\left(0.5\frac{W_i}{H_i}\right)^{1.23} \Theta_{db}{}^{0.552} K_{he}{}^{0.017} G_w{}^{-0.091} \tag{5.11}$$

valid for $0.8 \leq 0.5W_i/H_i \leq 3$, $55 \leq \Theta_{db} \leq 110$, $15 \leq K_{he} \leq 50$ and $1 \leq G_w \leq 2.4$ kg/m^{2}s.

5.3.3 Cascading collecting basin design model setup

The following is a discussion of the two cascaded basin designs for the induced draft configuration, V-shaped and rectangular shaped respectively. The cascaded design can only be used with the induced draft layout due to space constraints. The cascaded design has a lower collection point for the water, which means more

pumping power is required to overcome the elevation difference. The geometric parameters of the cascaded V-shaped basin design are shown in Figure 5.13. For this investigation the basin has a reference case where the half inlet width to inlet height ratio ($0.5W_i/H_i$) is 1.3, the half inlet width to inlet height$_2$ ratio ($0.5W_i/H_{i2}$) is 5 and the heat exchanger has a loss coefficient (K_{he}) of 38. The water falls under gravity onto a splash plate with a guide plate at the bottom edge. The splash plate is at a 45 degree angle and the guide plate is 100 mm in length as shown. The basin has a maximum capacity of 3 m^3 per meter length.

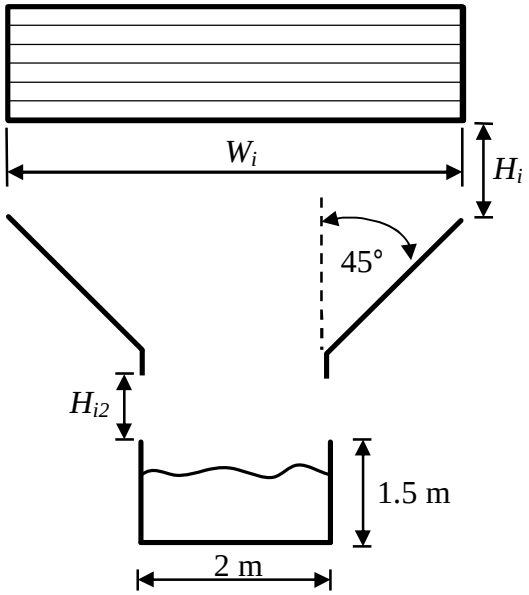

Figure 5.13: V-shaped cascaded design with two lateral inlets per side

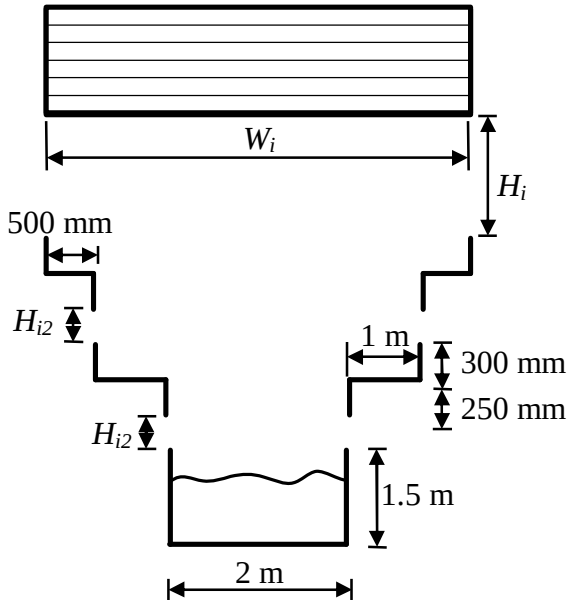

Figure 5.14: Rectangular shaped cascaded design with three lateral inlets per side

The rectangular shaped cascaded basin is shown in Figure 5.14. The segments act as splash plates for the water falling under the force of gravity. The splash plates direct the water to the collection area in the middle of the basin. The basin has a maximum capacity of 3 m^3 per meter length. For this investigation the basin has a reference case where the half inlet width to inlet height ratio ($0.5W_i/H_i$) is 1.3, the half inlet width to inlet height$_2$ ratio ($0.5W_i/H_{i2}$) is 5 and the heat exchanger has a loss coefficient (K_{he}) of 38.

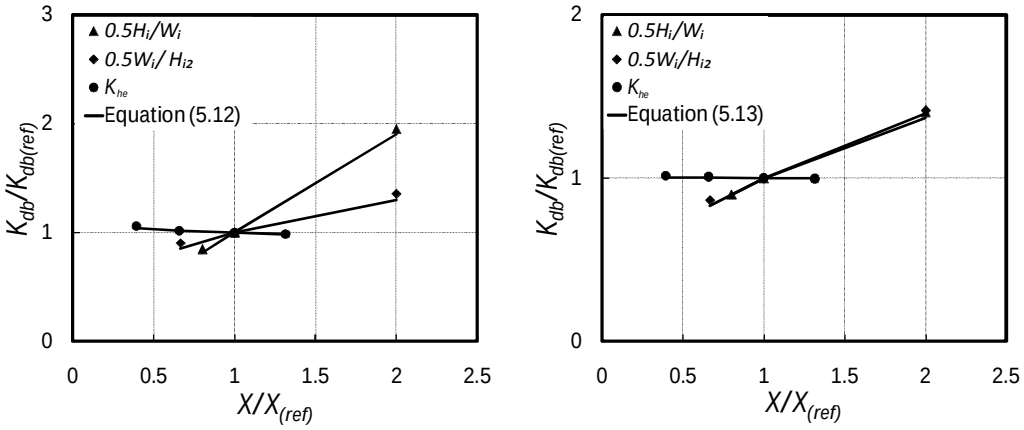

(a) V- shaped design (b) Rectangular design

Figure 5.15: Basin inlet loss coefficient regression curves for the cascaded designs

The following relation (equation 5.12) is proposed for the V-shaped cascaded basin. The effect of the water depth has been neglected for this simulation as it is too small to have an effect on the inlet loss coefficient.

$$K_{db,cv} = 2.689\left(0.5\frac{W_i}{H_i}\right)^{0.927}\left(0.5\frac{W_i}{H_{i2}}\right)^{0.384} K_{he}{}^{-0.043} \qquad (5.12)$$

valid for $1 \leq 0.5W_i/H_i \leq 2.5$, $3.3 \leq 0.5W_i/H_{i2} \leq 10$, and $15 \leq K_{he} \leq 50$

The following relation (equation 5.13) is proposed for the rectangular cascaded basin design. Similar to the V-shaped design, the water depth is neglected as the effect is too small.

$$K_{db,cr} = 1.517\left(0.5\frac{W_i}{H_i}\right)^{0.48}\left(0.5\frac{W_i}{H_{i2}}\right)^{0.457} K_{he}{}^{-0.0063} \qquad (5.13)$$

valid for $1 \leq 0.5W_i/H_i \leq 2.5$, $3.33 \leq 0.5W_i/H_{i2} \leq 10$, and $15 \leq K_{he} \leq 50$

5.4 Forced draft HDWD basin CFD modelling

5.4.1 Single collecting basin design

In Figure 5.16 the layout of the forced draft HDWD with a collecting basin can be seen. The air is forced through the fin tubes of the condenser and the lateral basin inlet by the fan. Both the fin tube and the HDWD are modelled as a porous medium in FLUENT®. The correlation (equation 2.3) for the loss coefficient (K_{ft}) of the condenser finned tubes is obtained from Kröger (2004).

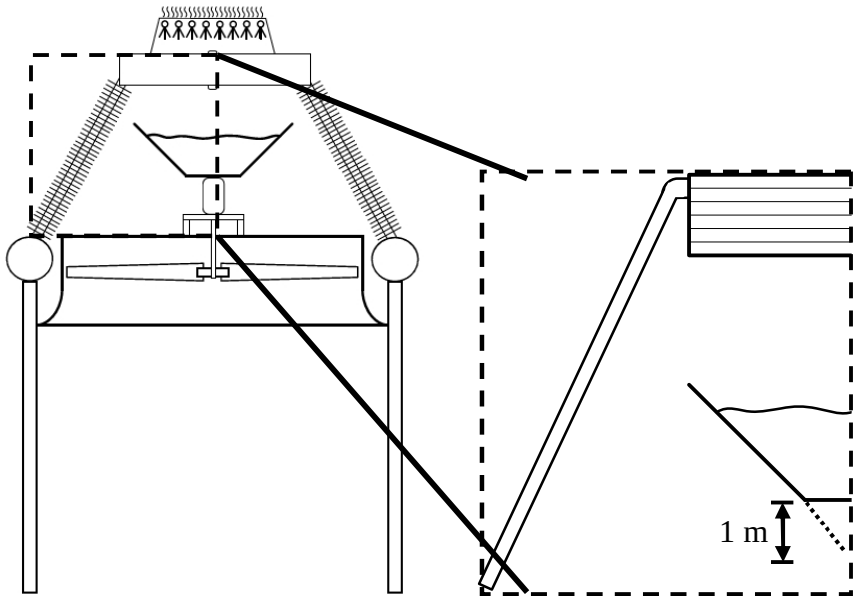

Figure 5.16: Forced draft symmetrical model layout

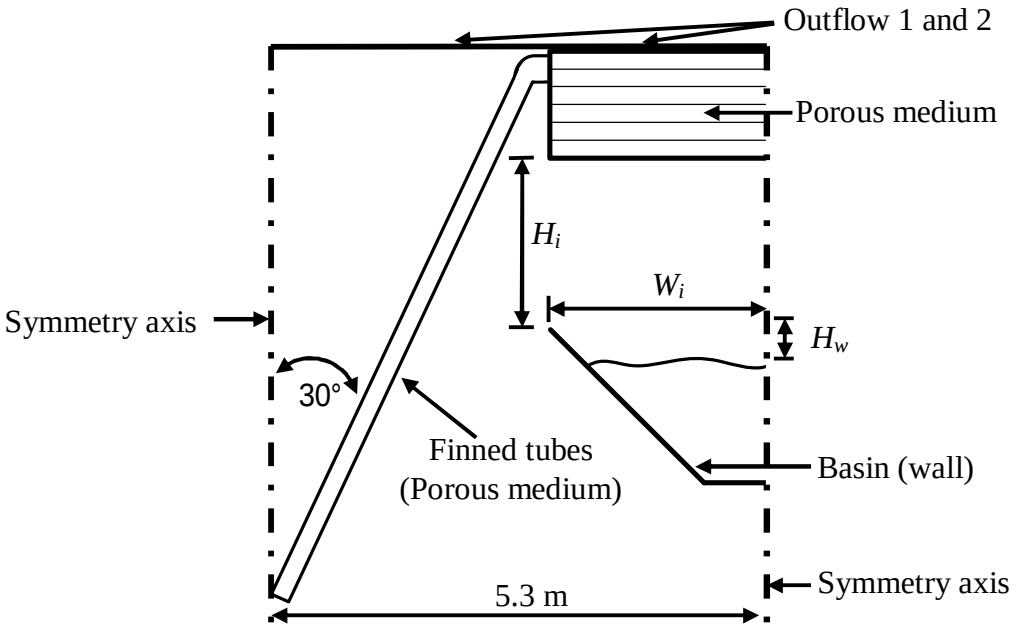

Figure 5.17: CFD model setup and boundary conditions for the forced draft basin

A symmetrical model is setup in FLUENT® for the forced draft layout. With regards to the geometry the model is the same as for the induced draft, apart from the finned tube which is seen in Figure 5.17. The standard for the condenser finned tubes are set at 30 degrees to the vertical and have a depth of 240 mm as taken from Kröger (2004). The finned tube causes a reduction in flow area at the inlet of the basin inlet. As mentioned, with the forced draft layout, space is needed to accommodate the fan motor and walkway above the fan; therefore the basin has a 1m cut out from what is used for the induced draft, which reduces the water capacity to 5.25 m^3 per meter of length as shown in Figure 5.16.

5.4.2 Single collecting basin design with a numerical fan model

The pressure jump method (PJM) is applied to the forced draft design. The PJM in FLUENT® is implemented to simulate the effect a fan will have on the flow patterns of the forced draft layout. This is done to ensure the above boundary condition (mass flow inlet) is a true reflection of the reality. The (PJM) function makes use of a static-to-static pressure increase, across a line (with a 2-D model) which represents the fan rotor. The amount, by which the pressure is increased, is a function of the volume flow rate passing through the plane. The PJM is simplified method with a minimal amount of information needed. The PJM is built on the published fan performance curves by the fan manufacturer. Details on the fan used for the PJM can be found in Appendix E. The PJM ignores the variation in blade properties along the length of the blade. The PJM is not a perfect simulation of how a fan would perform under the given circumstances, but a good indication on what the pressure contours might look like.

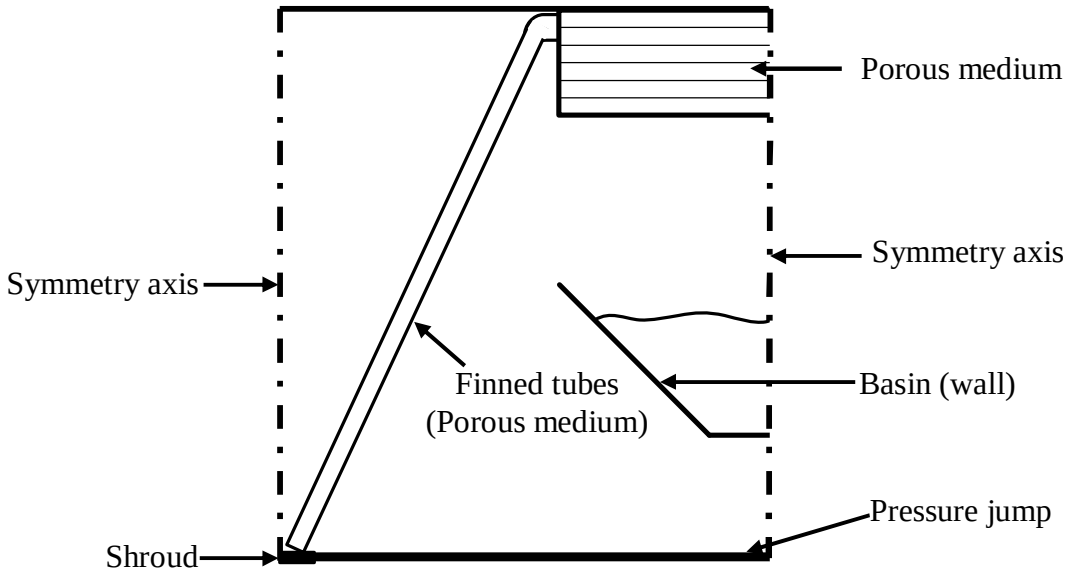

Figure 5.18: CFD model setup and boundary conditions for the forced draft basin with the numerical fan model

The model geometry and layout is the same as the forced draft model setup discussed above, with the addition of a line, representing a numerical fan. The fan casing has a diameter of 9.17 m. In the model a solid is used to replicate the shroud of the fan, to prevent flow recirculation at the tip of the fan blades

A 3rd order polynomial curve fit, shown in equation (5.14), is used to predict the pressure jump at a specific point along a surface similar to what is used by Owen (2010) for an air cooled condenser simulation. The 3rd order polynomial curve fit is in terms of total pressure (atmospheric pressure) upstream of the fan and static pressure downstream of the fan. Van der Spuy and von Backström (2009) showed an explicit method for the use of the PJM by converting the fan total-to-static pressure characteristics of the fan to static-to-static pressure.

$$\Delta p_{f(t-s)} = 320.0452 - 0.2975V_a + 6.3515 \times 10^{-4}V_a^2 - 8.14 \times 10^{-7}V_a^3 \text{ , N/m}^2 \quad (5.14)$$

The polynomial curve fit is needed in terms of velocity (normal to the pressure jump plane) for the pressure jump method in FLUENT®. The volumetric flow rate can be expressed in terms of velocity and area, where the fan's cross sectional area as shown in equation (5.15) below.

$$A_f = \pi(r_{shroud}^2 - r_{hub}^2) = \pi(4.585^2 - 1.83^2) = 55.53 \text{ m}^2 \quad (5.15)$$

and $v = \dot{V}/A$, m/s (5.16)

Therefore:

$$\Delta p_{f(t-s)} = 320.0452 - 16.52v + 1.96v^2 - 0.14v^3 \text{ , N/m}^2 \quad (5.17)$$

The PJM function in FLUENT® requires an input of static-to-static pressure function as shown in equation (5.18) below.

$$p_{s1} - (p_s + p_d)_2 = p_{f(t-s)}$$

$$p_{s1} - p_{s2} = p_{f(s)} + p_{d2}$$

$$p_{s-s} = p_{f(t-s)} + p_{d1} \quad (5.18)$$

The bell mouth inlet losses (K_i) are taken into account from Idelchik (1994), where the inlet loss coefficient is determined in terms of shroud flow area, as shown by Van der Spuy (2011) with equation (5.19) below. Now the following equation can be used assuming an air density of 1.2 kg/m^3. Therefore equation (5.20) is used in the PJM function of FLUENT®.

$$K_i = K_{iOD}\frac{A}{\pi r_s^2} = 0.095\frac{55.53}{66.04} = 0.079 \quad (5.19)$$

$$p_{s-s} = p_{f(t-s)} + (p_d)_2 + p_{inlet\ losses}$$

$$p_{s-s} = 320.0452 - 16.52v + 1.96v^2 - 0.14v^3 + \frac{1}{2}\rho v^2 + \frac{1}{2}\rho v^2 K_i$$

$$p_{s-s} = 320.0452 - 16.52v + 1.96v^2 - 0.14v^3 + \frac{1}{2}1.2v^2 + \frac{1}{2}1.2v^2 0.079$$

$$p_{s-s} = 320.0452 - 16.52v + 2.6074v^2 - 0.14v^3 \quad (5.20)$$

5.4.3 Single collecting basin design results

The single basin forced draft with the pressure jump model has the same reference values as the forced draft model discussed in section 5.4.1.

The regression curves for the forced draft V-shaped basin are shown in Figure 5.19 below. The inlet height and basin angle has the prominent effect on the basin inlet loss coefficient. The following empirical relation is proposed for the forced draft V-shaped basin inlet loss coefficient under dry conditions.

$$K_{db(Dry)} = 1.951\left(0.5\frac{W_i}{H_i}\right)^{1.274} \Theta_b{}^{0.447} K_{he}{}^{-0.033} K_{ft}{}^{0.064} \quad (5.21)$$

valid for $0.8 \leq 0.5W_i/H_i \leq 3$, $55 \leq \Theta_b \leq 110$, $15 \leq K_{he} \leq 50$ and $15 \leq K_{ft} \leq 30$.

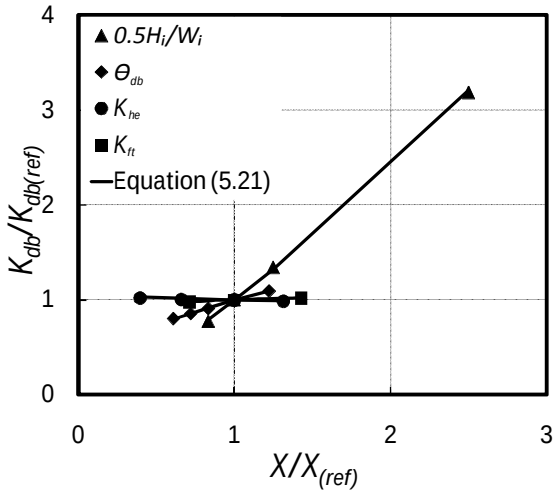

Figure 5.19: Inlet loss coefficient regression curves for the dry forced draft layout

5.4.4 Single collecting basin design with a numerical fan model results

The results from both models are compared. The basin inlet loss coefficient and the flow path lines are looked at when analyzed. In Figure 5.20 below the CFD results for the velocity path lines can be seen for a forced draft layout with (a) the mass flow inlet and (b) the numerical fan model with an inlet height of 1.5 m. The

inlet height of 1.5 m is used for the comparison as the reduction in inlet height amplifies changes in velocity and pressure. There is a good agreement between the inlet loss coefficients (K_{db}) of the two models. The inlet loss coefficient for the model with the mass flow inlet is seen to be 30.73 while the loss coefficient for the model with the numerical fan is 30.8. From the numerical results discussed, it can be reasoned that the inlet boundary with a mass flow inlet delivers similar results as the model with the numerical fan.

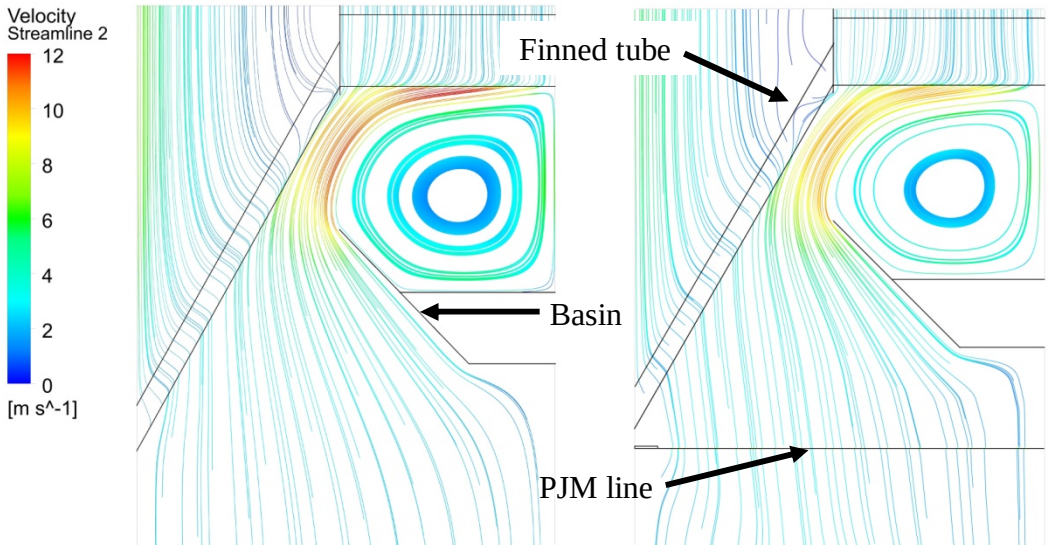

(a) Mass flow inlet (b) Numerical fan model

Figure 5.20: Velocity path lines for the single basin forced draft design with a 1.5 m inlet height

5.5 Summary of results

The validated two-dimensional symmetrical CFD model is used to explore different collecting basin designs for both induced and forced draft HDWD designs. The basin is deployed under a delugeable bundle to collect deluge water before the water is pumped back to the sprayers. The results are summarized in Table 5-1.

Table 5-1: Comparison of the basin designs for the reference cases (dry)

Basin design	**Draft type**	**Loss coefficient, K_{db}**	**Pumping head, h_p, m**
Single-V	Induced	8.3	6
Cascaded-V	Induced	5.16	5
Cascaded-R	Induced	4.25	6.5
Single-V	Forced	15.3	5

The grid size used for the simulations is 0.8 % of the width of the delugeable bundle. Good agreement is found between the CFD results and the experimental results for the rectangular cooling tower. A monodisperse droplet distribution is used to simulate a rain-zone. The results from the rain-zone are compared to an empirical relation, showing a good agreement. A good agreement between the CFD results and the inlet correction factor (C_{rz}) for rectangular cooling towers from Kröger and De Villiers (1997) are found.

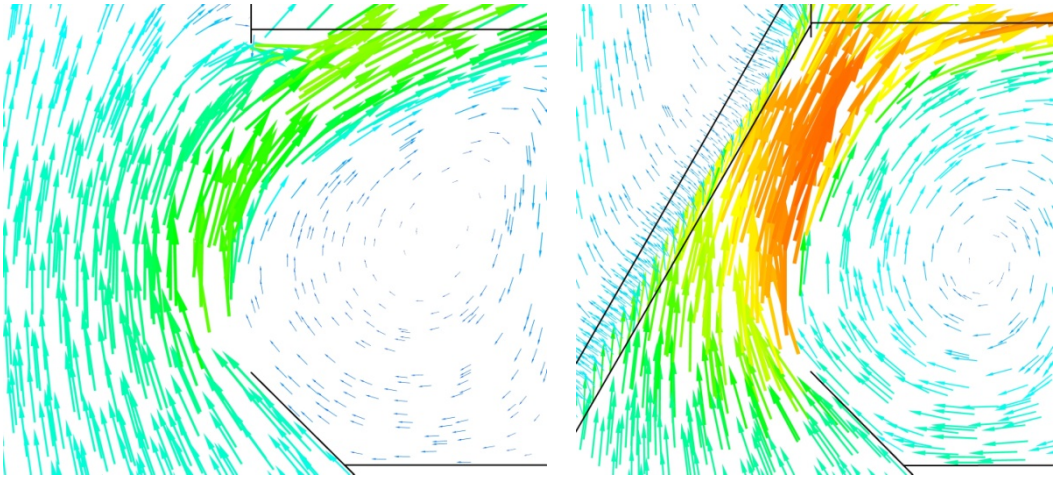

(a) Induced draft (b) Forced draft

Figure 5.21: CFD velocity vector diagrams basin comparison for $0.5W_i/H_i = 1$

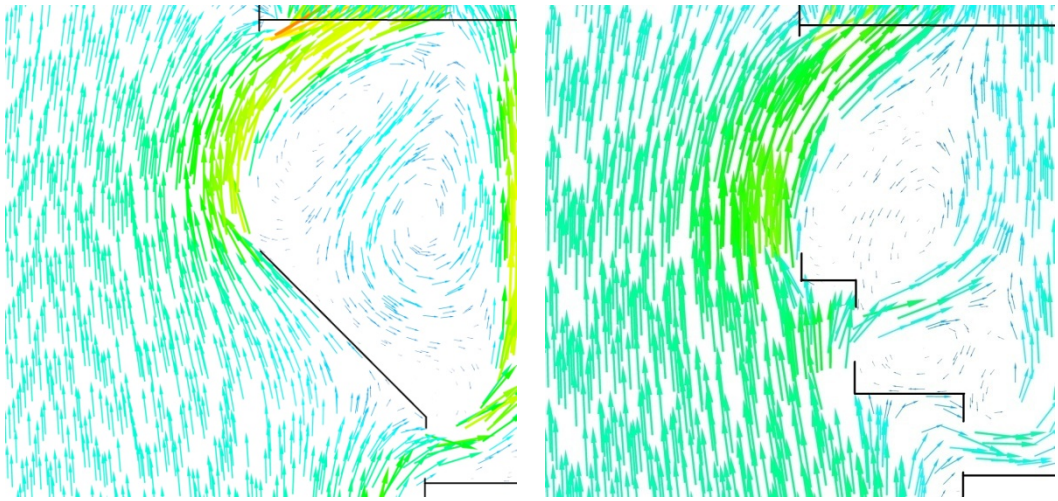

(a) V-shaped cascaded basin (b) Rectangular cascaded basin

Figure 5.22: CFD velocity vector diagrams cascaded basin comparison for $0.5W_i/H_i = 1$

Decreasing the basin angle makes the basin more streamline as the air flows around the outside. The water level inside the basin had a weak effect on the

empirical inlet loss coefficient and therefore it was discarded. The single basin induced draft layout has the lowest inlet loss coefficient = 8.3 for the single basins. The cascaded basin design has a lower inlet loss coefficient when compared to the single basin which is 5.16 and 4.25 for the V-shaped and rectangular cascaded basin respectively. The effect of the PJM is seen to be insignificant for this model. The velocity vector diagrams in Figure 5.21 and Figure 5.22, for the induced and forced draft system shows the reduction in inlet area with the forced draft design due to the finned tubes.

5.6 Conclusion

The lateral air inlet of a rectangular cooling tower is modelled in CFD and the data is compared to experimental work in Figure 5.4 to show the accuracy of the CFD model. The model is not sensitive to change in the mesh element size, within the mesh element size range of 50 to 20 mm. The k-ε Realizable turbulence model is used, and is an improvement on the standard k-ε turbulence model and Reuter (2010) found that the k-ε Realizable turbulence model produced similar results to the experimental data of Kröger and Terblanche (1994) at the tower inlet. There is a maximum of 4 % deviation between the experimental and CFD model results. The validation done with the CFD models provide confidence in the results.

The collecting basin should be made streamline (V-shaped) to reduce losses as the air flows from the bottom over the outside of the basin. An induced draft rectangular tower with $(0.5W_i/H_i) = 1$ has a loss coefficient of 1.1 and for the same case an induced draft V-shaped single basin inlet has a loss coefficient of 8.3. The HDWD forced draft basin design has a higher inlet loss coefficient of 15.3. The greater loss coefficient is due to the reduction in inlet area caused by the finned tubes at the basin inlets as shown in Figure 5.21. The forced draft basin design also has space constraints under the basin, due to the fan motor and walk way. The cascaded HDWD induced draft basin design has an inlet loss coefficient of 5.16 and 4.25 for the V-shaped and rectangular cascaded basin respectively. This is due to the increased lateral inlet area. The cascaded basin can only be used for the induced draft design due to space constraints. The rain-zone inlet loss correction factor (C_{rz}) can be used to correct for the effect the rain-zone has on the basin inlet loss coefficient. This can be used where inlet loss coefficient of only dry operation is given. Due to the large inlet loss coefficient of the forced draft design and the space constraints it is recommended that the collecting basin option is best suited for an induced draft HDWD design as there can be seen from the results and in Figure 5.21. The empirical relations for the different collecting basins are given to predict the air-side pressure drop through the collecting basin inlet. The volume of the deluge water needed to run the HDWD is needed to specify the volume of the collecting basin. If the basin cannot accommodate all the deluge water when the system is running dry a make-up tank can also be used in conjunction with the collecting basin as a holding tank for the deluge water.

6. COMPARATIVE SYSTEM ANALYSIS AND DESIGN GUIDELINES

6.1 Introduction

In this chapter the water trough and water basin systems are compared in terms of energy consumed over a year of operation, from both the air resistance and the elevation difference that needs to be overcome. The comparison is done to find the best balance between energy consumed by the fan (air-side) and the deluge water pump (water-side) to overcome the elevation difference between the collection point and the sprayers. From the information gathered in Chapter 4 and 5 it is seen that by scaling the size of a water collection system the loss coefficient (K) may be decreased, which subsequently increases the required water pumping head and vice versa. Furthermore this chapter provides guidelines and recommendations for a design engineer to assist with the selection of the system and the geometry the design and the selection of a specific design.

6.2 Water collection system comparison

After the deluge water is collected by either the water troughs or the water basin system it is drained to the lowest point of the collection system from which it is pumped back to the sprayers. The elevation difference will depend on the water collection system design. A summary of the loss coefficients and pumping head required for the different systems are shown in Table 6-1 below.

Table 6-1: Summary of input values for the comparison

System type	Design	Draft	Case	Loss coefficient, K	Pump head, h_p, m
Single basin	V-shaped	Induced	Ref case	8.3	6
Single basin	V-shaped	Induced	$0.5W_i/H_i$ = 0.8	6.4	6.5
Cascaded basin	V-shaped	Induced	Ref case	5.16	5
Cascaded basin	Rectangular	Induced	Ref case	4.25	6.5
Single basin	V-shaped	Forced	Ref case	15.3	5
Trough	Δx = 40 mm	Both	Ref case	7.4	0.99
Trough	Δx = 40 mm	Both	H_{tr} = 145 mm	3.65	1.045
Trough	Δx = 40 mm	Both	H_{tr} = 250 mm	1.76	1.15

For comparison it is assumed that the fan has an efficiency of 60 % and the deluge water pump has an efficiency of 80 %. It is assumed that the fan runs throughout the year while the deluge water pump is only used when needed. The air flows at 2.5 m/s while the deluge water pump delivers 1.7 kg/m^{2}s. The air density is taken at 1.225 kg/m^3. The energy usage of a system will depend on how often the

deluge water pump system is used. The comparison is done for when the deluge system is used 100 % of the year to when it is used 0 % per of the year with 20 % increments. The troughs all have 40 mm spacing between each trough as discussed in Chapter 4. The comparison is only due to inlet losses and water pump head. No other frictional or nozzle losses are taken into account. Equations are also provided to determine the power consumed by the collection system.

6.3 Results

The results of the water troughs and the water basin designs are directly compared to see the energy needed to operate each system over a time span of a year. The results are presented in a graph in Figure 6.1 below. A clear distinction in terms of energy consumed, between the water trough and basin can be seen.

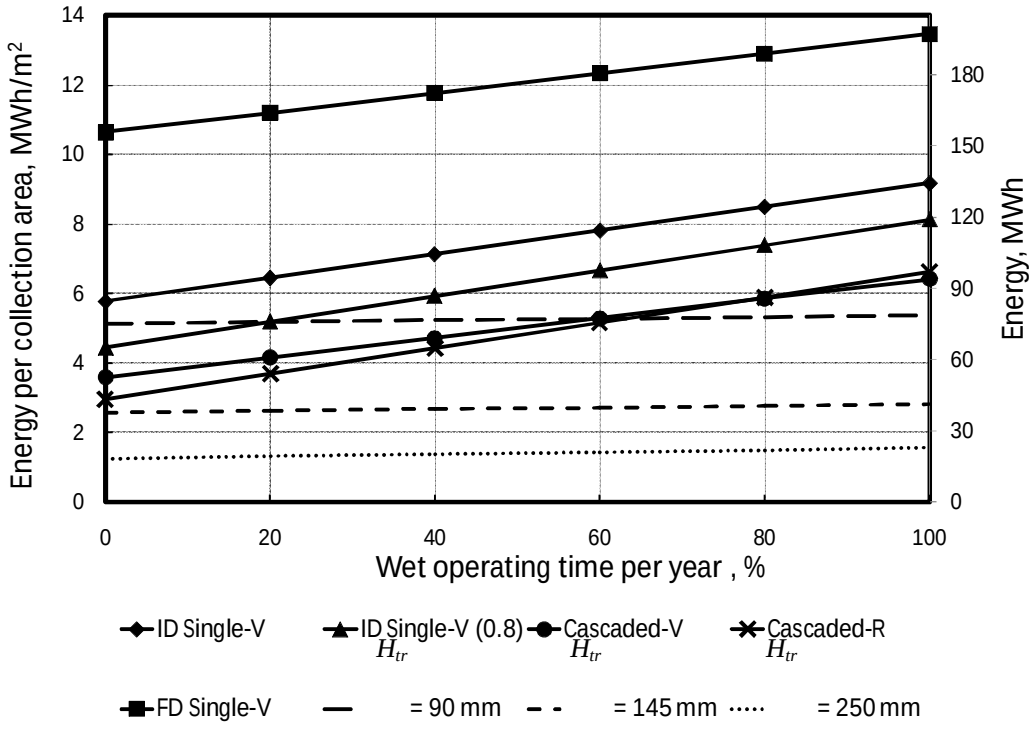

Figure 6.1: Energy consumption per year for the different water collection systems

The forced draft system (K_{db} = 15.3) is the most energy intensive while the 250 mm water trough (K_{tr} = 1.76) has the lowest energy consumption. The air velocity has an exponential effect on the energy consumption while the water height difference has a linear effect on the energy consumption. Equation (6.3) is used to estimate the energy consumption of a generic water collection system when the loss coefficient and water height is known. It is noted that the air velocity has the major effect on the energy consumed by the system.

$$\frac{P_f}{A_{db}} = \frac{\frac{1}{2}K\rho_a v_a^3}{\eta_f} \text{ ,W} \tag{6.1}$$

$$\frac{P_p}{A_{db}} = \frac{(\dot{m}_w \rho_w g H_w)}{(A_{db}\rho_w \eta_f)} = \frac{G_w g H_w}{\eta_f} \text{ ,W} \tag{6.2}$$

$$\frac{P_t}{A_{db}}\Delta t = \left(\frac{\frac{1}{2}K\rho_a v_a^3}{\eta_f} + (\%\, wet)\frac{G_w g H_w}{\eta_f}\right)\Delta t, \text{ kw.h} \tag{6.3}$$

6.4 Discussion of result

The total amount of energy consumed by the water collection system is dependent on how often the deluge water pump is used. This may vary with peak loading, seasons of the year, climate etc. The fan will run all the time, while the deluge system will run when necessary. The air velocity has the greatest effect on the energy usage of such a system.

The water troughs have the lowest loss coefficient and therefore the lowest energy consumption when compared to the water basin system. By increasing the inlet height of the water basin system the loss coefficient is decreased, but the pumping head is increased.

6.5 Design guidelines

Following in this section are guidelines on how a water collection system should be selected by a design engineer according to the results and findings in this thesis. In Figure 6.2 a process is shown on how the water collection system is selected.

The water collection system can be selected after the HDWD design is finalized. The cascaded basin should be used with a forced draft system due to space constraints and high loss coefficient. The water trough system is favoured over the basin system, due to the small loss coefficient. The water trough, single basin and cascaded basin designs may work with the induced draft system.

If the water mass velocity (G_w) exceeds 2.4 kg/m^{2}s the water troughs will not drain the water off at a sufficient rate, unless the angles of the troughs are exceeding 7 degrees. To reduce the water depth in the channels, which prevents splashing, the water troughs could be used with a water mass velocity up to 2.4 kg/m^{2}s. The trough depth can also be increased to accommodate more water, but a channel full of water may cause splashing. A water basin system will be able to accommodate most water mass velocity if the collection tank has sufficient capacity.

Next the dimensions of the system can be selected which is dependent on the dephlegmator size. The dimensions will influence the loss coefficient, therefore

the dimensions can be optimized to obtain a given loss coefficient by using the proposed correlations discussed in Chapter 4 and 5. The loss coefficient can be optimized to reduce the operating cost of the water collection system.

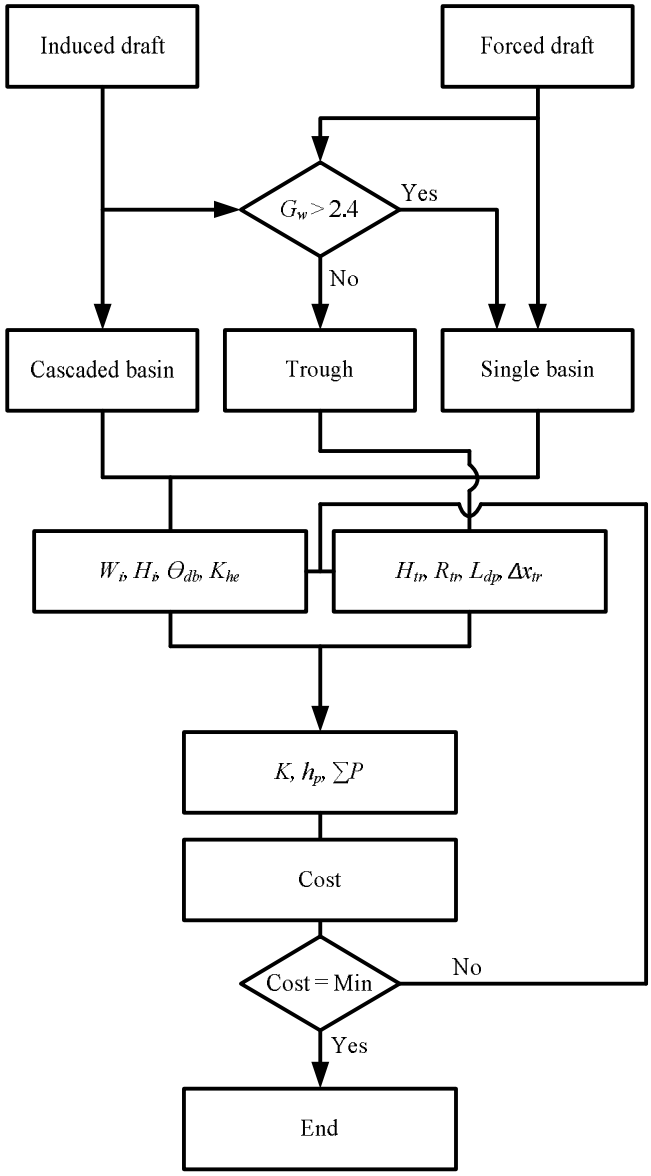

Figure 6.2: Design and system selection process diagram

6.5.1 Trough design recommendations

The water trough system may have the lowest air-side loss coefficient but is more likely to spill or leak water if the design is not done according to the following recommendations. The dimensions of the reference case are shown in Figure 4.4 in section 4.2. The deflector plate should have a minimum length of 30 mm and the overlap between the deflector plate and the next trough should be 10 mm as

shown in Figure 4.13 (i.e. Δx_{tr} = 40 mm) This will ensure the water drops are deflected onto the neighbouring water trough. The water channel should have a minimum radius of 10 mm. The dimensions may be varied as discussed in Chapter 4 to optimize the loss coefficient.

As shown in Chapter 4, the angle of the water troughs channels should be set between 3 and 7 degrees, depending on the water mass velocity of the design. The steeper the trough angle the better the water will be drained off. The channel depth can be increased to accommodate more water, but this may cause splashing as water is falling into the channel.

The frontal area of the troughs should be larger than that of the rain-zone (dephlegmator tube bundle) to prevent wall effects and localized flooding of the troughs. The troughs cannot store the water like the collecting basin design and therefore a large makeup tank is needed at the trough outflow to hold the water needed to run the HDWD system.

The water troughs can be supported from the bottom with slats running along the length of the trough. Shown in Figure 6.4 are the supporting slats and a stiffening rod. This will prevent water from adhering to the support structure and dripping off. This will also prevent the support structure to interfere with the deluge water flow.

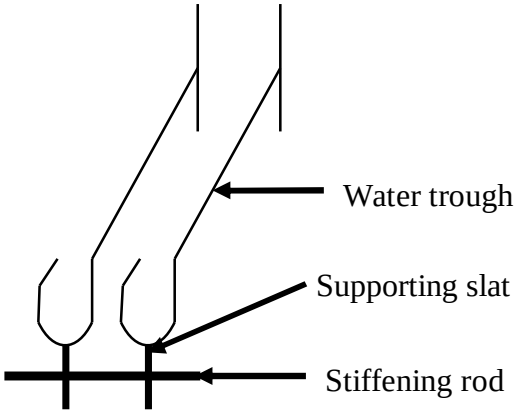

Figure 6.3: Water trough with support slats

6.5.2 Basin design recommendations

The V-shaped HDWD collecting basin geometry is discussed in Chapter 5. A collecting basin is effective in collecting water and will not have leakage problems. Water will not splash out of the basin inlets due to the angle of the basin wall and the air flow, dragging the water drops inwards. This effect is shown in Figure 6.4 below. Wind may have an effect but this can be solved by adding a wind shield in the middle of the water basin supported from the top. A wind shield will prevent water from being blown out of the basin.

The basin size will depend on the size of the delugeable bundle. The capacity of the basin is dependent on the design and size. The total volume of the water for the deluge system is required to design the basin system. A makeup tank can assist the basin in accommodating all the deluge water needed to operate the HDWD system.

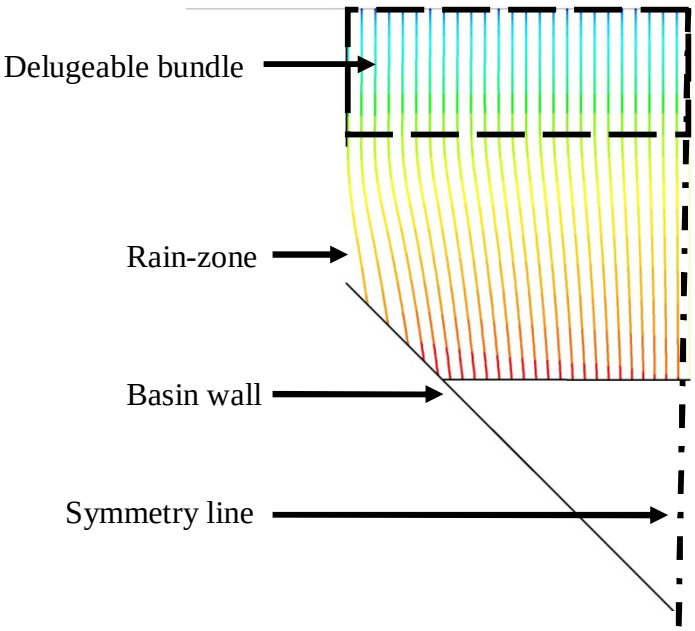

Figure 6.4: Water basin with a rain-zone and water drop flow path

7. CONCLUSION

A water collecting trough and water collecting basin systems are developed and the performance characteristics are presented in this thesis. The water trough system allows air to pass through vertically between the troughs while the water basin system has lateral air inlets, allowing air to enter laterally and pass through vertically. The water troughs design, identical in design to those in the counter-flow fill test facility at Stellenbosch University, are improved because they are not effective in collecting all the water in the counter-flow section. The experimental results and the CFD models are used to determine the loss coefficient, the deluge water pumping head for design purposes and to make recommendations. The water troughs are tested and analyzed with high speed digital cameras to improve the water collecting performance. The current design is improved by adding a 30 mm protruding deflector plate to the back edge of the trough and the spacing between each trough is reduced to have a 10 mm overlap. The effect of the deflector plate is that the water collection bypass is reduced from 4 % to 0.015 % with trough spacing of 50 mm. No water is bypassed when the trough spacing is reduced to 40 mm. The modified trough has a loss coefficient (K_{tr}) of 7.4. The water channel is tested to find the rate at which water can be drained out of the channel at different angles. The pressure drop over the water troughs is simulated with FLUENT® 14.0. The experimental results from the water trough tests validate the two-dimensional CFD model. The two-dimensional CFD model is used to conduct a parametric study from which an empirical relation is proposed to predict the loss coefficient for design purposes.

FLUENT® is used to develop and investigate a water basin system below the delugeable bundle. The DPM is used to simulate a rain-zone. The results are used to develop an empirical relation for the basin inlet loss coefficient. The CFD model is validated with work done by Kröger and Terblanche (1994) on a rectangular cooling tower inlet with a horizontal heat exchanger. A cascaded basin design is also considered with multiple lateral inlets which increase the inlet flow area subsequently decreasing the inlet loss coefficient. The finned tube from the forced draft layout reduces the flow area at the basin inlet and subsequently increasing the inlet loss coefficient. The induced draft rectangular tower with ($0.5W_i/H_i$) = 1 has a loss coefficient of 1.1 while the induced draft V-shaped single basin inlet as a loss coefficient = 8.3 for the same case and the forced draft basin has an inlet loss coefficient = 15.3. Therefore the basin system is not recommended for the forced draft HDWD layout due to space constraints and a high inlet loss coefficient.

A direct comparison is made between the trough and the basin system in terms of energy consumed by the system. The energy consumed is due to the air resistance of the water collection system and required pumping head. Design recommendations are made in terms of geometry and sizes for each system. The recommendations are important to decrease the loss coefficient and to ensure the troughs do not let water bypass.

8. REFERENCES

Anderson, N.R., 2014, *Evaluation of the performance characteristics of a hybrid (dry/wet) induced draft dephlegmator*. Stellenbosch University.

Bertrand, T.P., 2011, Evaluation *of a 1.5 x 1.5 m^2 counter-flow fill performance test facility with a view to contributing to a fill performance standard*. Stellenbosch University.

Cengel, Y. & Cimbala, J., 2006, *Fluid Mechanics Fundamentals and application*. Mc Graw Hill, Singapore.

Hamon thermal Europe., 2013, *Wet cooling towers: Natural draft cooling towers*. Mont-St-Guiber, Belgium.

Heyns, J.A., 2008, *Performance characteristics of an air-cooled steam condenser incorporating a hybrid (dry/wet) dephlegmator*. Stellenbosch University.

Idelchik, I.E., 1994, *Handbook of Hydraulic Resistance*, 3 rd Edition, Begell House.

Killion, J. D. & Garmimella, S., 2003, *Gravity-driven flow of liquid films and droplets in horizontal tube banks*. International Journal of Refrigeration, 26, 516-526.

Korsell, L., 1984, *Device in an evaporative cooler*. US Patent no 4427607

Kröger, D.G., 2004, *Air-cooled Heat Exchangers and Cooling Towers: Thermal Flow Performance Evaluation and Design*. Tulsa, Oklahoma, USA: PenWell Corporation.

Kröger, D.G. & De Villiers, E., 1997, *Analysis of heat, mass and momentum transfer in the rain-zone of counter-flow cooling towers*. Stellenbosch University.

Lefevre, M.R., 1985, *Drainage collection system*. US patent number 4521350

Oosthuizen, H.R., 1995, *Enhancement of Cooling Tower Performance by Manipulating of Rain-zone Drop Size*. University of Stellenbosch

Owen, M., 2013, Air-cooled condenser steam flow distribution and related dephlegmator design considerations. Stellenbosch University.

Pierce, J.D., 2007, *Evaluation and performance predictions of cooling tower rain zones*. Stellenbosch University.

Reuter, H.C.R., 2010, Performance *evaluation of natural draft cooling towers with anisotropic fills*. Stellenbosch University.

Shih, T., Liou, W., Shabbir, A., Yang, Z. & Zhu, J., 1995, *A new k-e Eddy-viscosity model for High Reynolds number turbulent flows- Model development and validation*. Computer fluids 24(3): 227-238.

Kröger, D.G. & Terblanche, J.E., 1994, *Experimental evaluation of the aerodynamic inlet losses in cooling towers*. Stellenbosch University.

Terblanche, R., 2008, Investigation *of performance enhancing devices for the rain zone of wet-cooling towers*. Stellenbosch University.

Terblanche, R., 2011, *Evaluation of drop break-up after impingement on horizontal slat grids and the effect of drop size of cooling tower rain zone performance*. Stellenbosch University.

Tower Tech, 2011, *Installation, operation and maintenance manual: TTXL series modular cooling tower*. Oklahoma, USA.

Van der Spuy, S.J., von Backström, T.W., & Kröger D.G., 2009, *Performance of low noise fans in power plant air cooled steam condensers.* Noise Control Engineering Journal, 57 (4).

Van der Spuy, S.J., 2011, *Perimeter fan performance in forced draught air-cooled steam condensers*. Stellenbosch University.

Yung, D., & Lorenz, J.J., 1980, *Vapour/Liquid Interaction in and Entrainment in Falling Film Evaporators.* ASME Journal of Heat Transfer, Vol. 102, pp. 20 – 25,

APPENDIX A: THERMOPHYSICAL PROPERTIES OF FLUIDS

A.1 Introduction

The following equations taken from Kröger (2004) are used to determine the fluid properties needed for all calculations in the thesis.

A.2 Thermophysical properties of dry air

The following fluid properties are for dry air from 220 K to 380 K at an atmospheric pressure of 101325 N/m^2.

Air density:

$$\rho_a = \frac{P_a}{287.08 \times T_a} \ , \mathrm{kg/m^3} \tag{A.1}$$

Dynamic viscosity of air:

$$\mu_a = 2.287973 \times 10^{-6} + 6.259793 \times 10^{-8} \times T_a - 3.131956 \times 10^{-11} \times T_a{}^2 + 8.15038 \times 10^{-15} \times T_a{}^3 \ , \mathrm{kg/ms} \tag{A.2}$$

A.3 Thermophysical properties of saturated water liquid

The following fluid properties are for saturated vapour from 273.15K to 380K.

Water density:

$$\rho_w = (1.49343 \times 10^{-3} - 3.7164 \times 10^{-6} \times T_w + 7.09782 \times 10^{-9} \times T_w{}^2 - 1.90321 \times 10^{-20} \times T_w{}^6)^{-1} \ , \mathrm{kg/m^3} \tag{A.3}$$

Dynamic viscosity of water:

$$\mu_w = 2.414 \times 10^{-5} \times 10^{(247.8 \ / \ (T_w - 140))} \ , \ \mathrm{kg/ms} \tag{A.4}$$

Water surface tension:

$$\sigma_w = 5.148103 \times 10^{-2} + 3.998714 \times 10^{-4} \times T_w - 1.4721869 \times 10^{-6} \times T_w{}^2 + 1.21405335 \times 10^{-9} \times T_w{}^3 \ , \mathrm{N/m} \tag{A.5}$$

APPENDIX B: CALIBRATION DETAILS OF THE HIGH SPEED CAMERA

B.1 Introduction

A free falling drop tests is conducted with steel ball bearings in order to confirm theoretical calculations and to calibrate the high speed cameras. Ball bearings are chosen for calibration because they are spherical in shape with a smooth surface and the diameter and mass can easily be measured. The high speed digital cameras are calibrated with a 5 mm by 5 mm grid paper at the focus point recoding at 150 frames per second, therefore a photo is taken every 0.0067 s. The pixels of each block in the grid paper are related to a distance. Three different sizes of steel bearings are recorded to measure the free falling velocity and the results are compared to a theoretical model. Following are the sample calculations for the 3.01 mm steel ball bearing and calibration test results. The calibration is also done with water drops in section B.4.

B.2 Theoretical speed calculation

The theoretical velocity of the ball bearing is calculated with an iterative force balance. The drop height is broken up in 1.25 mm increments (Δy) and the instantaneous forces for each increment are calculated individually to compensate for the acceleration of the ball bearing. The vertically free falling ball bearing has three forces acting on the ball bearing, namely the force of gravity (vertically downwards), the drag force (vertically upwards) and buoyancy force (vertically upwards). Terminal velocity is not reached with the tests conducted for this thesis and therefore the sphere drag coefficient of Turton and Levenspiel (1986) is used for the ball bearings and water drops, similar to what was done by Terblanche (2011) as shown in equation (B.5).

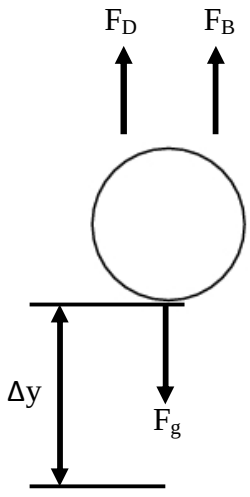

Figure B.1: Free body diagram for a vertically free falling ball bearing

The 3.01 mm ball bearing has a measured weight of 0.11258 g. Firstly the three forces acting on the ball bearing is calculated.

Volume of the sphere:

$$Volume_{bb} = \frac{4}{3}\pi\left(\frac{d}{2}\right)^3 = \frac{4}{3}\pi\left(\frac{0.003006}{2}\right)^3 = 14.2222 \times 10^{-9}, \text{m}^3 \quad \text{(B.1)}$$

Buoyancy force:

$$F_B = Vol_D \rho_a g = 1.42222e^{-8} \times 1.184 \times 9.81 = 0.165246 \times 10^{-6}\ \text{N} \quad \text{(B.2)}$$

Force due to gravity:

$$F_g = m_{bb} g = 0.00011258 \times 9.81 = 1.10441 \times 10^{-3}\ \text{N} \quad \text{(B.3)}$$

Force due to drag:

$$F_D = \frac{1}{2} C_D \rho_a {V_2}^2 A_f = \frac{1}{2}(1.059393)(1.184)(0.49)^2(7.09689 \times 10^{-6})$$

$$F_D = 1.09071 \times 10^{-6}\ \text{N} \quad \text{(B.4)}$$

where C_D is:

$$C_D = 24\frac{(1+0.173Re^{0.657})}{Re} + \frac{0.413}{(1+16300Re^{-1.09})} \quad \text{(B.5)}$$

where Re ≤ 2 x 10^5

The resultant force and ball bearing acceleration between drop height increments:

$$F_R = ma \quad \text{(B.6)}$$

$$a = \frac{F_g - F_D - F_B}{m} = \frac{0.00110441 - 1.09071 \times 10^{-6} - 0.165246 \times 10^{-6}}{0.00011258}$$

$$a = 9.7988\ \text{m/s}^2$$

Instantaneous calculated velocity for each drop height increment due to the acceleration:

$$v_1^2 + u^2 = 2 \times \Delta y \times a \quad \text{(B.7)}$$

$$v_1 = \sqrt{(-u)^2 + 2 \times 0.0125 \times 9.7988} = 0.49\ \text{m/s}$$

The initial guessed velocity (V_2) is varied until the difference between the V_1 and V_2 is as close to 0 as possible and the forces are balanced.

B.3 Ball bearing calibration results

Three different sizes of ball bearings (small, medium and large) are dropped from 500, 1000 and 1500 mm drop heights to measure the velocity and compare it to the calculated velocity. The ball bearings are free falling under the force of gravity with a 5 mm by 5 mm grid as a backdrop. The falling distance is measured per photo frame from which the velocity is calculated. The calibration velocity is measured over both two and three frames to ensure accuracy. In table B.1 below, the three different ball bearings' mass and diameter are shown used for the calculations. The calibration results are shown and the calculated velocity and measured velocity is compared.

Table B.1: Sphere ball bearing measurements

Ball bearing description	**Mass, m_{bb}, g**	**Diameter, d_{bb}, mm**
Small	0.113	3.01
Medium	2.138	8.04
Large	8.49	12.75

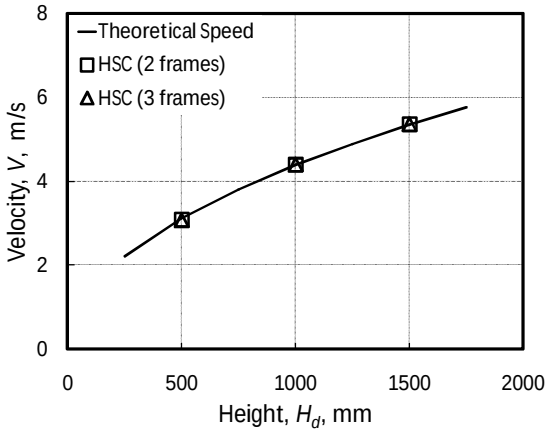

(a) Small ball bearing

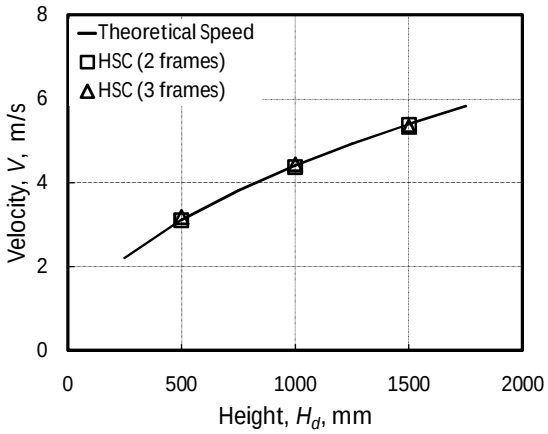

(b) Medium ball bearing

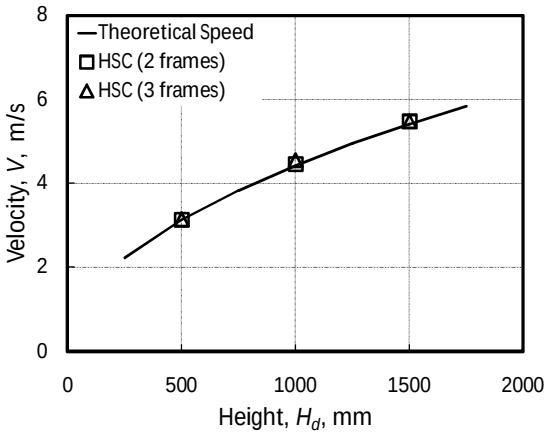

(c) Large ball bearing

Figure B.2: High speed camera calibration test done with different size spheres

B.4 Water drop measurements calibration

According to Terblanche (2011) the sphere drag coefficient of Turton and Levenspiel (1986) (equation B.5) can be used for water drops which has not reached terminal velocity. The theoretical velocity calculations mentioned above are used on the free falling water drop to validate the water drop diameter measurements and the free falling velocity. The drop diameter measurements can be confirmed by comparing the measured and calculated drop velocity. Presented in Figure B.3 below are the theoretical calculations for a water drop diameter of 4.5 mm and the measured drop velocity for different injection heights. The results validate the measurements techniques. The injection height is varied between 250 mm and 1750 mm with 250 mm increments.

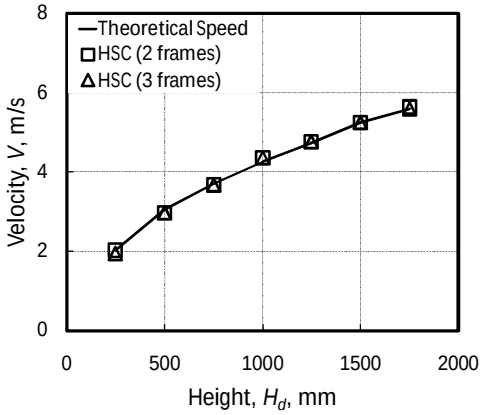

Figure B.3: Theoretical velocity calculations and measurements results for a 4.5 mm diameter water drop for different injection heights

B.5 Conclusion

The calibration test results show that the theoretical velocity calculations predict the free falling ball bearing velocity at different heights, with a maximum deviation of 1.2 %. The theoretical velocity calculations are validated and may be used for water drop velocity calibrations.

The validated velocity model is used to determine the water drop velocity and to confirm the water drop diameter measurements. This is done by reverse calculating the diameter from the measured drop velocity. The injection height is varied between 250 mm and 1750 mm with 250 mm increments. The water drop velocity and diameter measurements are made accurate with a maximum difference of 1.9 %.

APPENDIX C: CALIBRATION DETAILS OF THE COUNTER-FLOW TEST SECTION

C.1 Introduction

Following are the instrumentation calibration details for the counter-flow fill test facility at Stellenbosch University. The instrumentation consists of three differential pressure transducers and an electromagnetic flow meter. The calibration constants are used in a Visual Basic Excel programme for data logging on an Agilent data acquisition system.

C.2 Pressure transducers calibration

The three Endress and Hauser differential pressure transducers, as shown in Figure 4.5, are calibrated against a Betz manometer. Following is the calibration procedure.

Calibration Procedure

1. Level the Betz manometer with the built-in water level by adjusting the four legs.
2. Switch on the backlight of the Betz manometer, making the pressure reading visible.
3. Blow air through the positive port to remove all water drops from the line.
4. Zero the pressure reading by adjusting the knob at the top.
5. Connect a common line between the negative and positive ports of the Betz manometer and the differential pressure transducers.
6. Apply a differential pressure by blowing on the line, connected to the positive side. Close the line off to keep the applied pressure.
7. Record the reading on the Betz manometer, differential pressure transducers display and the pressure transducers' voltage output.
8. Release some of the air and take down the next data point.
9. Repeat the above until the working range is covered.

With reference to Figure 4.5, the differential pressure transducers A, B and C have pressure ranges of 1000, 450 and 450 N/m^2 respectively. From this a linear regression between the pressure and voltage is obtained to relate the voltage to a pressure reading when data is logged.

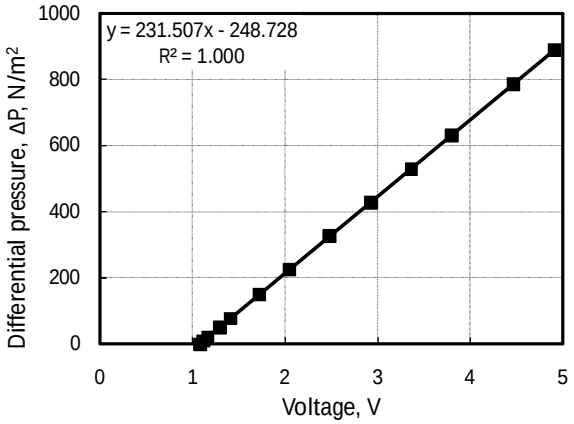

(a) 0 - 1000 N/m^2 pressure transducer used across the inlet nozzles.

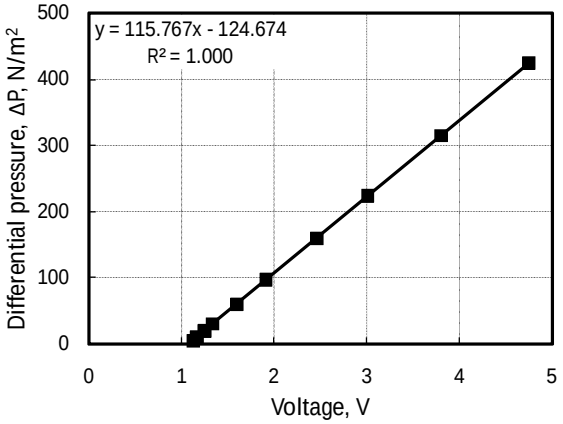

(b) 0 - 450 N/m^2 pressure transducer used over the water troughs

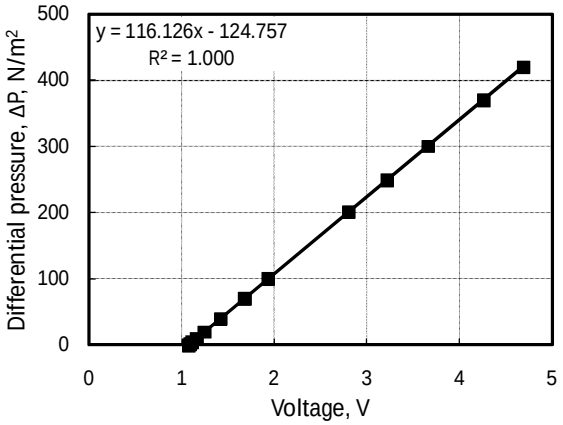

(c) 0 - 450 N/m^2 pressure transducer used over the water troughs

Figure C-1: Calibration details of the Endress and Hauser differential pressure transducers

C.3 Electromagnetic flow meter

The electromagnetic flow meter is used to measure the volume flow rate of the water supplied to the sprayers. The electromagnetic flow meter is calibrated against a calibrated water tank and the LCD display on the flow meter. Following is the calibration procedure.

Calibration Procedure

1. Calibrate the volume of the water tank by measuring each amount of water that is added to the tank. Mark each volume with reference lines on the tank. The tank dimensions are shown in Figure C-2.
2. Remove the supply pipe from the sprayer, and direct the water to flow into the calibrated water tank.
3. Start the pump with all valves fully open to bleed the system.
4. With each run, record the time it takes to fill the calibrated tank, the reading on the LCD display and the current output.
5. Close the supply side valve slightly to produce the next data point.
6. Repeat steps 4 and 5 over the working range.

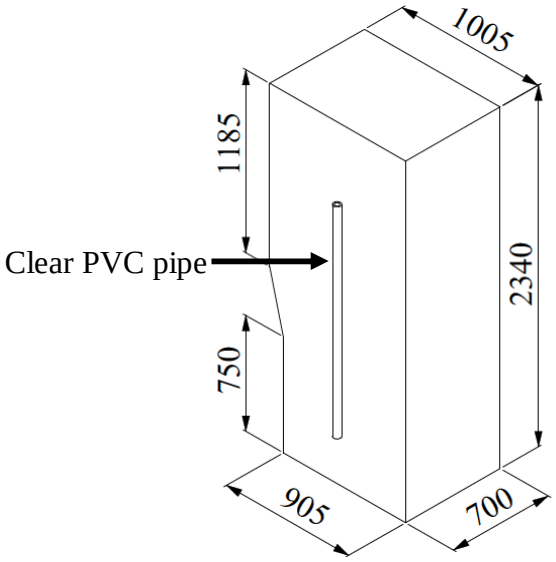

Figure C-2: Calibration tank with dimensions

The percentage deviation between the measured flow rate and the flow meter LCD display is plotted. A linear regression between the volumetric flow rate from the calibration tank and current output is obtained to relate the current to a flow rate reading. See Figure C-3 below for the regression curve.

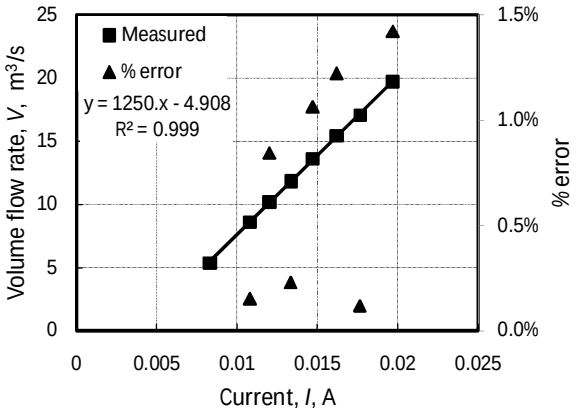

Figure C-3: Electromagnetic flow meter calibration

APPENDIX D: WATER TROUGH DRAINING PERFORMANCE AT DIFFERENT ANGLES

D.1 Introduction

Following are the theoretical calculations used to determine the water depth in the draining trough as discussed in Chapter 4. The theoretical water depth is compared to the measured water depth, to find the water drainage characteristics of the water trough. The water depth at the outlet is calculated while the trough angle and water mass velocity are varied.

D.2 Theoretical water depth

Open channel flow theory is used to calculate the water depth in the channel, 2.5m in length. The theory is based on work done by Gauckler and Manning taken from Cengel and Cimbala (2006) as shown in equation (D.8). The water flow rate and the slope of the trough are kept constant while the depth is calculated iteratively. The dimensions of the water channel are shown in Figure D-1. The water channel is divided into control volumes along the length of the channel. The outlet flow rate and water depth of the first control volume is the inlet conditions of the following control volume as shown in equation (D.6). The water flow is uniformly distributed along the length of the channel, this value is used as an input to the Manning equation. Following are the equations used to calculate the depth of the water at the outlet. The initial water depth is guessed for the first iteration. The water depth is either increased or decreased after each iteration to get the calculated volume flow rate equal to the desired water flow rate. The mean value for the Manning coefficient (n) is taken as 0.012 from Cengel and Cimbala (2006) for smooth stainless steel.

The flow area is:

$$A_c = (W \times \Delta y) + \frac{1}{2}\left(\pi \frac{D^2}{4}\right) = (0.02 \times 0.01) + \frac{1}{2}\left(\pi \frac{0.02^2}{4}\right) = 0.000357 \text{ m}^2 \quad \text{(D.1)}$$

Wetted parameter:

$$p = S + (W + 2\Delta y) = 0.029845 + (0.02 + 2 \times 0.01) = 0.069845 \text{ m} \quad \text{(D.2)}$$

Hydraulic radius:

$$R_h = \frac{A_c}{p} = \frac{0.00035707}{0.069845} = 0.00511 \quad \text{(D.3)}$$

Slope:

$$S_o = \frac{\Delta x}{\Delta y} = \frac{0.39}{2.5} = 0.156 \quad \text{(D.4)}$$

Desired water mass flow rate for the 2.5 m channel:

$$\dot{m} = G_w \times A = 1.7 \times (2.5 \times 0.05) = 0.2125\ \text{kg/s} \quad \text{(D.5)}$$

Mass flow rate for the control volumes:

$$\dot{m}_1 + \dot{m}_2 = \dot{m}_3 \quad \text{(D.6)}$$

Water volume flow rate:

$$\dot{V}_1 = \frac{\dot{m}}{\rho_w} = \frac{0.2125}{998} = 0.000213\ \text{m}^3/\text{s} \quad \text{(D.7)}$$

Calculated water volume flow rate:

$$\dot{V}_2 = \frac{a}{n} A_c R_h^{2/3} S_o^{1/2} \quad \text{(D.8)}$$

$$\dot{V}_2 = \frac{1}{0.012} 0.000357 \times 0.00511^{2/3} \times 0.156^{1/2} = 0.0002045\ \text{m}^3/\text{s}$$

Difference in flow rate:

$$\Delta\dot{V} = \dot{V}_1 - \dot{V}_2 = 8.5 \times 10^{-12} \quad \text{(D.9)}$$

With the next iteration the water depth is increased to reduce the difference in volume flow rate.

Water depth in the channel:

$$H_w = R_{ch} + \Delta y = 10\ \text{mm} + 10\ \text{mm} = 20\ \text{mm} \quad \text{(D.10)}$$

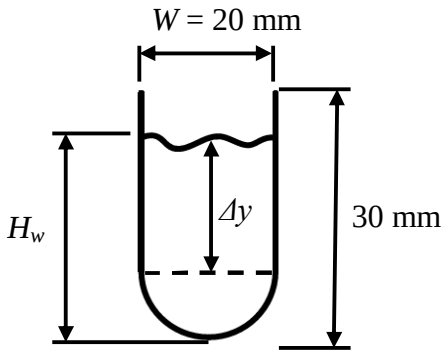

Figure D-1: Water channel with dimensions

APPENDIX E: INPUT DATA TO THE TWO DIMENSIONAL CFD MODEL OF THE WATER BASIN

E.1 Introduction

Following in this appendix are tables containing the input data for the two-dimensional CFD model presented and discussed in Chapter 5.

E.2 CFD model input data

The standard input vales and settings are used in the FLUENT® model unless stated otherwise. The input data for the two-dimensional FLUENT® model is summarized below in Table E-1 to E-4.

Table E-1: FLUENT® model input data

Description	**Settings**	**Input value**
Solver	Pressure based	-
Space	Planar	-
Gravity	y-direction	-9.81
Porous formulation	Superficial velocity	-
Viscous/Model	*k-ε* Realizable	-
DPM/Interaction	Interaction with continues phase	-
DPM/Tracking parameter	Max number of steps	50 000
DPM/Tracking parameter	Step length factor	2
DPM/Drag law	Spherical drag law	-

Table E-2: FLUENT® boundary conditions input data

Description	**Settings**	**Input value**	**Units**
Domain inlet	Mass flow inlet	13	kg/s
	Turbulence intensity (Induced draft)	4	%
	Turbulence intensity (Forced draft)	8	%
	Turbulence length scale	0.15	m
Domain outlet	Outflow	-	-
Wall-part-surface (Basin wall)	DPM/Escape	-	-

Table E-3: FLUENT® fluid material input data

Description	Settings	Input value	Units
Material type	Fluid/Air	-	-
Properties / Density	Constant	1.225	kg/m^3
Properties / Viscosity	Constant	1.79e^{-5}	kg/m-s
Properties / Reference temperature	Constant	288.16	K

Table E-4: FLUENT® (DPM) fluid material input data

Description	Settings	Input value	Units
Material type	Fluid/Water liquid		
Properties / Density	Constant	998.2	kg/m^3
Properties / Viscosity	Constant		kg/m-s
Properties / Reference temperature	Constant		K
Injection type	Surface	Air outflow 1	-
Diameter distribution	Uniform	0.005	m
Variable	x-velocity	0	m/s
Variable	y-velocity	-0.0075	m/s

E.3 Fan data for the PJM

Following are the dimensions of the generic ACSC fan used for the PJM.

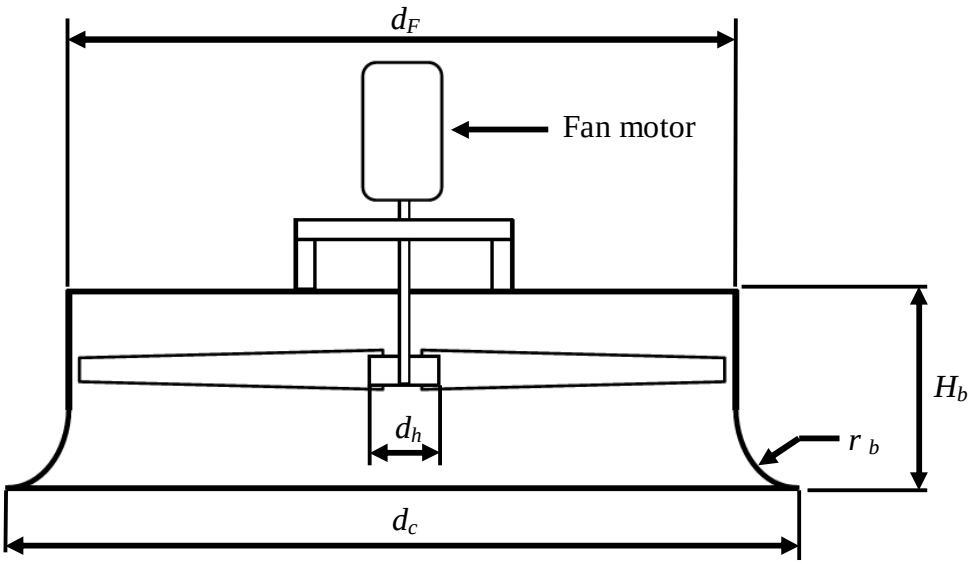

Figure E-1: Axial flow fan dimensions

Table E-5: Generic ACSA axial flow fan details

Description	Symbol	Value	Units
Fan diameter	d_f	9.145	m
Fan casing diameter	d_c	9.17	m
Height of inlet shroud	H_b	1.92	m
Inlet shroud radius	r_b	1.16	m
Number of blades	N_{bl}	8	-
Rotational speed	N	125	rpm

E.4 CFD mesh element data

The mesh element size independence study is done with the validated model used for validation of the CFD model with to experimental results by Kröger and Terblanche (1994) on induced draft rectangular tower inlets with a horizontal heat exchanger. The results are shown in section 5.2. In Figure E-2 is a screen shot of the mesh used for the model, with refinement closer to the tower walls where the flow re-circulation is expected at the basin inlet near the vicinity of the wall. This is repeated for all CFD models around the basin inlets.

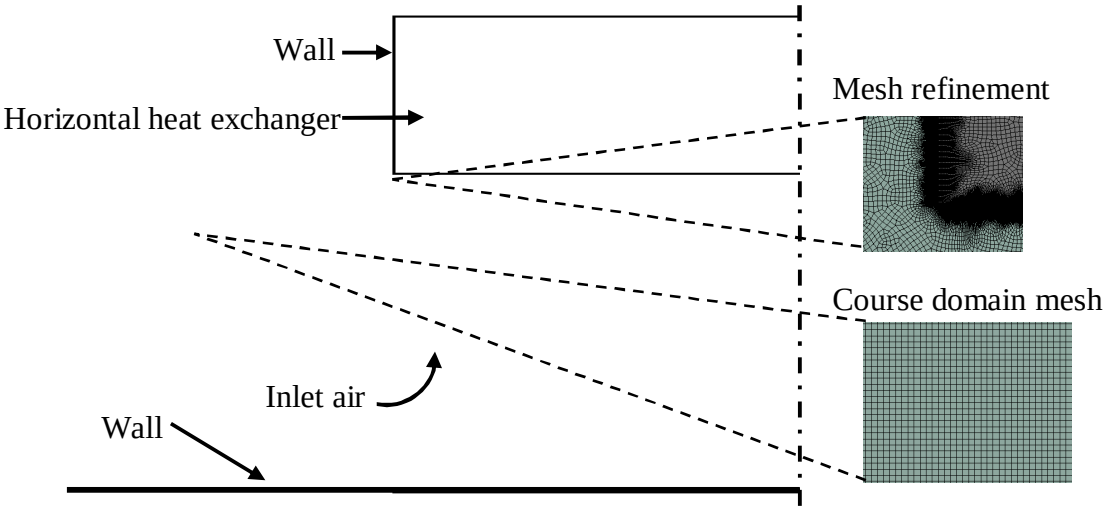

Figure E-2: Mesh elements for the rectangular tower with horizontal heat exchanger

APPENDIX F: BASIN INLET LOSS COEFFICIENT CALCULATIONS

F.1 Introduction

Following is a sample calculation for the validation of the inlet loss coefficient. The sample calculation of the inlet loss coefficient of the water basin with an induced draft with a rain-zone and a 2.5 m lateral inlet is shown below. The similar approach is used with the cascaded and forced draft basin layouts.

F.2 Calculations

The CFD models are validated by comparing the result of the CFD model to the correlation (equation 5.5) for inlet loss coefficient developed from experimental work by Kröger and Terblanche (1994). Following is the sample calculation for the loss coefficient of the rectangular cooling tower with a 5 m width and a 2.5 m inlet height.

$$K_{ct} = \left[1.1 + 1.1\left(0.5\frac{W_i}{H_i}\right)^3 - 0.05\left(0.5\frac{W_i}{H_i}\right)e^{\left(0.5\frac{W_i}{H_i}\right)}\right] \times K_{he}^{\left[-0.29+0.079cos\left(0.5\frac{W_i}{H_i}\right)+0.102sin\left(0.5\frac{W_i}{H_i}\right)\right]}$$

$$K_{ct} = \left[1.1 + 1.1\left(0.5\frac{5}{2.5}\right)^3 - 0.05\left(0.5\frac{5}{2.5}\right)e^{\left(0.5\frac{5}{2.5}\right)}\right] \times 38^{\left[-0.29+0.079cos\left(0.5\frac{5}{2.5}\right)+0.102sin\left(0.5\frac{5}{2.5}\right)\right]}$$

$$K_{ct} = 1.15 \quad \text{(F.1)}$$

After the two-dimensional symmetrical CFD model is run, the mass-weighted average total pressure (P_t) is taken from the inlet and the outlet.

The basin inlet coefficient:

$$K_{db(wet)} = K_t - K_{he} - K_{rz} \quad \text{(F.2)}$$

$$K_{db(wet)} = \frac{P_{t1}-P_{t2}}{\frac{\rho_i v^2}{2}} - K_{he} - K_{rz}$$

Where the total loss coefficient is:

$$K_t = \frac{P_{t1}-P_{t2}}{\frac{\rho_i v^2}{2}} = \frac{(-1.737-(-131.61))}{\frac{1.225\times 2.123^2}{2}} = 47 \quad \text{(F.3)}$$

The loss coefficient (K_{he}) of the heat exchanger is an input value of 38. The loss coefficient of the rain-zone is determined from work done by Kröger and De Villiers (1997) and the correlation is shown in equation (F.4).

$$K_{rz} =$$

$$a_v v_w \frac{3}{2}\left(\frac{H_i}{d_d}\right)\left\{\begin{array}{c} 0.219164 + 8278.8a_\mu\mu_a - 0.30487a_\rho\rho_a \\ +0.954153 \times [0.328467exp(135.7638a_L d_d) + 0.47] \\ \times [26.28482(a_L H_i)^{-2.95729} + 0.56] \\ \\ \times exp\left[\begin{array}{c} \ln[0.204814\, exp(0.133036a_L W_i) + 0.21] \\ \times [3.9186\, exp(-0.3a_L H_i)] \\ \times [0.31095\, \ln a_L d_d + 2.63745] \end{array}\right] \\ \\ \times [2.177546(a_v v_a)^{-1.46541} + 0.21] \end{array}\right\} \qquad \text{(F.4)}$$

with $10 \leq T_w \leq 40$ °C, $0.927 \leq \rho_a \leq 1.289$ kg/m^3, $0.002 \leq d_d \leq 0.007$ m, $0.0075 \leq v_w \leq 0.003$ m/s, $2 \leq H_i \leq 8$ m, $1 \leq v_a \leq 5$ m/s and $4 \leq W_i \leq 40$ m

where

$$a_\mu = 3.061 \times 10^{-6}\left[\frac{\rho_w^4 g^9}{\sigma_w}\right]^{0.25} = 3.061 \times 10^{-6}\left[\frac{998.2^4\ 9.81^9}{0.0720348342}\right]^{0.25} = 1.004501$$

$$a_p = \frac{998}{\rho_w} = \frac{998}{998.2} = 0.9998$$

$$a_v = 73.298\left[\frac{g^5\sigma_w^3}{\rho_w^3}\right]^{0.25} = 73.298\left[\frac{9.81^5 \times 0.07203^3}{998.2^3}\right]^{0.25} = 0.9963$$

$$a_L = 6.122\left[\frac{g\sigma_w}{\rho_w}\right]^{0.25} = 6.122\left[\frac{9.81 \times 0.07203}{998.2}\right]^{0.25} = 0.9986$$

Water mass flow rate:

$$\dot{m} = G_w \times A = 1.75 \times 2.5 = 4.25\ \text{kg/s} \qquad \text{(F.5)}$$

Water droplet initial velocity

$$v_w = \frac{\dot{m}}{A\rho} = \frac{5kg/s}{2.5 \times 998.2} = 0.0017\ \text{m/s} \qquad \text{(F.6)}$$

For the induced draft reference case with an inlet height of 2.5 m, and a drop diameter of 4 mm the rain-zone loss coefficient can be determined as follows with equation (F.4). The air density is taken as 1.225 kg/m^3 and the viscosity is 0.17894 x 10^{-6} kg/m-s.

$$K_{rz} =$$

$$a_v(0.0017)\frac{3}{2}\left(\frac{2.5}{0.004}\right)\left\{\begin{array}{c}0.219164 + 8278.8a_\mu(0.179 \times 10^{-6}) - 0.30487a_\rho(1.225) \\ +0.954153 \times \left[0.328467exp\left(135.7638a_L(0.004)\right) + 0.47\right] \\ \times [26.28482(a_L \times 2.5)^{-2.95729} + 0.56] \\ \\ \times exp\left[\begin{array}{c}\ln[0.204814\ exp(0.133036a_L \times 2.5) + 0.21] \\ \times [3.9186\ exp(-0.3a_L \times 2.5)] \\ \times [0.31095\ \ln a_L(0.004) + 2.63745]\end{array}\right] \\ \\ \times [2.177546(a_v \times 2.123)^{-1.46541} + 0.21]\end{array}\right\}$$

$K_{rz} = 0.95$

Now equation (F.1) can be solved:

$$K_{db(wet)} = K_t - K_{he} - K_{rz} = 47 - 38 - 0.95 = 8.05$$

For the dry basin the same process will be followed, except for the rain-zone loss coefficient will be omitted.

The rain-zone correction factor (equation 5.9) sample calculation is shown below for the reference case. The empirical correlation is only applicable to induced draft rectangular cooling towers

$$C_{rz} = 1 - G_w\left(0.123 - 12.1d_d - 272.26d_d + 5.04e^{-4} \times e^{\frac{0.466W_i}{H_i}}\right)(1 - 1.16 \times 10^{-3}e^{G_a})$$

$$C_{rz} = 1 - 1.7\left(0.123 - 12.1 \times 0.004 - 272.26 \times 0.004 + 0.504 \times 10^{-3} \times e^{\frac{0.466\times5}{2.5}}\right)$$
$$(1 - 1.16 \times 10^{-3}e^{2.5})$$

$C_{rz} = 0.875$